Characterizing methane (CH4) and carbon dioxide (CO2) emissions through mobile platforms from local to national scale

Yunsong Liu

THESE DE DOCTORAT

NNT : 2022UPASJ021

Characterizing methane (CH_4) and carbon dioxide (CO_2) emissions through mobile platforms from local to national scale

Caractériser les émissions de CH_4 et de CO_2 via des plateformes mobiles de l'échelle locale à nationale

Thèse de doctorat de l'université Paris-Saclay et de The Cyprus Institute

École doctorale n° 129: Sciences de l'Environnement d'Ile-de-France (SEIF)
Spécialité de doctorat: Sciences du climat, de l'atmosphère et des océans, terrestres et planétaire

Graduate school: Géosciences, climat, environnement et planètes
Référent : Université de Versailles Saint-Quentin-en-Yvelines

Thèse préparée dans l'unité de recherche LSCE (Université Paris-Saclay, CNRS, CEA, UVSQ), sous la direction de Philippe BOUSQUET, Professeur des universités, la co-direction de Jean SCIARE, Professeur, le co-encadrement de Jean-Daniel PARIS, Chargé de recherche et de Mihalis VREKOUSSIS, Professeur

Thèse soutenue à Paris-Saclay, le 22 décembre 2022, par

Yunsong LIU

Composition du Jury

Membres du jury avec voix délibérative

Maria KANAKIDOU Professeur, University of Crete	Présidente et Rapporteure
Nikolaos MIHALOPOULOS Professeur, University of Crete	Rapporteur et Examinateur
Anke ROIGER Chercheuse, DLR	Examinatrice
Martina SCHMIDT Professeur, Universität Heidelberg	Examinatrice

Titre : Caractériser les émissions de CH_4 et de CO_2 via des plateformes mobiles de l'échelle locale à nationale

Mots clés : méthane, dioxyde de carbone, mesures mobiles, véhicule aérien sans pilote, gaz naturel, estimations des émissions

Résumé : Le méthane et le dioxyde de carbone sont les gaz à effet de serre (GES) d'origine humaine les plus abondants dans l'atmosphère. Leur concentration croissante dans l'atmosphère est la principal cause du changement climatique. Il est donc essentiel de surveiller l'évolution de leurs sources et de leurs puits. Une caractérisation et une quantification précises de leurs émissions territoriales provenant de différents secteurs sont nécessaires pour déterminer et gérer des actions et des politiques d'atténuation efficaces. L'objectif principal de cette thèse est d'améliorer la caractérisation des émissions de CH_4 et de CO_2 secteur par secteur, de l'échelle locale à l'échelle nationale, via le développement de stratégies d'observation mobiles exploitant des plateformes telles que la voiture, le drone et l'avion.

Cette étude comporte trois parties. La première partie vise à vérifier un inventaire national de CH_4 avec une méthode reproductible, en prenant pour base Chypre. Je me concentre sur la quantification des émetteurs de méthane significatifs (décharges et zones d'élevage) qui représentent cumulativement 28% des émissions nationales de méthane. L'approche se base sur des mesures mobiles en voiture et une modélisation par dispersion gaussienne. Les émissions de méthane calculées provenant des décharges et de la fermentation entérique du bétail étaient environ 160% et 40% plus importantes, respectivement, que les estimations sectorielles ascendantes utilisées dans l'inventaire national. Ces enquêtes mobiles montrent qu'un ensemble de mesures in situ ciblant des points chauds représentatifs des émissions de méthane avec une couverture temporelle et spatiale cohérente peut largement améliorer les inventaires nationaux ascendants des émissions.

La deuxième partie se concentre sur les méthodes de quantification des émissions de CH_4 pour l'industrie pétrolière et gazière. Elle compare dix systèmes commerciaux de pointe de quantification du méthane par le biais d'une série d'expériences de rejet contrôlé dans une station de compression inerte. Les rejets contrôlés couvraient une série de situations, y compris différents taux de fuite et conditions de vent. Les résultats indiquent que les systèmes "source-level" (proches d'une fuite unique) sous-estiment généralement les émissions, tandis que les systèmes "site-level" (intégrant les émissions pour le site) reposant sur la dispersion atmosphérique surestiment légèrement les taux d'émission. L'analyse de cette partie souligne que les drones (UAV) ont le potentiel de combler le fossé entre les observations au sol et les observations aériennes, mais sont fortement sensibles au vent.

La dernière partie était consacrée au développement des mesures de GES par drone. J'ai

développé et validé un nouveau système de capteur portable UAV-CO_2 qui est léger mais reste suffisamment précis. Grâce à une procédure minutieuse de caractérisation, de correction et de calibration du capteur, nous atteignons une précision en vol de ± 2 ppm (1σ) à 1 Hz et de ± 1 ppm (1σ) à 1 min. Ce système est relativement peu coûteux et facile à reproduire, et a le potentiel pour réaliser une large gamme d'applications sur le terrain, telles que la surveillance des émissions urbaines et des sources ponctuelles.

En bref, ce doctorat fait un pas en avant pour la réconciliation future des estimations d'émissions de GES basées sur divers systèmes d'observation et différentes approches, et recherche des méthodes facilement duplicables et applicables à d'autres régions et secteurs d'émission. Alors que les approches mobiles présentées ici représentent clairement des options importantes pour le suivi des émissions, des défis significatifs demeurent dans la capacité actuelle d'estimer régulièrement les trajectoires d'émissions de GES anthropiques avec une précision suffisante et à grande échelle.

université PARIS-SACLAY | ÉCOLE DOCTORALE Sciences de l'Environnement d'Île-de-France (SEIF)

Title : Characterizing methane (CH_4) and carbon dioxide (CO_2) emissions through mobile platforms from local to national scale

Keywords : methane, carbon dioxide, mobile measurements, unmanned aerial vehicles, natural gas, emission estimates

Abstract : Methane and carbon dioxide are the most abundant human-induced greenhouse gases (GHG) in the atmosphere. Their increasing atmospheric concentration is the main driver of climate change. Therefore, it is critical to monitor the evolution of their sources and sinks. Accurate characterization and quantification of their territorial emissions from different sectors are required in order to determine and manage efficient mitigation actions and policies. The main goal of this Ph.D. is to improve the characterization of CH_4 and CO_2 sectoral emissions from local to national scale through the development of mobile observation strategies including platforms such as car, drone and aircraft.

This study consists of three parts. The first part aims at verifying a national CH_4 inventory with a replicable method. I focus on surveying and quantifying significant methane emitters that represent 28% of national (Cyprus) methane emissions. These are essentially landfills and cattle farm areas. The approach is based on car-based mobile measurements and Gaussian plume dispersion modelling. The calculated methane emissions from landfills and enteric fermentation of cattle were about 160% and 40% larger, respectively, than the bottom-up sectoral estimates used in the national inventory. These mobile surveys show that an ensemble of in situ measurements targeting representative methane emission hotspots with consistent temporal and spatial coverage can largely improve national bottom-up emission inventories.

The second part focuses on methods to quantify CH_4 emissions for the oil and gas industry. It compares ten state-of-the-art commercial methane quantification systems through a series of controlled release experiments at an inert compressor station. The controlled releases covered a range of situations including various leak rates and wind conditions. The results indicated that 'source-level' systems (close to single leak) generally underestimate emissions, while 'site-level' systems (integrating emissions for the site) relying on atmospheric dispersion slightly overestimate emission rates. The analysis of this part highlights that unmanned aerial vehicles (UAV) have the potential to bridge the gap between ground-based and airborne observations but are strongly wind sensitive.

The last part focused on the development of UAV GHG measurements. I have developed and validated a novel portable UAV-CO_2 sensor system that is lightweight but remains sufficiently precise. Through a careful sensor characterization, correction and calibration procedure, we reach an in-flight precision of ± 2 ppm (1σ) at 1 Hz and ± 1 ppm (1σ) at 1 min. This system is relatively

inexpensive and easy to reproduce, and has the potential to perform a wide range of field applications, such as urban and point source emissions monitoring.

In short, this Ph.D. makes a step forward for future reconciliation of GHG emission estimates based on various observation systems and different approaches, and seeks methods that are easily duplicated and applicable to other regions and emission sectors. While mobile approaches presented here clearly represent important monitoring options, significant challenges remain in current capability to estimate routinely anthropogenic GHG emission trajectories with sufficient precision and at large scale.

Acknowledgments

This has been a very nice and fulfilling four years' journey. Although the global pandemic made it more difficult, this trip becomes more meaningful and memorable. I would like to express my gratidude here and thank the people and institutes I shared with during this journey.

First, I would like to show my deepest gratitude here to my supervisors Jean-Daniel Paris, Philippe Bousquet, Jean Sciare and Mihalis Vrekoussis for your continuous support, help and trust. Thank you, Jean-Daniel for showing me how to do research and giving me guidance whenever I got lost. Our weekly intellectual discussions not only allowed me to dig and expand this topic, but also encouraged me a lot during tough times. Besides science, our conversations on various topics inspired my thoughts. Thank you Jean for guiding me to look at my work from bigger perspectives. Your support and help on all my research activities during COVID 19 motivated me to complete this topic and pass the most difficult time. Thank you Philippe for guiding me to dig this topic, and helping me get some perspectives during our talks and email exchange, and making our lab life abundant with different activities. Thank you Mihalis for your prompt replies, nice suggestions and guidance on my work, and helping me improve my scientific writing ability, and hope we will meet soon in person.

Additional thanks to Gregoire for the nice suggestions, guidance and brainstorms for Chapter 3, and the constructive discussions made significant progress on this part. Many thanks to Sébastien Biraud and Huilin Chen for being my thesis committee members to evaluate and supervise my work each year, and the discussions shared with you prompted the development and progress of this thesis.

Many thanks to my colleagues at LSCE and CyI whose assistance and support were a milestone in the completion of this project. Especially, thank you Olivier, Carole and Luc for your help and guidance on laboratory tests for the instruments used in this thesis and providing me remote support during my stay in Cyprus. Thank you Christos, Panayiota, CC, Andreas and all my USRL colleagues for your continuous help, support and efforts on all field campaigns and lab tests in Cyprus. Without your help, I could not imagine how I would complete this topic. Thanks to people at the graduate school of CyI for all of your kind help during my stay in Cyprus. Thank you

my working partner Pierre-Yves for numerous hours spent with me in the car and all your efforts whenever I need. Also, specific thanks to the ICOS volleyball teams for getting me my first siliver medal.

The most valuable part of this journey belongs to beautiful friendships, full of precious memories. Thank you, Stijn, my first non-chinese speaking friend, for all the trips and your impressive driving skill; Sara for the accompanies, help and support from the beginning to the end; Yitong and Yang for your coding helps, sharing my pressure and enriching my everyday life in France; Anna for your welcome and all the meals shared with me; Max, *tu es mon frère français,* thank you for all the trips and can't wait for our next trip; Pierre-Yves, you are not only a working partner but also a unique friend who can read my mind magically; Aliki, my greek sister, your endless energy and passion for life impact me a lot, thanks to you and your families for making me feel at home in Europe; Constantina and Panayiota, I miss your hugs, and thank you for taking care of me like families, and Cyprus becomes special to me because of you. Thank you my housemates Fabian and Charis for your companies, sharing my pressure and everyday life, and teaching me swimming and driving. Thank you Nikoleta for driving me to markets and your unique humor. Thank you Ayche for your amazing cook skill and showing me Belgium. Thank you Jacopo, Laurence, Elena, Cagla, Elefteria, Pan, Chiara, Emeric, Xinwei, Siteng and others for all the lunches, trips, hikes, camps, parties, beach volleyball, badminton and all the wonderful memories.

In the end, thanks to my families and dear friends in China and Australia. thank you for all the video calls, messages and your confidence in me to complete this Ph.D. You gave me continuous energy to support me to pass all the difficulties. Finally, thanks to my parents who always support my decisions and stay on my back. Your love gave me the motivation to start this journey and also supported me to complete it. Please make dumplings for me once I am back home.

CONTENTS

FIGURES

TABLES

1 INTRODUCTION

1.1 CLIMATE IS CHANGING

Climate change is characterized by long-term changes in temperatures and precipitations and other components at the local, regional and global scales. Climate change is caused by forcing factors leading to a change in the Earth's energy balance. The greenhouse gas concentrations increasing in the atmosphere because of human activities is the main climate forcing. According to the IPCC (2021), the global mean temperature will increase by at least 1.5 ℃ in the next 20 years relative to the pre-industrial period (1750s) for five future scenarios (SSP1-1.9, SSP1-2.6, SSP2-4.5, SSP3-7.0 and SSP5-8.5). Such temperature increase has already resulted in profound alterations to human societies and natural systems, for example, increases in heat waves, longer warm seasons and shorter cold seasons. Notably, some of the observed changes are unprecedented and irreversible over hundreds to thousands of years, such as sustained sea level rise (IPCC, 2018 and 2019).

Climate change is a severe global threat that has become one of the most critical challenges of the 21st century from both a scientific and societal perspective. Recently and worldwide, together with non-governmental organizations (NGO), citizen movements have put growing pressure on many governments to agree on the reduction in greenhouse gas emissions and to act rapidly. Acknowledging the challenge associated with mandatory reduction (Kyoto Protocol) has resulted in establishing the Paris Agreement for the climate in 2015. The main goal of the Paris Agreement is to limit climate change by keeping the warming below 2 ˚C (ideally 1.5 ˚C) compared to pre-industrial levels by this century. This very ambitious objective implies achieving a reduction of atmospheric GHG as soon as possible during the 21st century, with large reductions of their emissions to the atmosphere.

In this context, it is critical to curb GHG concentrations in the atmosphere and to plan, implement and monitor policies that ensure emission reduction. This entails monitoring the evolution of GHG in the atmosphere from local to global scales. To do so, we need to strengthen our capability of having high-quality and accurate observations of atmospheric GHGs at all scales, including local, regional and global measurements at the surface and

vertically resolved. Carbon dioxide (CO_2) and methane (CH_4) are the top two abundant and the most significant human-induced greenhouse gases in the atmosphere. They are the major drivers of the ongoing global climate change and key actors of global biogeochemical cycles (IPCC, 2013, 2021; Ciais et al., 2013). Therefore, accurately identifying their source categories and their magnitudes is a critical pre-requisite for the effective implementation of climate change mitigation policies (Le Quéré et al., 2018; Saunois et al., 2016). Since this study will focus on the characterization of CO_2 and CH_4 atmospheric content and emissions, the following two subsections will introduce atmospheric CO_2 and CH_4 and their sources and sinks in detail.

1.2 CARBON DIOXIDE (CO_2)

Carbon dioxide (CO_2), the most important human-induced greenhouse gas in the atmosphere, is implicated as the foremost gas responsible for climate change, whose mole fraction has reached a new high in 2020 at 413.2 ± 0.2 μmol mol^{-1} (unit also referred to as 'ppm'), which is 49 % higher than its pre-industrial levels (WMO, 2021). Moreover, the growth of atmospheric CO_2 mole fraction in 2021 makes it to a new recorded level, more than 50% higher than its preindustrial level (Friedlingstein et al., 2022). In order to implement efficient mitigation policies and project future global warming, an accurate assessment of the global carbon budget (anthropogenic CO_2 emissions and their redistributions among the atmosphere, ocean and terrestrial biosphere) is needed (Friedlingstein et al., 2020). Worldwide, scientists have engaged in quantifying spatial and temporal distributions of CO_2 for the long term to identify global CO_2 trends and the characterization of CO_2 sources and sinks from global to local scales (e.g. Ciais et al., 2013; Millar et al., 2017; Le Quéré et al., 2018; Rogelj et al., 2019; Dlugokencky and Tans, 2022).

Figure 1.1 presents the perturbation of the global CO_2 cycle caused by anthropogenic activities. Friedlingstein, et al. (2022) found a near-balanced global carbon budget between estimated sources and sinks from 2011 to 2020. Also, their study suggested a 5.4% decrease in fossil CO_2 emissions for 2020 relative to 2019 due to the COVID-19 pandemic (Friedlingstein et al., 2022). The methods used to estimate the global carbon budget include bottom-up inventories based on activity data and emission factors, global models based on dynamic and biogeochemistry processes and top-down

atmospheric measurements and inverse models (DeVries et al., 2019; Hauck et al., 2020).

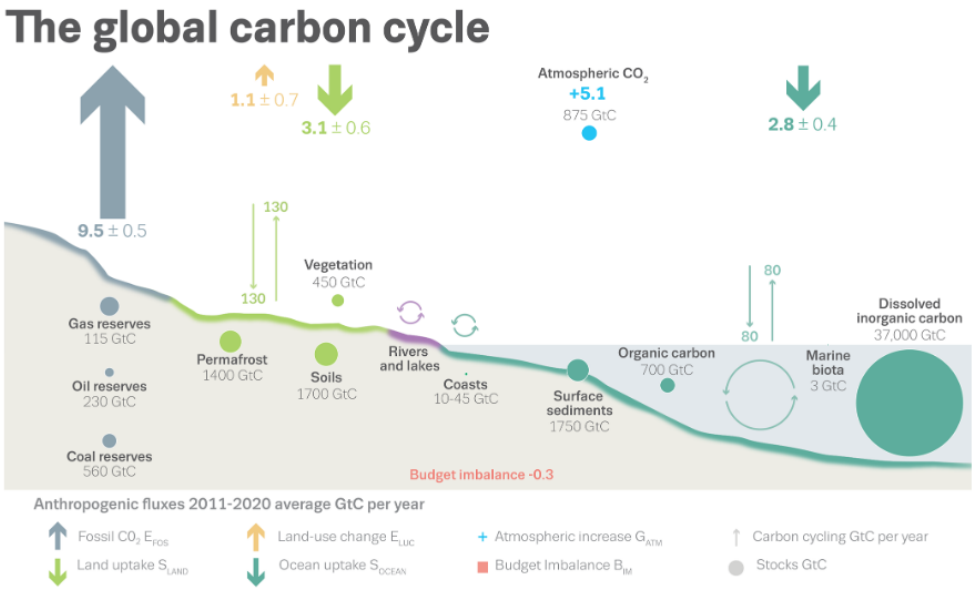

Figure 1.1 Schematic representation of the overall perturbation of the global carbon cycle caused by anthropogenic activities, averaged globally for 2011-2020 (figure from Friedlingstein et al., 2022).

1.2.1 Sources and sinks

About 90% of total CO_2 emissions in the atmosphere are from fossil fuel combustion, which includes various anthropogenic activities like transportation, power plants, heating and air conditioning, cement production and others. Global fossil CO_2 emissions kept increasing by about 3.0 GtC yr^{-1} every decade from the 1960s. Coal combustion contributed about 40%, followed by oil combustion (about 35%) for 2020 (Friedlingstein et al., 2020, 2022). The largest regional contributions to this sector were from China (31%), the USA (14%), the EU27 (7%) and India (7%) in 2020 (Friedlingstein et al., 2022). As the second largest CO_2 emission source, land use changes, accounting for 10% of the total CO_2 emissions have been relatively constant since the 1960s (as shown in Fig.1.2).

The growth rate in atmospheric CO_2 increased by about 3.3 GtC yr^{-1} from 1960s to the last decade (Fig.1.2) (Friedlingstein et al. 2020). The terrestrial biosphere (plants and soils) and the ocean as major natural sinks are taking

up an amount of anthropogenic CO_2 emissions. As shown in Fig.1.2, ocean and land as CO_2 sinks have increased in pace with anthropogenic emissions (Friedlingstein et al. 2020). Since the 1850s, the ocean and terrestrial CO_2 sinks have removed 26% and 30%, respectively, of the total anthropogenic CO_2 emissions (Friedlingstein et al., 2022). Over the past decade (2011-2020), the CO_2 emission was partitioned by 47%, 26% and 29% among the atmosphere, ocean and land, respectively, with a nearly zero imbalance (about 3%) (Friedlingstein et al. 2022).

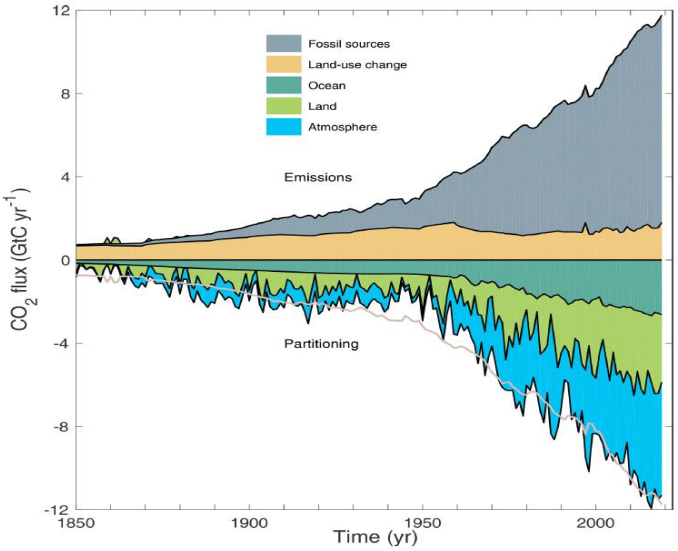

Figure 1.2 Combined components of the global carbon budget illustrated in Fig.1.1 as a function of time, for fossil CO_2 emissions (E_{FOS}, including a small sink from cement carbonation; grey) and emissions from land-use changes (E_{LUC}; brown), as well as their partitioning among the atmosphere (G_{ATM}; blue), ocean (S_{OCEAN}; turquoise) and land (S_{LAND}; green). The partitioning is based on nearly independent estimates from observations (for G_{ATM}) and process model ensembles constrained by data (for S_{OCEAN} and S_{LAND}) and does not exactly add up to the sum of the emissions, resulting in a budget imbalance which is represented by the difference between the bottom pink line (reflecting total emissions) and the sum of the ocean, land, and atmosphere (figure from Friedlingstein et al. 2020).

1.3 METHANE (CH_4)

Methane (CH_4), a potent greenhouse gas with a 9-year lifetime in the atmosphere, has about 28 times the global warming potential of CO_2 on a

100-year horizon (IPCC, 2018). The globally averaged surface mole fraction of CH_4 increased 2.6 times above pre-industrial levels (WMO, 2021). The annual methane increase in 2021 reached 17 ppb, the largest since direct measurements started in 1983. Such rapid increase makes CH_4 the second most important greenhouse gas after CO_2. The current growth trend in CH_4 emissions is estimated between the two warmest scenarios (RCP8.5 and RCP6.0), which corresponds to a 3 ˚C temperature increase by the end of this century (Nisbet et al., 2020; Saunois et al., 2020). Therefore, large reductions in CH_4 emissions are essential and urgently needed to meet the 1.5-2.0 ˚C target of the Paris agreement (Collins et al., 2013; Nisbet et al., 2019). Moreover, methane's shorter lifetime and stronger radiative forcing than CO_2 makes it an efficient target for rapid climate change mitigation on decadal time scales (Nisbet et al., 2020; Saunois et al., 2020).

In order to implement emission mitigation strategies, a better understanding of CH_4 source and sink distributions at local and global scales is needed. Currently, methane source distributions are still poorly constrained due to the large variety of CH_4 sources that overlap geographically (Saunois et al., 2016, 2020). A combination of top-down approaches based on atmospheric constraints and bottom-up approaches using inventories and process-based models is used to determine the global CH_4 budget (Saunois et al., 2020; Stavert et al., 2022). Figure 1.3 presents the global CH_4 budget by sector and shows that CH_4 emissions from anthropogenic and natural sources are partially balanced by the four sinks (Saunois et al., 2020).

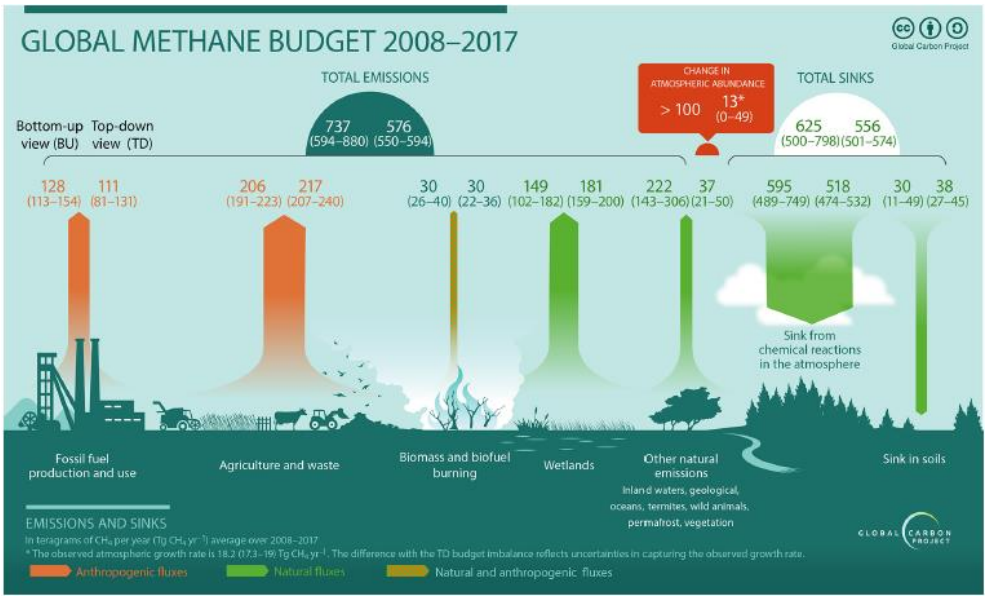

Figure 1.3 Global methane budget for the 2008-2017 decade. Both bottom-up (left) and top-down (right) estimates (Tg CH_4 yr^{-1}) are provided for each emission and sink category, as well as for total emissions and total sinks (figure from Saunois et al. 2020).

1.3.1 Sources and sinks

In a synthesis paper, Saunois et al. (2020) showed that 60% of global methane emissions is from anthropogenic activities and 40% is attributed to natural sources for the decade 2008-2017 based on a top-down approach. For the same decade, bottom-up approaches suggest about 30% larger global emissions since the estimates for natural sources are higher than top-down estimates. Based on the outcome of the same study, atmospheric observation-based emissions suggest a latitudinal distribution, a predominance of tropical emissions (65%), mid-latitudes (about 30%) and high northern latitudes (about 4%). China and the Middle East have the largest regional emission increases in total emission rates (above 20%) during 2000-2017. In contrast, Europe, Korea and Japan show a decline of 10% in emission rates over the same period. China and South Asia emit more than 25% of global anthropogenic emissions (Stavert et al., 2022).

Methane is generated through different processes, categorized as biogenic, thermogenic and pyrogenic paths, and can be further divided into anthropogenic and natural sources. Biogenic methane is produced from the decomposition of organic matter by methanogens in anaerobic environments,

such as rice paddies, landfills, sewage and wastewater treatment or through animal digestive systems. Thermogenic methane is formed on the breakup of organic matter at elevated temperatures and pressures in the Earth's crust, forming coal, oil and gas reservoirs. Natural methane leaks occur through marine and land geological gas seeps. Pyrogenic methane is emitted due to the incomplete combustion of biomass and other organic materials.

Anthropogenic CH_4 sources include fossil fuel production and use, rice agriculture, ruminant animals, waste management and anthropogenic biomass burning. The emissions related to fossil fuels come from exploitation, transportation and use of coal, oil and natural gas, together accounting for about 35% of total anthropogenic emissions. In the subcategory of oil and natural gas systems, CH_4 emissions can be either fugitive (e.g. leaks) or planned (e.g. venting). However, it is difficult to quantify fugitive emissions since they can be persistent or intermittent. These emissions vary greatly among areas depending on the infrastructure and maintenance (McKain et al., 2015; Wunch et al., 2016; Zavala-Araiza et al., 2021).

Under the agriculture and waste categories, livestock (especially enteric fermentation) is the largest CH_4 emission source in most countries, accounting for about one-third of total anthropogenic CH_4 emissions, followed by waste management (predominantly solid waste disposal) and rice cultivation.

Additionally, about 8% of total anthropogenic CH_4 emissions is from biomass and biofuel burning, mainly in the tropics and subtropics where forests and grasslands are used for agricultural land (Saunois et al., 2020). Biofuel burning emissions are mainly from domestic cooking and heating in developing countries (Bakkaloglu et al., 2021).

Above all, coal mining, solid waste disposal and enteric fermentation are dominant drivers of observed anthropogenic CH_4 emission increases and declines appear to be a combination of waste and fossil emission reductions according to the study by Stavert et al. (2022), which means these sectors could be the risks in increasing atmospheric CH_4 and the opportunities for atmospheric CH_4 reductions.

Natural methane sources include wetlands, inland water systems, land geological sources, wild animals, termites, thawing terrestrial and marine

permafrost and oceanic sources. Natural emissions especially from wetlands and other inland waters, are the most important source of uncertainty in the global methane budget estimate (Saunois et al., 2020).

Methane is a well-mixed and reactive trace gas in the troposphere. It plays a key role in both tropospheric and stratospheric chemistry. Three major atmospheric sinks are balancing these CH_4 sources. The most important atmospheric sink is the reaction with tropospheric OH radicals, which accounts for about 88% of the total sink (Stavert et al., 2022). The reaction with tropospheric atomic chlorine accounts for about 2% of the total sink.

Moreover, the third reaction happens in the stratosphere with excited atomic oxygen O (^{1}D), atomic fluorine (F), and OH, accounting for 5% of the total sink (Stavert et al., 2022). In addition to atmospheric CH_4 sinks, biological consumption of CH_4 by methanotrophic bacteria in the soil and other environments is another sink. This process is estimated to account for 5% of the total CH_4 sink (Saunois et al., 2020).

1.4 SOURCE DETERMINATION AND QUANTIFICATION

Two main approaches have been used to monitor GHG emissions and sinks. Bottom-up methods rely on process models or inventories to estimate individual or sectorial emissions (Deng et al., 2022; Scarpelli et al., 2020). Top-down approaches use atmospheric GHG concentrations to infer emissions based on transport modelling and a prior knowledge of emissions usually originating from bottom-up studies (Helfter et al., 2019; Ren et al., 2018). Such inversions methods have originally been developed at the global scale but have been increasingly adapted/modified to smaller scales (Lauvaux et al., 2016; Kumar et al., 2022). Indeed, in general, methods developed to estimate emissions at regional or larger scales are not, at least not directly, suitable for local or smaller scales. As my study will focus on characterizing atmospheric CO_2 and CH_4 emissions through in-situ measurements based on various platforms from local to national scales, I detail below different methods suitable for the different scales.

1.4.1 From global to continental scale

Various estimates are available for global sources and sinks of GHG. As suggested in the study of Friedlingstein et al. (2022), the approach used to

estimate global fossil CO_2 emissions is the standard bottom-up method of inventories with activity data and emission factors based on data collection by many parties such as the United Nations Framework Convention on Climate Change (UNFCCC, https://unfccc.int/ghg-inventories-annex-i-parties/2021) and the Emissions Database for Global Atmospheric Research (EDGAR, https://data.jrc.ec.europa.eu/collection/edgar) (e.g. Deng et al., 2022; Solazzo et al., 2021). Additionally, global dynamic process models are applied to estimate land-use change emissions of CO_2 (Gasser et al., 2020; Friedlingstein et al., 2022). Moreover, the worldwide network of in situ atmospheric measurements and satellite-derived atmospheric CO_2 column observations also constrain atmospheric CO_2 changes (top-down approach).

Similar to CO_2, one approach to estimating global anthropogenic CH_4 emissions relies on bottom-up inventory estimates For example, EDGAR inventory provides global gridded anthropogenic emissions at 0.1×0.1 degree resolution. Moreover, process-based models are also used to estimate methane emissions, such as biogeochemical models for wetland emissions. Additionally, as the top-down estimates, atmospheric inversions are used to report the global methane budget (Saunois et al., 2020). Atmospheric data from different networks assimilated in top-down atmospheric inversions also provide a constraint on the total global source using surface observations (Yver-Kwok et al., 2021) or satellite data (e.g. GOSAT) inversions reduce global estimate uncertainties (Fraser et al., 2013; Buchwitz et al., 2017).

1.4.2 From territorial to regional scale

When going to sub-regional or sub-continental scales, inventory methods based on country reporting of GHG emissions to UNFCCC may have difficulties identifying all possible point sources and quantifying all emissions of complex and diffuse sources. In addition, it requires independent verification as uncertainties in anthropogenic activities, and emission factors can have large biases (Cheewaphongphan et al., 2019a; Hristov et al., 2017). Hence, for these scales, it is critical to better document activity data and emissions factors, and to develop top-down approaches to constrain or cross-check bottom-up inventories and detect inconsistencies with atmospheric observations.

There are several top-down methods for the territory to regional scales, including direct measurements, the equilibrium boundary layer approach based on the mass balance in the atmospheric boundary layer, and regional inverse modeling (Davis et al., 2003, Peters et al., 2007). Networks of direct measurements on tall towers exist around the world to monitor and model emissions from local to continental scales with attempts to reach global scales by extrapolations or neural networks (Feng et al., 2011; Zhang et al., 2014; Stanley et al., 2018). The mass balance approach uses atmospheric measurement data collected by mobile platforms (e.g. ship and aircraft) to calculate emissions (Helfter et al., 2019; Karion et al., 2015a; Gordon et al., 2015; Guha et al., 2020). Aircraft-based mass balance approaches attempt to capture the total integrated emissions, some of which may be difficult to assess or missed by inventories. This approach has been used to assess regional inventories in recent studies. Ren et al. (2018) conducted mass balance aircraft measurements over the Baltimore-Washington area. They suggested that the observed CH_4 emission rate was about twice that given in the inventory. Guha et al. (2020) derived methane emissions from landfills and wastewater treatment plants were about twice the current inventory estimates in the San Francisco Bay area using airborne mass-balance observations. The measurement-derived estimate was consistent with that reported to UNFCCC. Inverse modelling determines emissions using atmospheric transport models constrained by satellite and in situ measurement data. Such top-down methods are widely applied to optimize global, continental or national-scale emissions (Bergamaschi et al., 2010, 2015; Paris et al., 2021). They do not always agree at sub-continental scales. For instance, recent top-down inversion studies using TROPOMI data suggested that CH_4 bottom-up emissions were underestimated by 21% in China (Chen et al., 2022a), contrary to surface-based inversions from the global carbon project (Saunois et al., 2020). Additionally, anthropogenic CH_4 emissions in Europe, the United States, Canada and Mexico are found to be underestimated by about 20-40%, 40%, 30% and 20%, respectively, compared to bottom-up national emission inventories (Cheewaphongphan et al., 2019; Bergamaschi et al., 2015; Peng et al., 2016; Lu et al., 2022).

1.4.3 From site to local scale

Cities, as the center of human activities, are attributed to about 70% of anthropogenic GHG emissions, and by 2050, the population in urban areas is expected to double (Tadić et al., 2017; Ryoo et al., 2019). Therefore,

cities will focus on future mitigation to address climate change. Up to now, urban greenhouse gas emissions have been estimated using bottom-up and top-down methods. Since 2010, the high spatial and temporal resolution greenhouse gas emissions inventory for urban areas has been constructed in developed and developing countries by using different methods, such as the developed framework IPCC and other official guidance (Wright et al., 2011; Sanna et al., 2014; Cai et al., 2019). Cai et al. (2019) assembled a dataset of GHG emissions for 305 Chinese cities based on a high-resolution emissions database and on-site data collection and verification using a bottom-up method.

Moreover, top-down approaches based on atmospheric observations are also used to quantify urban CO_2 and CH_4 emissions either with a mass-balance method or inverse modeling (Klausner, et al., 2020; Moran et al., 2021). Atmospheric measurements can include low-cost and dense sensors (Müller et al., 2020), high-precision ground-based or tower-mounted instruments and flask samples, mobile measurements through different platforms (e.g. vehicles, aircraft and drones), space- and ground-based remote sensing measurements, and combinations of all of the above (Mueller et al., 2018; Maazallahi et al., 2020; Dietrich et al., 2021a). As suggested in the study of Muller et al. (2020), more than 300 low-cost non-dispersive infrared (NDIR) CO_2 sensors were evaluated and integrated into portable units to be used for a CO_2 observation network to monitor CO_2 emissions in Switzerland. Airborne measurements have been conducted to quantify CO_2 and CH_4 emissions for some cities (e.g. Berlin, London and Indianapolis) in the US and Europe to compare with inventorial data. For example, in the study of Klausner et al. (2020), the estimated CO_2 emission is in agreement with current inventories, and the estimated CH_4 emission is almost twice larger than the reported value in the inventory. Besides airborne studies, vehicle-based atmospheric measurements have also been conducted to characterize and map CH_4 emissions in cities like Paris and Hamburg (Defratyka et al., 2021b; Maazallahi et al., 2020). It is found that 50%-80% and 63% of all measured CH_4 emissions is attributed to the natural gas distribution network in Hamburg and Paris, respectively. Lately, Moran et al. (2021) provide a new pan-European model estimating emissions at the urban level and presented a new CO_2 emissions inventory for all municipal and local-government units in Europe.

Additionally, atmospheric measurements can determine and quantify CO_2

and CH_4 emissions from site-level and localized point sources. Notable developments regarding instruments, platforms and analysis have been emerging in the last decade. Mobile measurement laboratories using moving platforms (e.g. vehicles and ships) achieve spatial coverage for specific emission sites and point sources (Lan et al., 2015; Liu et al., 2018a; Lowry et al., 2020a; Paris et al., 2021b). However, mobile laboratories may have limited access to region downwind of emitters, depending on meteorological conditions and of road configurations, and have less temporal coverage compared to stationary measurements. Therefore, hybrid approaches have been evaluated to optimize the determination and quantification of point or multiple sources (Edie et al., 2020; Kumar et al., 2022).

Furthermore, the tracer release method (Yver Kwok et al., 2015) has been developed to quantify emissions from industrial sites emitting CO_2 or CH_4 from single or multiple point sources within a defined area. It is deployed in the form of mobile measurements across the emission plumes of the target and a tracer purposely emitted at a well-known rate close to the suspected source (Lamb et al., 1995; Mønster et al., 2019; Ars et al., 2017). The application of unmanned aerial vehicle (UAV)-based measurements to characterize and quantify point emissions is attractive in recent years' studies. Morales et al. (2021a) developed a drone-based system to measure atmospheric methane and estimate emission fluxes using a mass-balance method for point sources. Reuter et al. (2021) developed a lightweight (about 1.2 kg) UAV system to quantify CO_2 emissions of power plants with a precision of 3 ppm at 0.5 Hz. More recently, Vinković et al. (2022) used an innovative UAV-based active AirCore system to perform accurate atmospheric CH_4 measurements at the farm scale and quantify the emission rate using a mass balance approach.

Depending on this study's objectives, targeted resolution, and topography, such models can be simple mass balance approaches, Gaussian models, Lagrangian dispersion models or more sophisticated computational fluid dynamics models. However, the local-scale transport models can bear large uncertainties (Gao et al., 2009; Hanna et al., 2011; Lan et al., 2015; Ars et al., 2017). Generally, meteorological measurements are performed in parallel with the targeted gas to support the setup of these models. The statistical inversion can account for uncertainties in the model and a statistical estimate of emission rates is derived to optimize the fit to the measurements, accounting for the statistical uncertainties in the transport

modelling and the measurements (Goyal et al., 2005; Ars et al., 2017; Kumar et al., 2021). In theory, the transport model and the inversion procedure can be applied for a point source and multiple sources. Therefore, atmospheric transport inverse modeling relies on atmospheric dispersion modeling. Its statistical inversion has been used to determine the localization and quantification of emissions from facility-scale and site-level (Mønster et al., 2019; Kumar et al., 2022).

In order to evaluate and support the development of different atmospheric measurements and modeling approaches to improve the accuracy and reliability of monitoring anthropogenic emissions at the facility- and site-level scales, controlled release experiments with known emitting locations and emission rates have been conducted in several studies (Feitz et al., 2018; Ravikumar et al., 2019; Bell et al., 2020; Sherwin et al., 2021). In particular, with the development of various atmospheric measurement technologies, promising measurement systems are emerging to detect and quantify anthropogenic methane emissions in the natural gas supply chain ranging from facility to site scale. Recent studies involved these systems in conducting blind controlled releases to assess the accuracy and compare their performances under different emission protocols and meteorological conditions (Albertson et al., 2016; Edie et al., 2020; Morales et al., 2022). Bell et al. (2020) assessed twelve CH_4 emission measurement technologies. They found that localization by handheld and mobile technologies is more accurate than continuous monitoring systems. However, Kumar et al. (2022) showed a 20%-30% precision for the estimate of controlled CH_4 release rates when relying on either mobile or fixed station networks. They also found that the localization of the releases was better when relying on fixed stations. Sherwin et al. (2021) have shown that an airplane-based hyperspectral imaging CH_4 emission detection system can detect and quantify over 50% of total emissions from super-emitting sources.

Moreover, the airborne CH_4 measurement technology reported in Johnson et al. (2021) can detect, locate and quantify individual sources at or below the magnitudes of recently regulated venting limits with ± 31%-68% quantification uncertainties. These different studies raise contrasting or similar conclusions depending on the specific experimental set-up or the specific mobile of fixed platforms, sensors, sampling strategies, and models used. In fine, new inter-comparisons based on controlled releases and involving a wide range of technologies are needed to be performed regularly.

1.4.4 Reconciling top-down and bottom-up approaches

As mentioned in Section 1.4, the bottom-up inventory approach relies on statistical activity data and data-driven emission factors to estimate emissions, or uses process-based modeling, while top-down approaches derive emission rates from atmospheric measurements assimilated in atmospheric transport models forced by a prior knowledge of emissions. However, according to the literature, large discrepancies can be found between top-down and bottom-up estimates at all scales. For example, airborne-based CH_4 calculated emissions in the San Francisco Bay Area were about twice as large as the respective values given on regional scale inventories (Guha et al., 2020). At the global scale total bottom-up methane emissions are 25% larger than the top-down budget (Saunois et al., 2020). Kondo et al. (2015) found large differences about 23 Pg C yr^{-1} in the mean global CO_2 budgets from June 2009 to October 2011, estimated by top-down and bottom-up approaches.

Therefore, it is important to better coordinate and reconcile top-down and bottom-up approaches to obtain a more accurate estimate to design and follow robust mitigation strategies. Some efforts have been made to compare top-down and bottom-up estimates at urban and regional scales, or for sector-specific emissions (Miller and Michalak, 2017; Wolf et al., 2017; Vaughn et al., 2018; Neininger et al., 2021). Some studies pointed out that bottom-up inventories underestimate methane emissions from natural gas production in the US (Lyon et al., 2015; Zavala-Araiza et al., 2015; Rutherford et al., 2021; Morales et al., 2022). This discrepany could be attributed to assumptions of past years' activity while activity increases, lack of accounting for all sources in emission inventories, lack of accounting for specific, time-limited venting operations, challenging spatial or temporal aggregation of activities, or missing specific super-emitters. Some studies focused on the comparison of methane emissions inventories with top-down measurements from waste and agriculture sectors (e.g. landfills, wastewater treatments and livestock). It is still challenging to reconcile these estimates due to separating interspersed sources and rarely verified estimates (Guha et al., 2020; Scheutz et al., 2022; Wolf et al., 2017; Desjardins et al., 2018). More efforts are needed to combine currently existing top-down datasets and expand intensive atmospheric measurement campaigns, improve activity data and revise emission factors those drive emission inventories. These would obtain more accurate spatial and temporal gridded inventory esti-

mates, along with more extensive observations to estimate and revise current emission factors for specific source sectors to achieve reconciliation between top-down and bottom-up approaches. An important point to do so, with a top-down perspective, is to rely on an ensemble of atmospheric observations, each one being able to cover one or more scales (spatial and temporal).

1.5 ATMOSPHERIC MEASUREMENTS AND PLATFORMS

1.5.1 Ground-based observation stations

Systematic atmospheric CO_2 measurements started in 1958 in Mauna Loa in Hawaii (Pales and Keeling, 1965). Blake et al. (1982) started systematic atmospheric CH_4 measurements in 1978 with discrete air samples collected in the Pacific at latitudes from 67° N to 53° S. From then on, the spatial and temporal coverage of atmospheric CO_2 and CH_4 measurements were improved by regional observation networks using in situ measurements and discrete flask measurements, which are set up by a variety of academic institutes around the world such as NOAA/ESRL (the Earth System Research Laboratory from the US National Oceanic and Atmospheric Administration) and ICOS (Integrated Carbon Observation System) under the coordination of WMO/GAW (the World Meteorological Organization Global Atmosphere Watch Programme) (Steele et al., 1987; INGOS, 2018; WMO, 2019). Figure 1.4 presents GAW global CO_2 measurement network. The CH_4 network is similar. These ground-based stations and stationary observations like instrumented masts and towers can deliver continuous, highly precise and accurate, and for some networks near real-time data streams over long periods of time. These ground-based datasets provide the longest time series of globally averaged atmospheric CO_2 and CH_4 measurements. Flask sampling programmes, progreesively replaced by robust in situ laser spectrometers such as the one developed by Picarro (USA) based on Cavity ring-down spectroscopy (CRDS), have been used for long-term atmospheric CO_2 and CH_4 measurements within worldwide observation networks (Crosson, 2008). However, they only provide single-point location measurements at the Earth's surface, and their footprints are limited and determined largely by the height of the structure (Berman et al., 2012a; Kunz et al., 2018).

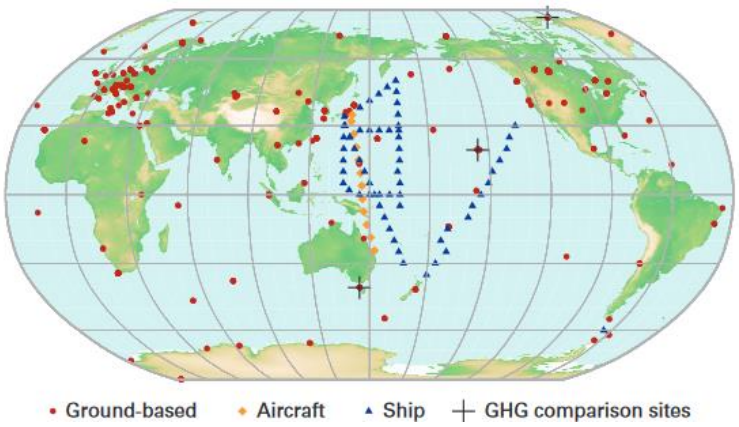

Figure 1.4 The GAW global CO_2 measurement network (WMO, 2018), for ground-based measurements (red), aircraft measurements (orange), shipborne measurements (blue).

1.5.2 Remote sensing

Since the 2000s, atmospheric CO_2 and CH_4 measurements were complemented by remote sensing from space and from the surface, providing column-averaged mole fractions (Wunch et al., 2017). Measurements of total CO_2 and CH_4 columns by solar backscatter start with SCIAMACHY instrument for 2003-2012 (Frankenberg et al., 2006) and continue to the present with the Greenhouse Gases Observing Satellite (GOSAT), the Orbiting Carbon Observatory-2 (OCO-2), the TROPOspheric Monitoring Instrument (TROPOMI), the Carbon Dioxide Observation Satellite (TanSat) and the Greenhouse Gas Satellite (GHGSat), and more satellites targeting GHGs are planned in doing so. GOSAT has higher precision and pixel resolution but its observations are not that dense (Kuze et al., 2016). In 2014, OCO-2 was launched successfully and the main product is the column-averaged dry air CO_2 mole fraction (X_{CO2}) with high precision, which improves our understanding of the global carbon cycle (Wunch et al., 2017) although systematic errors still limit the potential of such data to consistently infer regional emission. Chevallier et al. (2019) have tested and proved that the quality of some OCO-2 retrievals over land is high enough to provide comparable results in credibility to the reference surface air sample network. The TROPOMI instrument launched in 2017 expands the capability to observe CH_4 from space by providing complete daily global coverage at the cost of lower precision and accuracy than surface observations. In addition, its high resolution with the high signal-to-

noise ratio provides CH_4 emissions from localized to larger scale sources (Lorente et al., 2021). Moreover, the IASI (Infrared Atmospheric Sounding Interferometer) launched on the European MetOp-A platform since 2007 has yielded a complete view of methane sensitivities (e.g. geographical distributions, seasonality and long-term tendency) in the mid-troposphere (Crevoisier et al., 2013), and the second-generation has been launched to provide continuous monitoring on a fine spatiotemporal scale (De Wachter et al., 2017). GOSAT-2 launched in 2018 provides seamless global CO_2 and CH_4 observations and observes local emissions and uptake with an additional CO channel (Suto et al., 2021). Satellite data from sun-synchronous orbits have almost global coverage and multi-species detection advantages. In contrast, it still experiences critical limitations, including accuracy issues, difficulties to observe high latitudes (when sunlight is requested), or difficulties to resolve properly the boundary layer (Gålfalk et al., 2016; Khan et al., 2012). Moreover, Ground-based Fourier transform infrared (FTIR) measurements, for example the Total Carbon Column Observing Network (TCCON) established in 2004 and the Collaborative Carbon Column Observing Network (COCCON) based on EM27/SUN FTIR spectrometers, can also provide GHG column observations as an essential validation resource for the satellite measurements (Houweling et al., 2014; Alberti et al., 2022). What's more, The AirCore, as a balloon-borne atmospheric sampling system, has the capability to provide full-column measurements of CO_2 and CH_4 (Karion et al., 2010). The profiles obtained from Aircore can be used to assess and compare with FTIR measurements within TCCON (Zhou et al., 2019).

1.5.3 Mobile measurements

In order to improve the quantification of CO_2 and CH_4 emissions, atmospheric measurements through various mobile platforms (e.g. vehicles, ships, aircraft and unmanned aerial vehicles) can provide additional constraints on sources and sinks by bringing the gaps between fixed ground-based stations and remote satellite columns retrievals (Liu et al., 2018; Defratyka et al., 2021a; Schuster et al., 2009; Paris et al., 2021). Car-based mobile measurements have the capability to provide short-term and intensive measurements close to individual sources, documenting individual sources. It is an efficient way to identify and quantify local emissions in urban areas (Weller et al., 2018; Lowry et al., 2020; Maazallahi et al., 2020). These measurements have covered a variety of cities in Europe and US (Lan

et al., 2015; Weller et al., 2020; Maazallahi et al., 2020) to characterize methane emissions and they reveal that the pre-dominant source is natural gas distribution network in megacities (e.g. Paris and Hamburg). Shipborne measurements expand the geographic coverage of atmospheric CO_2 and CH_4 measurements (e.g. in the Arctic and the Mediterranean and Middle East areas) and improve our understanding of atmospheric CO_2 and CH_4 distributions (Bukosa et al., 2019; Berchet et al., 2020). Additionally, shipborne measurements provide a way to evaluate satellite measurements over the oceans using EM27/SUN Fourier transform spectrometer (FTS) on board (Klappenbach et al., 2015; Knapp et al., 2021). Moreover, Helfter et al. (2019) estimated the seasonal and annual emission budget of CO_2 and CH_4 at a national scale using shipborne measurements and a mass balance approach, which provided independent verification for emission budgets.

Additionally, atmospheric measurements based on aircraft and unmanned aerial vehicles (UAVs) platforms have appeared since 2000 (around 2005 for UAVs), and they provide additional constraints through 3-D observations directly reflecting nearby sources and sinks, with a more complete view of emitted plumes than car measurements. They help reduce uncertainties on emission factors of individual source types by using high-frequency and high-precision instruments onboard (Jr et al., 2002; Paris et al., 2009; Frish et al., 2013; Filges et al., 2015; Thorpe et al., 2016; Krautwurst et al., 2017; Barker et al., 2020). For example, Barket et al. (2020) provided new datasets of African biomass burning emission factors and modified combustion efficiencies by aircraft measurements. Airborne measurements can quantify emissions of specific sources and areas to provide an independent assessment of bottom-up inventories (Karion et al., 2015; Johnson et al., 2017; Palmer et al., 2018; Ren et al., 2018; Guha et al., 2020) which is critical to make effective mitigation policy and action. Guha et al. (2020) implemented an airborne mass-balance system to quantify methane emission rates of different sources (including landfills, wastewater treatment plants and refineries) in the San Francisco Bay Area to assess regional emission inventories. However, flying aircraft is costly, complex to organize and requires frequent maintenance. Moreover, it is difficult for aircraft to properly cover the region due to the limitations on the minimum flight altitude and their high speed (Bara Emran et al., 2017; Kunz et al., 2018).

Compared with aircraft, UAVs experience fewer limitations and have

other advantages. First, it is a cost-effective solution for routine observations to complement global networks. It has the capability to characterize specific source emissions close to the ground and from unreachable areas. Moreover, it can operate at lower altitudes and slower speeds to provide high temporal and spatial resolution data, creating less interference with the local airflow (Barchyn et al., 2017). In addition, UAVs improve the documentation of CO_2 and CH_4 spatial distributions around fixed points. However, UAVs' measurements require instruments that can sustain rapid changes in pressure and temperature. The payload and volume are also limited on UAVs. In the past decade, research has been underway to develop and implement compact, lightweight, low-powered systems with high accuracy for UAV applications. A caveat so far is also the limited flight time due to battery capacity and weight. Table 1.1 presents historical studies of atmospheric GHG measurements on UAVs in the past decade. In summary, the payload is reducing over time, and UAV measurements have been widely applied for different purposes, such as quantifying anthropogenic emissions close to the ground (e.g. power plants, landfills and pastures). Additionally, high-precision and commercial analyzers of CO_2 and CH_4 for UAV applications are emerging currently such as the ABB light Micro-portable Greenhouse Gas Analyzer (pMGGA) (Shah et al., 2020).

Table 1.1 A summary of UAV-based measurement of atmospheric CO_2 and CH_4 in the past decade.

Analyzers	Species	Payload	UAVs	Significance	Studies
A single-cell nondispersive infrared (NDIR) analyzer (LI-800, LI-COR)	CO_2	3.5kg	Sky Remote	Quantify the temporal and vertical variations of CO_2	Watai et al.(2006)
Near infrared off-Axis Integrated Cavity Output Spectroscopy (Off-Axis ICOS)	CO_2, CH_4	19.5kg	NASA SIERRA	Develop a system for UAV measurements	Berman et al. (2012)
Vertical cavity surface emitting laser (VCSEL) sensor	CO_2, CH_4	2kg	TREX Align 700E	Improve emissions estimates of GHGs	Khan et al.(2012)

Near-infrared standoff tunable diode laser absorption spectroscopy (sTDLAS)	CH_4	1.4kg	A small quadrotor	Measure pipeline leaks	Frish et al.(2013)
Custom laser based open-path sensor	CH_4	3.1kg	Fixed-wing UAV	Quantify the methane leak rate	Nathan et al.(2015)
Metal oxide resistive sensor (MOX); off-the-shelf NDIR sensor	CO_2, CH_4	3285g	The Green Falcon UAV	Validate gas sensing application on UAVs	Malaver et al.(2015)
Laser Methane mini-G (SA3C50A)	CH_4	530g	EVO Arm F800-R hexacopter	Map CH_4	Emran et al.(2017)
SenseAir AB HPP sensors	CO_2	1.2kg	Fixed-wing UAV	Develop a compact UAV system with high precision	Kunz et al.(2018)
Off-axis integrated cavity output spectroscopy	CO_2	1.0kg	Fixed-wing UAV	GHGs hotspot flux calculation	Allen et al.(2019)
A NDIR CO_2 sensor (the Vaisala GMP343)	CO_2	1.2kg	DJI Matrice 210v2	Derive anthropogenic point source emissions	Reuter et al.(2021)
Active AirCore	CO_2, CH_4	1.1kg	Quadrotor	Quantify CH_4 emissions from dairy cows	Vinkovic et al.(2022)

1.6 THESIS OUTLINE

The main goal of my Ph.D. study is to improve the characterization of CH_4 and CO_2 emissions from the local to national scale through the development of mobile platforms. To achieve this goal, the main approach is the design, realization and analysis of field campaigns, taking benefit of various mobile measurement systems. One additional goal is to reconcile top-down and bottom-up estimates of methane emissions up to the national scale of Cyprus, a Country-Island of the European Union. I benefited from a collaboration between LSCE and the Cyprus Institute to implement my objectives for the Country-Island of Cyprus as the main terrain for my experiments.

Cyprus is located in the Eastern Mediterranean and Middle East (EMME) region, which has been considered a climate change hotspot based on

observation-based and modeling studies (Giorgi, 2006; Lelieveld et al., 2012a; Zittis et al., 2016, 2022). Zittis et al. (2022) found that anthropogenic greenhouse gas emissions in the EMME region have increased by six-fold during the past six decades according to the bottom-up country-reported emission datasets. Figure 1.5 shows historical emissions of CO_2 and CH_4 across selected countries and regions (Zittis et al., 2022). It shows that annual CO_2 emissions of the EMME are now similar to those of the EU27 and annual CH_4 emissions of the EMME are now larger than those of most selected countries and regions (Fig.1.5). In short, the EMME region is becoming a significant global greenhouse gas emitter mainly for CO_2 and CH_4. For the countries in the EMME region, the energy and transportation sectors dominate anthropogenic CO_2 emissions. Besides the energy sector, methane emissions emanate are from various sources, including major contributions from the agricultural and waste sectors. To achieve efficient mitigation plannings, only using information from inventories is not enough. Therefore, mobile measurements are implemented for this region as a part of this Ph.D., focusing on methane emissions from agricultural and waste sectors, to improve our understanding to support the reduction of CH_4 emissions. In **Chapter 2**, I report on the 24 mobile surveys that were conducted in one year at representative methane emission areas in Cyprus (e.g. landfills and cattle farms). Emission rates of these measured objectives were determined using the Gaussian plume model on the Polyphemus platform (Mallet et al., 2007) based on multiple downwind plume transects obtained during each mobile survey. Furthermore, the comparison with bottom-up inventories and the reconciliation of top-down and bottom-up estimates are discussed in this chapter. In addition to vehicle-based mobile measurements, airborne measurements based on an off-axis Integrated Cavity Output Spectroscopy (OA-ICOS) were also applied for Cyprus, as shown in Appendix A.

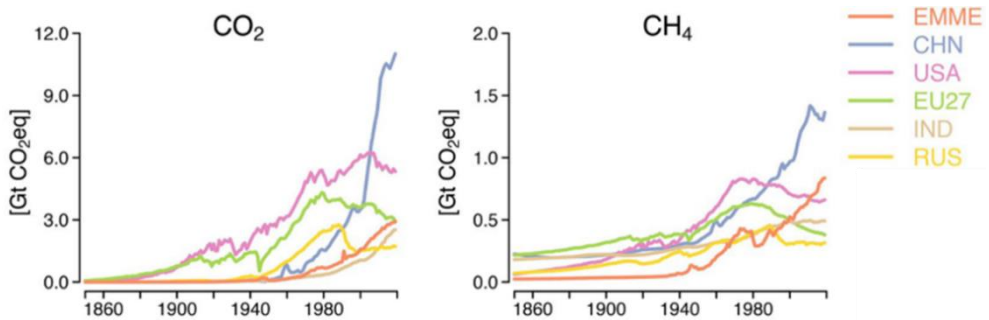

Figure 1.5 Historical emissions of CO_2 and CH_4 across selected countries and regions (EMME = Eastern Mediterranean and Middle East; CHN = China; USA = United States of America; EU27 = European Union; IND = India; RUS = Russia) (figure from Zittis et al. 2022).

In the past decade, high precision and lightweight instruments or sensors based on different platforms (e.g. drones, aircraft and trucks) are developed rapidly for atmospheric greenhouse gas measurements, which has already been discussed in Section 1.5. In order to assess their performance and support future development, **Chapter 3** describes an inter-comparison of ten start-of-the-art methane quantification systems through a series of blind controlled release experiments at an inert compressor station is presented in this thesis. According to recent studies, methane emissions in leaks, venting, and other parts associated with natural gas supply chains erode the climatic advantage of natural gas as transition energy ((Balcombe et al., 2017; Zimmerle et al., 2020a; Cooper et al., 2021). Improving CH_4 emission reporting across the natural gas value chain is thus critical to understanding the climate implications of a large-scale transition to natural gas. Controlled release experiments and inter-comparison studies have already been used in this field (e.g. Ravikumar et al., 2019; Bell et al., 2020; Sherwin et al., 2021; Kumar et al., 2022). These various studies raise contrasting or similar conclusions depending on the specific experimental set-up or the specific mobile and fixed platforms, sensors, sampling strategies and models they use. With the regular improvement of instruments and techniques, new inter-comparisons based on controlled releases involving various techniques are needed. Therefore, the study of this part (Chapter 3) aims to evaluate these quantification systems at source and site scales (including mobile, ground-based, and handheld measurement platforms) by analyzing their respective strength, weaknesses and potential complementarity depending on the emission and atmospheric conditions, to provide an update on the current capabilities to make efficient mitigation actions and policies.

Chapter 4 describes a mid-precision CO_2 UAV system intended to perform measurements close to large sources. As shown in Chapter 3, each measurement system has its own strengths and weaknesses. The existing measurement methods and systems could cover all the relevant spatial scales for emissions thanks to the development of unmanned aerial vehicles (UAV), which help fill the gap between the vehicle and airborne measurements. An appropriate sensor for UAV platforms would have the potential to provide independent measurements across source plumes to verify miti-

gation strategies since a large part of anthropogenic greenhouse gas originates from point emission sources (Pinty et al., 2017). Another potential application is to document the spatial distribution around fixed observations, since UAV measurements help separate signal variability into a large-scale footprint of ground stations and variability due to local influences. Although UAVs have some advantages, measurements on UAVs require instruments that can sustain rapid changes in pressure and temperature. The payload and volume are also limited on UAVs, referring to Section 1.5.3. However, until now, very few calibrated CO_2 measurements have been reported in the literature (Kunz et al., 2018; Reuter et al., 2021). These works have faced the difficulty of miniaturizing high-precision, fast-response CO_2 sensors. Very high-precision and commercial sensors for UAV applications are emerging currently, such as the ABB light micro-portable greenhouse gas analyzer (pMGGA) (Shah et al., 2020). However, the weight (about 3 kg) is still large for small UAVs, and the price is high. As a part of this Ph.D. study, a compact and lightweight UAV-CO_2 sensor system is developed and validated. It has been applied to monitor and map atmospheric CO_2 in urban area (Nicosia, Cyprus). The system is based on a low-cost commercial nondispersive near-infrared (NDIR) sensor (Senseair AB, Sweden). A series of laboratory tests have been conducted to ensure the accuracy, linearity and performance of the instrument before integration, after which intensive flights of the developed system were presented (Chapter 4).

Finally, **Chapter 5** summarizes my findings and perspectives of this study and provides an outlook of possible future research directions.

2 ON THE VERIFICATION OF NATIONAL METHANE EMISSIONS IN CYPRUS

2.1 OVERVIEW

The Eastern Mediterranean and the Middle East (EMME) region is highly sensitive to climate change. It has been identified as a global climate change hot-spot with adverse impacts such as extreme weather events (Giorgi, 2006; Lelieveld et al., 2012). The hot conditions that (strong warming of 3.5 ˚C-7 ˚C) rarely happened in the reference period (1961-1990) may be normal by the middle and the end of this century (Lelieveld et al., 2014; Zittis et al., 2016). With the intense population growth and strong industrialization, anthropogenic emissions in EMME have increased rapidly in recent decades (Lelieveld et al., 2002; Georgiou et al., 2018). The increasing CO_2 emissions are mainly driven by fossil fuel combustion in EMME (Zittis et al. 2022). The increasing CH_4 emissions from the energy sector after 2007 are mainly from Africa-Middle East (McNorton et al., 2018).

Cyprus is geographically placed at the center of EMME, an island country with 9251 km^2. There are mainly four cities, namely Nicosia, Limassol, Larnaca and Paphos, gathering about 70% of the total population (about 1.2 million) as shown in Fig.2.1 (Vrekoussis et al., 2022). Cyprus represents a valuable GHG observatory of regional and local anthropogenic emissions that can supplement our current knowledge on GHG distribution in the EMME. The latter is needed to design and apply efficient mitigation actions and policies. The presented research outcome focuses on the south of Cyprus. Although monitoring stations already exist in Cyprus for aerosols and gaseous pollutants like SO_2 and NO_x, atmospheric GHG surface measurements are still missing in this area so far. Cyprus is joining the Integrated Carbon Observation System (ICOS) Atmosphere network to set up its first GHG monitoring station, complementing the lack of ICOS atmosphere stations in EMME.

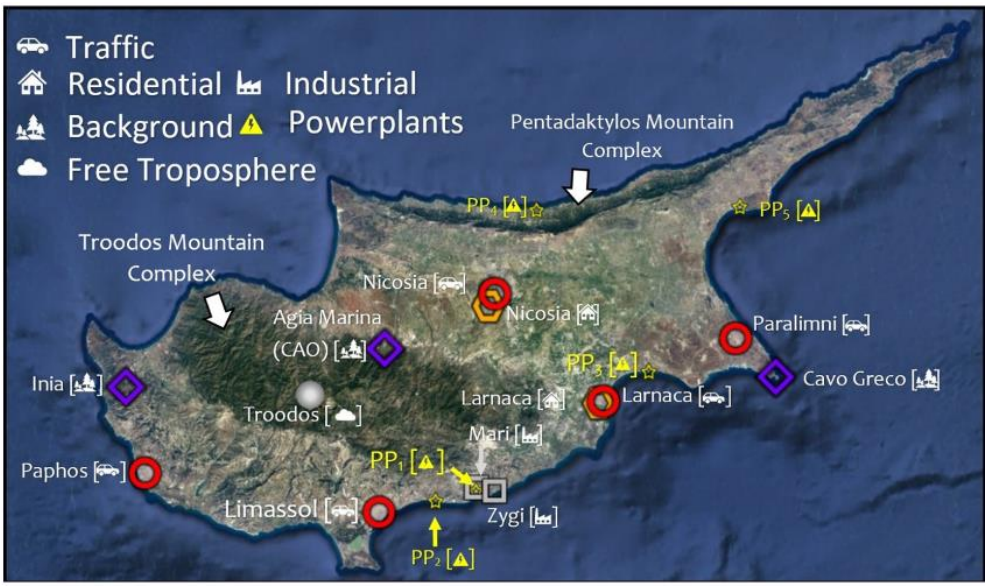

Figure 2.1 From Vrekoussis et al., 2022: spatial distribution of urban-traffic (red circles), residential (orange hexagons), industrial (grey squares), background (blue rhombus) and free-troposphere (white sphere) monitoring stations in Cyprus. The yellow star symbols indicated with PPx (X=1 to 5) labels show the location of the five power plants on the island. The two white arrows depict the two major mountain complexes in Cyprus, namely Troodos and Pentadaktylos.

This chapter focuses on the atmospheric methane measurements performed in Cyprus through vehicle-based mobile measurements. It is the first systematical investigation of atmospheric methane in Cyprus. This study aims at bridging the gap between top-down and bottom-up approaches and improving our understanding of CH_4 emissions on the national scale. Section 2.2, organized as a paper to be submitted, depicts car-based mobile measurements of CH_4 from October 2020 to September 2021 (24 survey days) in Cyprus. The surveyed areas include an active landfill (Koshi), a closed landfill (Kotsiatis) and a concentrated cattle farm area (Aradippou). Methane emission rates from these sources were estimated using a Gaussian plume model (Mallet et al., 2007). It is found that calculated methane emissions from solid waste disposals and livestock are about 160% and 40% larger, respectively, than the national bottom-up estimated inventory. A typical 21% uncertainty coupled for mobile measurements attributes to the meteorological parametrization of the Gaussian plume model. The result highlights that closed landfills may be a significant, underestimated CH_4

emission source. The survey method used in this study is suitable for many developing countries which have limited resources to develop atmospheric networks or sophisticated inventories. Besides vehicle-based mobile measurements, airborne investigations were also applied for Cyprus, as shown in Appendix A.

2.2 PAPER TO BE SUBMITTED: ON THE VERIFICATION OF NATIONAL METHANE EMISSIONS IN CYPRUS

On the verification of national methane emissions in Cyprus

Yunsong Liu (1) (2), Jean-Daniel Paris (1) (2), Mihalis Vrekoussis (2) (3), Pierre-Yves Quéhé (2), Maximilien Desservettaz (2), Jonilda Kushta (2), Florence Dubart (2), Demetris Demetriou (2), Philippe Bousquet (1), Jean Sciare (2)

(1) Laboratoire des Sciences du Climat et de l'Environnement, 91191 Gif sur Yvette, France

(2) The Cyprus Institute, Climate and Atmosphere Research Center (CARE-C), Nicosia, Cyprus

(3) University of Bremen, Institute of Environmental Physics and Remote Sensing (IUP) & Center of Marine Environmental Sciences (MARUM), D-28359 Bremen, Germany

Abstract

Reconciling top-down and bottom-up country-level emission estimates remains a key challenge in the MRV (Monitoring, Reporting, Verification) paradigm. Here we propose a first attempt to independently quantify cumulative emissions from a significant number of methane (CH_4) emitters in Cyprus and derive robust constraints for the national inventory. We performed 24 survey days of mobile measurements of CH_4 from October 2020 to September 2021 at emission 'hotspots' in Cyprus. Methane emissions in Cyprus emanate primarily from waste and agricultural activities. The surveyed areas include a large active landfill (Koshi), a large closed landfill (Kotsiatis), and a concentrated cattle farm area (Aradippou), accounting together for about 28% of national CH_4 emissions. Emission rates for each site were estimated using repeated downwind transects and a

Gaussian plume dispersion model. The calculated methane emissions from landfills of Koshi and Kotsiatis (25.9±6.4 Gg yr^{-1}) and enteric fermentation of cattle (10.4±4.4 Gg yr^{-1}) were about 160% and 40% larger, respectively than the bottom-up sectorial estimates used in the national UNFCCC inventory. The parameterization of the Gaussian plume model dominates the uncertainty in our method, with a typical 21% uncertainty. Seasonal variations have little influence on the results. We show that using an ensemble of in situ measurements targeting representative methane emission hotspots with consistent temporal and spatial coverage can vastly improve national bottom-up emission inventories.

Section 1: Introduction

Methane (CH_4) is a potent greenhouse gas with a nine-year atmospheric lifetime and 28 times the global warming potential of CO_2 on a 100-year horizon (IPCC, 2018). The globally averaged surface mole fraction of CH_4 has already increased 2.6 times above pre-industrial levels, from 722 ppb to 1896 ppb (WMO, 2021). The annual growth rate reached 17 ppb in 2021, the largest rate since the start of direct measurements in 1983. Methane's short lifetime compared to CO_2 and its strong radiative forcing make it a key target in the climate change mitigation action portfolio (Nisbet et al., 2020). However, CH_4 emissions and sinks are still poorly constrained at all scales due to the variety, heterogeneity and variability of anthropogenic and natural sources and sinks, with emissions often overlapping geographically (Saunois et al., 2020).

Anthropogenic CH_4 inventories derive emissions based on activity data and emission factors. Other bottom-up approaches for biogenic fluxes may rely on numerical simulations of emission processes at all relevant scales, typically for biogenic processes such as wetland models (Wania et al., 2013). Atmospheric measurements, either from space or in-situ from long term networks and mobile platforms (e.g., vehicles, ships and aircraft) can provide valuable insight on bottom-up emissions from local to global scales (Brantley et al., 2014; Defratyka et al., 2021; Lan et al., 2015; Turner et al., 2016; Johnson et al., 2017; Paris et al., 2021). At large scales, inverse modeling uses atmospheric measurements to correct CH_4 emissions inventories. These top-down methods have been applied to optimize global, continental or national-scale emission estimates (Bergamaschi et al., 2015; Lu et al., 2022). Recent top-down inversion studies using TROPOMI data

suggested that CH_4 bottom-up emissions were underestimated by 21% in China (Chen et al., 2022), a result contrasting the synthesis of Saunois et al. (2020). Additionally, anthropogenic CH_4 emissions estimated using inverse modeling in Europe, the United States, Canada and Mexico are higher by about 20%-40%, 40%, 30% and 20%, respectively, compared to bottom-up national emission inventories (Cheewaphongphan et al., 2019; Bergamaschi et al., 2015; Peng et al., 2016; Lu et al., 2022).

It has been debated whether atmospheric-based approaches at local scales could be more relevant to inform the reported national inventories (Leip et al., 2017). However, large discrepancies do exist between top-down and bottom-up estimates at local/regional scales (Hsu et al., 2010; Lamb et al., 2016; Ren et al., 2018; Lu et al., 2022; Vechi et al., 2022). For example, airborne-based CH_4 calculated emissions in the San Francisco Bay Area were approximately twice as large as the respective values given on regional scale inventories (Guha et al., 2020). Foulds et al. (2022) found that methane emissions estimates from offshore oil and gas facilities were 42% larger than the inventory for the area. Similarly, Vechi et al. (2022) found that bottom-up inventories underestimate CH_4 emissions by about 30%.

Reconciling top-down and bottom-up approaches at the national level is required to establish a reliable estimate of global methane emissions and to monitor the impact of mitigation strategies on emissions. National total inventories are more robust than spatialized inventories because emissions are not arbitrarily distributed along proxy parameters. However, comparing national emission inventories with atmospheric measurements is still hindered by several factors. First, atmospheric dynamics have to be characterized and simulated properly as the atmosphere is an integrator of any combination of emitters along air mass trajectory and a dispersion mechanism for individual sources. Second, the activity sectors identified in national inventories are not necessarily spatially separated on the ground and disentangling their contributions in individual measurements may be challenging. Finally, both top-down and bottom-up methods are associated with significant methodological uncertainties and there is no single ground truth. Therefore, discrepancies are difficult to interpret because approaches cannot be easily reproduced with complete, independent, temporally and spatially consistent data (Schwietzke et al., 2017).

Methane inventories in “small” countries and emerging hotspots of

climate change, such as the Eastern Mediterranean and the Middle East (EMME) region, are still poorly developed (Giorgi et al., 2006). It remains challenging to characterize, validate and quantify spatial distributions and emission magnitudes in these regions. Such countries may present a relatively small number of large emitters and their national inventories cannot be easily compared to global or regional inversions. We therefore investigate a representative EMME country to assess whether independent, mobile, repeatable atmospheric measurements can be robustly used in the verification of reported national inventories.

We performed mobile CH_4 measurements (24 survey days within one full year) in Cyprus, an island country of 9251 km2 in the eastern Mediterranean Sea with a population of 1.2 million. Cyprus provides a very relevant framework to work on the bottom-up versus top-down discrepancies: it is located in an emerging hotspot of GHG emissions (EMME region), it has only two main sectors emitting methane (agriculture and waste), and its reasonable surface area makes it possible to monitor a larger part of national emissions with mobile platforms. According to the United Nations Framework Convention on Climate Change (UNFCCC) 2021, in Cyprus, 57% of CH_4 is emitted from waste and 41% from agricultural activities. The representative local CH_4 emission hotspots Koshi (active landfill), Kotsiatis (closed landfill) and Aradippou area (cattle farms), accounting for about 28% of CH_4 national emissions (UNFCCC, 2021), were selected to validate the national bottom-up inventory. We quantified the emission rates of these hotspots using a Gaussian plume model (Mallet et al., 2007). This comprehensive study aims at bridging the gap between top-down and bottom-up approaches and improving our understanding of CH_4 emissions on the national scale for Cyprus. After presenting this work's methodology (Section 2), we detail and discuss the results obtained (Section 3).

Section 2: Materials and methods

Mobile system

We conducted 24 mobile surveys (24 days) between October 2020 and September 2021. A cavity ring-down spectrometer (CRDS) model G2401 manufactured by Picarro Inc. (USA) was employed to measure CH_4 with 1 Hz time resolution (Crosson et al., 2008). The analyzer was calibrated every month using the WMO X2004 scale (Yver Kwok et al., 2015). All the data

reported in this study were quality controlled with the Integrated Carbon Observation System-Atmosphere Thematic Center (ICOS-ATC) (Hazan et al., 2016). The precision in measured CH_4 is below one ppb. The instrument was installed into a vehicle equipped with a GPS device (NEO-M8N-0-10 U-Blox) and a sonic anemometer (150WX RS232 WeatherStation Instrument) on the roof. In addition, the air inlet was added to the roof of the car, close to the anemometer (about 190 cm above the ground), as shown in Fig.2.2 A real-time charging system was setup in the vehicle, allowing the battery to get charged while driving. The latter allowed for prolonged observations. All the data recorded were accessible and used for decision-making during each mobile measurement survey. Data logs accounted for the time delay of air traveling from the inlet to the analyzer for each survey day.

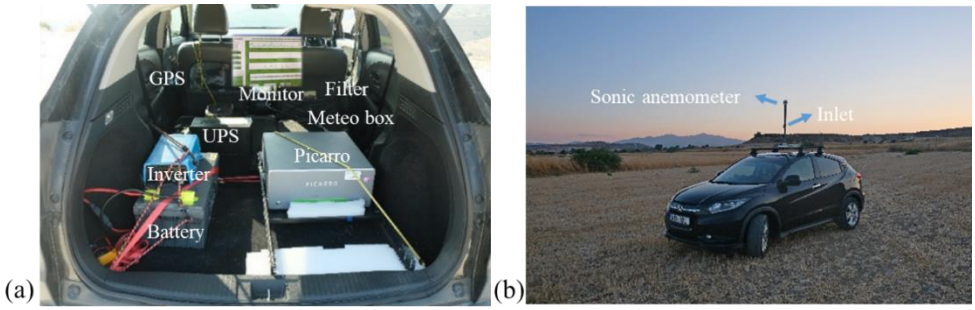

Figure 2.2 Components of the mobile measurement system, (a) shows the setup inside the car and (b) presents the outward of the car.

Survey area

We conducted mobile GHG measurements throughout Cyprus. Most people live in the following four cities Nicosia, Larnaca, Limassol, and Paphos. The national methane inventory indicate that agriculture (mostly ruminants) and waste management (mostly solid waste) are the highest emitting sectors. Energy only represents 2% of methane emissions. The active landfill Koshi was selected as a major CH_4 emission hotspot. Kotsiatis, the largest closed landfill still emitting CH_4, was selected as another major survey hotspot. Aradippou, with relatively concentrated cattle farms and about 5.2% of the total cattle population (82904 cows in total), was selected as the last survey area. In summary, surveyed areas should account for about 28% of the total CH_4 emissions in Cyprus, as shown in Fig.2.3.

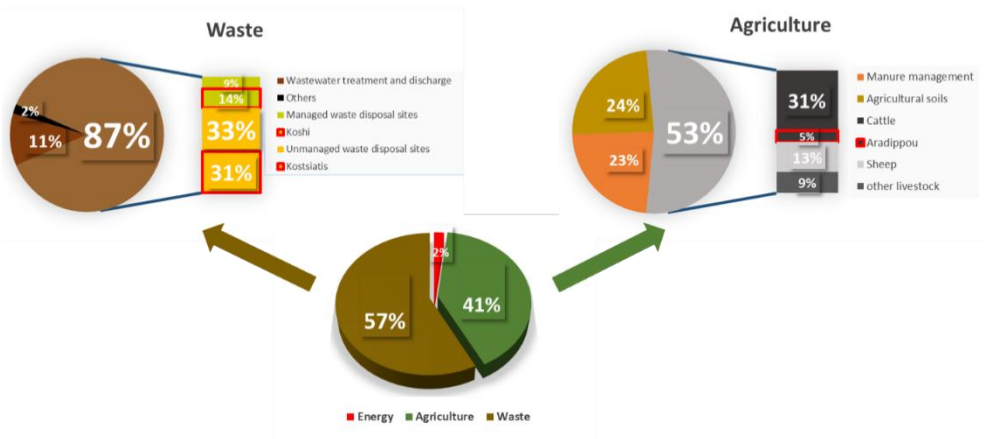

Figure 2.3 The source categories of methane emissions in Cyprus (UNFCCC, 2021).

Measurement protocol and data collection

Every month, two consecutive days of mobile survey were carried out around midday, when the air was well mixed in the planetary boundary layer. This allowed us to collect data in all seasons and under different wind conditions for each emitter. Each fieldwork day surveyed the three selected sites. Whenever CH_4 emission plumes were visible on the monitoring screen, 3-5 repeated transects, used to investigate gradual changes in CH_4 concentrations, were followed at a driving speed of 20-30 km h^{-1}, if the traffic condition permitted. This speed range has been identified optimal during Gaussian plume peak shape characterization (Lowry et al., 2020). Generally, the duration of each survey was 6-7 h.

The second percentile of measured methane mole fractions in each survey was selected as the daily background for emission rate calculations of all transects. Figure 2.4 shows the geographical locations of these three hotspots and an example of a one-day survey path at each site (about 15 km between sites).

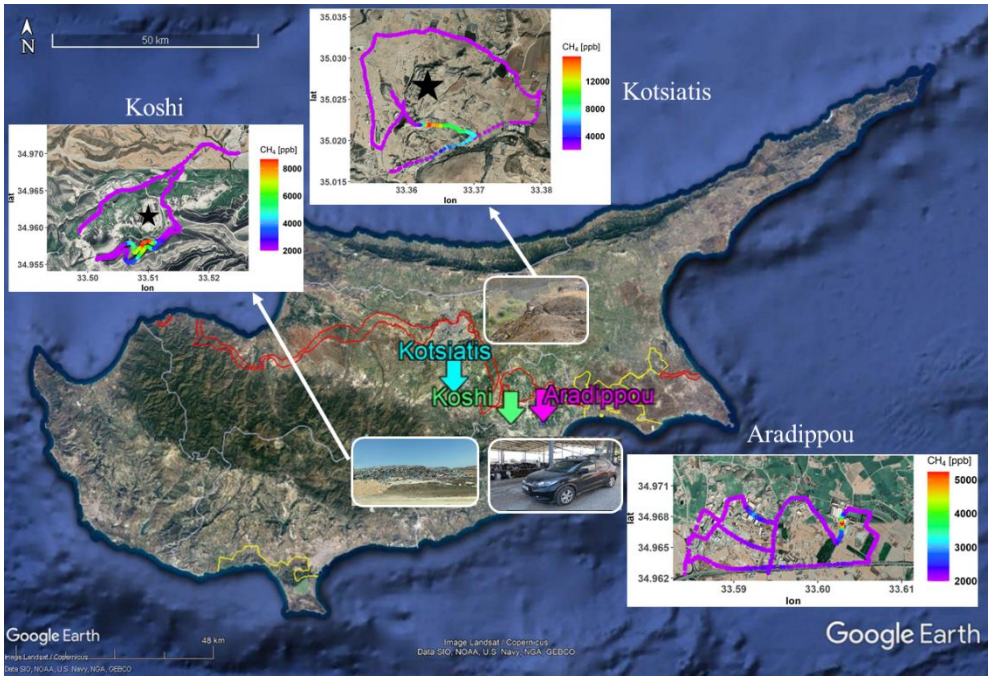

Figure 2.4 Locations and pictures of surveyed areas (Koshi, Kotsiatis and Aradippou) and an example of one-day survey paths at each site. Base map © Google Earth 2022.

Emission rate estimates from in-situ measurements

The emission rates were estimated using the Gaussian plume model by comparing the model output to the observations for each measured transect. We obtained 65, 81 and 108 transects for Koshi, Kotsiatis and Aradippou, respectively. However, in some cases, the model cannot reasonably reproduce the observations and obtain similar plume structure due to excessive atmospheric variability (e.g. wind direction and wind speed), long source-receptor distance (above 800 m), the presence of obvious turbulent structures or unfavourable transport conditions for the model (e.g. low wind condition) (Ars et al., 2017; Caulton et al., 2018). In such situations, the confidence in about 40% of the transects was deemed too low and disregarded from the analysis. Finally, only 41, 50 and 53 transects were considered for analysis at Koshi, Kotsiatis and Aradippou, respectively.

The Gaussian plume model

The Gaussian plume model used in this study is embedded in the Polyphemus air quality modeling system

(http://cerea.enpc.fr/polyphemus/introduction.html) (Mallet et al., 2007). This model is described in the study by Korsakissok and Mallet (2009), and has been proven to be adequate for gas emission estimates at a local scale. Some assumptions are generally made in analyzing the Gaussian plume model, including constant wind speed and direction with time and elevation and the terrain is relatively flat and open country. Gaussian plume models are based on a simple formula, which provides the concentration of a pollutant emitted from a point source during ambient stationary weather conditions:

$$C(x,y,z) = \frac{Q}{2\pi\bar{u}\sigma_y\sigma_z}\exp\left(-\frac{(y-y_s)^2}{2{\sigma_y}^2}\right) \times [\exp\left(-\frac{(z-z_s)^2}{2{\sigma_z}^2} + \exp\left(-\frac{(z+z_s)^2}{2{\sigma_z}^2}\right)\right)] \quad (1)$$

Here, C is the pollutant concentration at coordinates (x,y,z); the x-axis is in the wind direction, the y-axis refers to the horizontal crosswind direction, and the z-axis is the vertical coordinate. Further, ys is the source ordinate, zs refers to the release height above the ground (e.g. for stack emissions), and σ_y and σ_z are the Gaussian plume standard deviations in the horizontal and vertical directions, respectively. Q is the source emission rate and $\overline{u}$ is the wind speed. The outcome concentration is strongly dependent on these parameters. There are several ways to determine them in the Polyphemus platform by using the Doury formulations (Doury, 1976), Briggs parametrization (Briggs, 1971) or a parametrization on similarity theory (Ars et al., 2017). The Briggs parametrization, the most flexible one, has been selected for this study. Because it considers the atmosphere's stability via six classes of the Pasquill classification from extremely unstable (class A) to extremely stable (class F) based on wind speed and solar irradiance, and it considers the type of urban environment for emission sources surrounded by buildings and rural environment for isolated sites (Ars et al., 2017). The study of Korsakissok and Mallet (2009) has validated that the Briggs parametrization has a good representation of measurements by comparing it with different parametrizations at different distances from emitting sources. The following equation gives the associated standard deviations:

$$\sigma_y = \frac{\alpha x}{\sqrt{1+\beta x}} \text{ and } \sigma_z = \alpha x(1+\beta x)^{\gamma} \quad (2)$$

Where α, β, γ are coefficients depending on the Pasquill-Turner stability class (Pasquill, 1961).

In addition to meteorological data (temperature, wind direction and speed, stability class), source identification is required as input, including source position and diameter, and source input strength. The measurements and modeled concentrations are integrated along y, and the concentration is linear with the emission rate, as shown in the Eq. 1. Therefore, the emission rate can be estimated by the following formula:

$$Q = \frac{\sum C_{Observation} - C_{Background}}{\sum C_{Model}} \times Q_{input} \quad (3)$$

where Σ means summation over y (Caulton et al., 2018). Different factors could impact the calculated emission rate, as discussed in Section 3. The mass loss of dry/wet deposition was neglected since CH_4's solubility is small (Ars et al., 2017). Methane chemistry is neglected for the temporal and spatial scales of the study.

UNFCCC inventory calculations

Methane emissions are estimated and reported in national GHG inventories under UNFCCC for countries participating in the Kyoto protocol, following the International Panel of Climate Change (IPCC) guidelines (IPCC, 2006). For Cyprus, the landfill CH_4 emissions in 2020 were calculated at 21.66 ± 9.19 Gg by applying Tier 2 approach referring to IPCC (2006), which is based on the first-order degradation (FOD) model. The active landfill Koshi and the closed landfill Kotsiatis is reported to emit 3.34 Gg and 6.74 Gg CH_4 in 2020 respectively, accounting for about 47% of solid waste CH_4 emissions in Cyprus. The activity data used in this approach for Cyprus include disposed waste amounts, compositions and population (urban and rural). The suggested default values for degradable organic carbon (DOC) cover the whole southern Europe region, and the methane generation rate constant is the default one for dry temperatures. Landfill CH_4 emissions are calculated by reducing the fraction of collected CH_4 and the fraction of oxidized CH_4 in the landfill cover soil from CH_4 generation (IPCC, 2006). Thus, the uncertainty is related to CH_4 production/generation, variances in time collection efficiency and the part being oxidized (Scheutz et al., 2022). The uncertainty given for reported landfill CH_4 emissions is 42%.

For the category of agriculture, 53% methane emissions is from livestock and among which 31% is from cattle. They are calculated by IPCC Tier 2

method (IPCC, 2006) to estimate gross energy intake and determine the country-specific emission factor of activity data, such as pregnancy rate, digestibility, and nutrient content of the feed. Errors in feed intake estimation mainly determine the uncertainty of this method (Bannink et al., 2011; Million et al., 2022). In 2020, the partition between dairy and non-dairy cattle was 48% and 52% respectively. Only dairy cattle emissions were calculated using the Tier 2 method. Tier 1 approach (IPCC, 2006), with a default emission factor, was used for non-dairy cattle. Finally, in 2020, the enteric methane emission from dairy and non-dairy cattle was 4.82 Gg and 2.47 Gg, respectively. The uncertainty given for this sector is 50%.

Section 3: Results and discussion

Regarding solid waste disposal, emission rates were estimated at 10.1 Gg yr^{-1} (5% to 95% confidence range: 7.3 to 12.9 Gg yr^{-1}) and 15.8 Gg yr^{-1} (5% to 95% confidence range: 12.2 to 19.4 Gg yr^{-1}), for the active landfill (Koshi) and the closed landfill (Kotsiatis) respectively. Those findings suggest that the methane emission estimated from the closed landfill is about 50% larger than from the active landfill.

Regarding livestock, in the Aradippou area, the initial surveys revealed ten emitters (livestock farms). Due to their geographic clustering, the ten-point sources were surveyed and analyzed as three distinct groups, as shown in Fig.2.5. Then, summing up the emission rates estimated from these three parts yielded the total CH_4 emission rate for this area. That sum is calculated at 0.54 Gg yr^{-1} (5% to 95% confidence range: 0.31 to 0.77 Gg yr^{-1}).

The Aradippou area includes 5.2% of cattle emissions in Cyprus. It is assumed that the dairy and non-dairy cattle population distribution of the Aradippou area follows the national dairy and non-dairy cattle population distribution (48% dairy cattle and 52% non-dairy cattle in Cyprus). This assumption was used to obtain the amount of enteric CH_4 emission from cattle in Cyprus. Additionally, different emission factors for dairy cattle (120.5 kg CH_4 $head^{-1}$ yr^{-1}) and non-dairy cattle (57 kg CH_4 $head^{-1}$ yr^{-1}) are used to calculate the total emission from cattle. Based on the above, Cyprus CH_4 emission rate from cattle, under the sub-category livestock is estimated at 10.4 Gg yr^{-1} (5% to 95% confidence range: 6.0 to 14.8 Gg yr^{-1}).

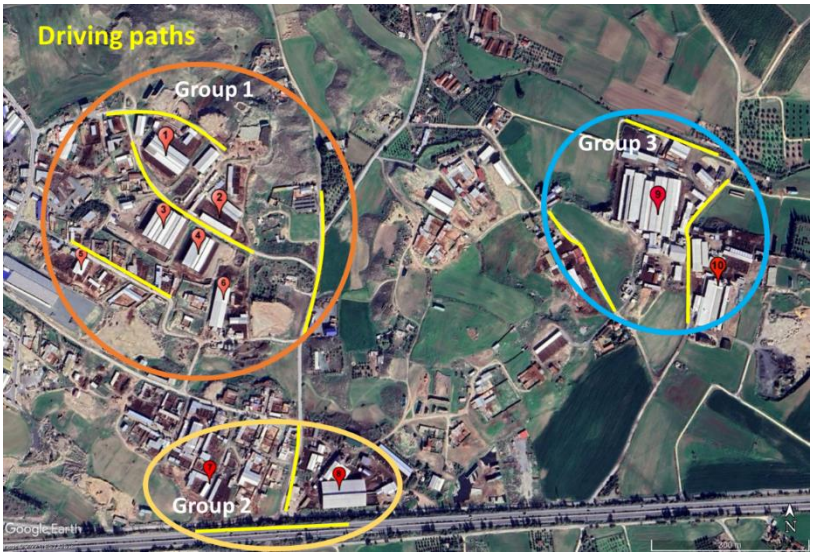

Figure 2.5 The selected ten-point sources at the Aradippou area combined with driving paths of the vehicle during measurement transects (yellow lines). Base map © Google Earth 2022.

Figure 2.6 shows the seasonal variability of the estimated emission rates from the three studied hotspots. There are only small seasonal variabilities (2.3 Gg yr^{-1} for Koshi active landfill, 3.3 Gg yr^{-1} for Kotsiatis closed landfill and 0.02 Gg yr^{-1} for Aradippou cattle farms). We estimate that this limited seasonality is due to the stable subtropical stable climate with an annual average temperature of 25 ˚C in Cyprus (Giannakopoulos et al., 2010). Several factors may potentially influence the seasonal variation of methane emissions of landfills. Emissions can be impacted by meteorological conditions, soil/cover conditions and waste and landfill conditions (Kjeldsen, 1996). Besides, landfills are generally managed to mitigate CH_4 emissions using gas collection and recovery systems, and CH_4 oxidation installations (Mønster et al., 2019), although we did not have access to management information for these landfills. Regarding livestock, manure management situation and animal number changes in time are probably the potential drivers. Therefore, strengthening cooperation with operators and managers would help better understanding seasonal fluctuations of these significant methane emitters.

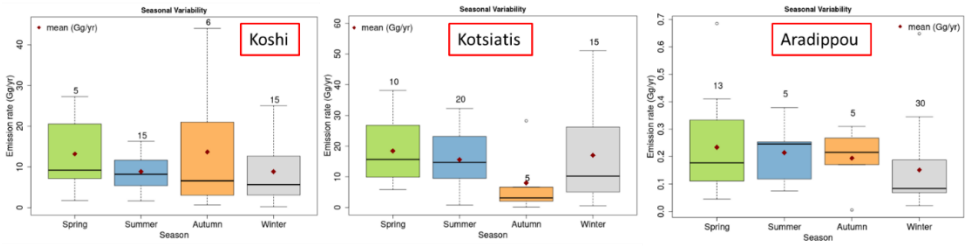

Figure 2.6 Seasonal variabilities of the three sites, from left to right respectively Koshi, Kotsiatis, and Aradippou.

Uncertainty of atmospheric estimations

Different input factors can result in under- or over-estimating emission rates. The main one would be the temporal variability, although we found limited seasonality in the emissions. Uncertainty can also be induced by poor representation of the dispersion downwind of the sites. To assess it within a single Gaussian plume estimate, we propagate the uncertainties linked to variability of wind speed and wind direction, and the choice of stability class. During this calculation, wind speed and wind direction were weighted by the statistical distribution according to the observed wind data during a single transect. The propagated uncertainty estimates for the active landfill (Koshi), the closed landfill (Kotsiatis) and the pasture area (Aradippou) are 18%, 22% and 23%, respectively. The stability class contributes 38% of the uncertainty due to one stability class discrepancy. On average, wind speed and direction changes contribute to 23% and 39% of the overall uncertainty, respectively.

Reconciling top-down and bottom-up estimates

In our survey, the three measured hotspots account for about 28% of the total CH_4 emission in Cyprus according to the bottom-up inventory. Figure 2.7 summarizes the results, combined with the bottom-up values from the Cyprus national inventory. Our estimation, based on mobile in-situ measurements for the sub-category of solid waste disposal, was 160% larger than that reported in the bottom-up inventory. The significant difference may result from i) obsolete inventory data, possibly due to empirical/regional/default input values based on limited and outdated research; ii) incorrect attribution of emissions from the closed landfill, which is unmanaged and did not meet the standards for landfills of European Union directives, iii) uncertainties in the top-down estimates,

including country-scale extrapolation. By considering top-down uncertainties, our results strongly suggest that the approach with default values of the FOD model (IPCC, 2006) at the national level is not appropriate for estimating landfill CH_4 emissions in Cyprus. Mobile surveys reveal that it is essential to reevaluate and revise the inventory data for the national waste sector. For livestock, methane emissions from enteric fermentation estimated using in situ measurements are 40% greater than that reported in the national inventory. The result is comparable to that reported Hiller et al. (2014) and Vechi et al. (2022) for other areas. However, the bottom-up estimate is within the lower end of the confidence interval of our top-down estimate. The possible reasons for this difference include i) time variability in the number of animals, ii) non-specific emission factors, iii) diurnal variation in the strength of cattle enteric fermentation, and iv) the measured emission rates may contain a fraction of manure methane emissions.

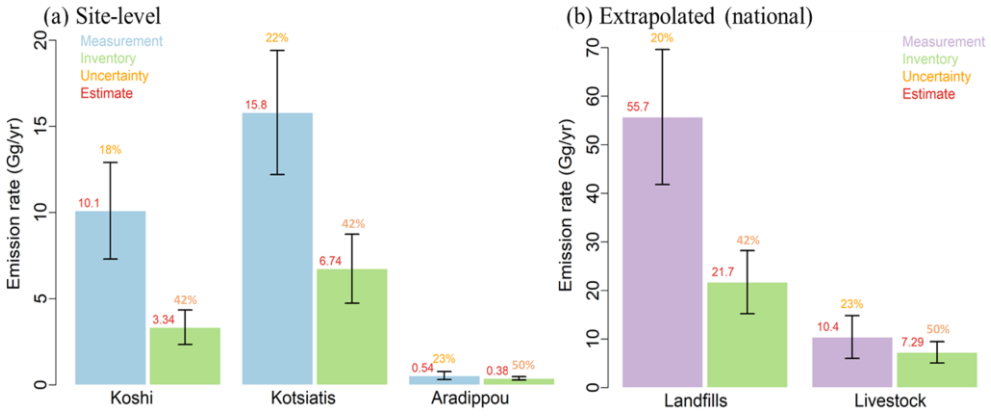

Figure 2.7 Methane emission rates calculated from in situ CH_4 measurements and bottom-up inventory estimates: (a) presents the site scale and (b) presents the extrapolated estimates (national scale).

Section 4: Conclusions and implications for verifying national inventories

This study provides one year of site-level atmospheric methane observations at three selected hotspots, representing 28% of Cyprus national methane emissions. It sheds light on the discrepancies between bottom-up and top-down estimation approaches. After extrapolation, our calculated top-down estimates of methane waste and livestock emissions for Cyprus

were 160% and 40% larger than the reported values in the bottom-up national inventory. Due to the ambient meteorological conditions of the subtropical climate, we expect only small seasonal changes in biogenic methane emissions from landfills and cattle farms.

For livestock, this study provides a method to quantify enteric methane emissions from cattle bridging the site scale to the national scale, whereas previous studies focused essentially on animal- or farm-scale (Golston et al., 2020; Storm et al., 2012; Vinković et al., 2022). Our study assumed that the dairy and non-dairy cattle distribution at the surveyed area is representative of the national-level dairy and non-dairy cattle population distribution, which may have a significant impact on national estimates of enteric CH_4 emissions from livestock.

Our study also highlights that closed landfills may be a significant, underestimated CH_4 emission source, even if active landfills are properly accounted for. Therefore, to achieve efficient mitigation of CH_4 emissions, closed landfills should be monitored regularly and targeted by mitigation approaches.

Additional measurements would be required to cover more emission source categories and extend our understanding of local to national methane emissions in Cyprus.

Also, different observation platforms and calculation methods could complement top-down estimates of this study and help to move towards a top-down vs. bottom-up reconciliation (Guha et al., 2020). For example, aircraft mass balance estimates (Lamb et al., 2016) for methane were 1.4-2.8 times higher than a city inventory. Our findings indicate that the bottom-up methane emissions from solid waste disposal are clearly underestimated by a factor of 2.6 for Cyprus. The development of an inventory including more site-specific and more contemporary emission factors is equally vital in reconciling top-down/bottom-up approaches, as hinted by Lyon et al. (2015) and Amini et al. (2022).

This survey method can be applied for other regions or small-surface countries aiming to assess the methane emission structure independently from inventories and support policymakers in designing and implementing efficient mitigation action. The use of commercially available sensor, car platform and open-source modeling ensure easy reproduction. Indeed, the

method presented here is suitable for countries where it is possible to directly estimate a significant and representative amount of the total emissions of major emitting sectors. In order to obtain comparable data, it is necessary to select the largest and most representative emission sources and areas. Actually, with only slightly more resources it would be feasible to monitor almost 100% of Cyprus methane emissions and therefore make more robust top-down estimates but also test the extrapolation hypotheses for different fractions of partial monitoring.

This approach is suitable for methane in livestock and waste sectors, with point sources and limited seasonal variability. The method would be easily applied to upstream and mid-stream fossil fuel methane emissions but would be more challenging for more diffuse leaks of natural gas distribution networks. The method covers a large fraction of global emissions and is promising for many developing countries which have limited resources to develop atmospheric networks or sophisticated inventories.

Author Contributions. YL led field measurements, data analysis and writing of the manuscript. JDP conceived the study. JDP, MV, PB and JS contributed to project advising, reviewing and editing the manuscript. PYQ and MD contributed to conduct field measurements and data collection. JK, FD and DD contributed to the calculation of bottom-up inventory estimates, review and editing of the manuscript.

Competing Interests. The authors declare that they have no conflict of interest.

Acknowledgements. We would like to thank the Integrated Carbon Observation System (ICOS) teams at Le Laboratoire des Sciences du Climat et de l'Environnement (LSCE) for their support on calibrations and data quality control for the instrument Picarro. We are grateful for all the technical support from the Unmanned Systems Research Laboratory (USRL) at the Cyprus Institute (CyI).

Financial support. This research has been supported by the project Eastern Mediterranean Middle East-Climate & Atmosphere Research Center (EMME-CARE) which has received the funding from the European Union's Horizon 2020 research and innovation programme under grant agreement No. 856612 and the Cyprus Government, and the project Air Quality Services for clean air in Cyprus (AQ-SERVE) INTEGRATED/0916/0016 is

co-financed by the European Regional Development Fund and the Republic of Cyprus through the Research and Innovation Foundation.

Here, we performed mobile GHG measurements with instruments deployed on various vehicle and aircraft platforms used to investigate the strength of methane emissions sources. Such mobile platforms have been largely developed worldwide (Paris et al., 2008; Chang et al., 2014; Barker et al., 2020; Defratyka et al., 2021). Indeed, with the rapid development of relevant instruments, sensors and various measurement platforms during the past decade, high-precision quantification measurement systems are emerging. They are used in several applications, including methane emissions determination from natural gas supply chains (Allen et al., 2013; Atherton et al., 2017; Barchyn et al., 2017; Golston et al., 2018). However, the performance of these instruments needs to be systematically evaluated to assess the degree of accuracy when quantifying emissions (e.g. Ravikumar et al., 2019; Bell et al., 2020; Sherwin et al., 2021). Therefore, as a part of this Ph.D. study, ten quantification measurement systems are evaluated through a series of blind controlled release experiments in the following chapter. These inter-comparisons analyze the strength and weaknesses of these measurement systems based on various platforms (e.g., trucks, drones and aircraft) depending on emission protocols and atmospheric conditions during the release experiments, providing an update on the current capabilities.

3 INTERCOMPARISON OF CURRENT METHANE EMISSIONS QUANTIFICATION TECHNIQUES THROUGH CONTROLLED RELEASE EXPERIMENT

3.1 OVERVIEW

Fossil fuel production and use is responsible for the release of 112 Mt CH_4 yr^{-1} to the atmosphere, representing 33% of the total anthropogenic emission of CH_4 (Saunois et al., 2020). Within fossil fuel emissions alone, 68% of the emissions is linked to oil and gas (O&G) while the rest is associated with coal mining. Emission of CH_4 arises at each step from the production site to the consumption site but a large fraction of the net emission is associated with the production, transport and processing (Alvarez et al., 2018), especially for oil production. In the gas industry, emission of CH_4 occurs either as fugitive emission (leaks from valves, connectors and compressors, intentional venting) or as incomplete combustion during flaring (GIE-MARCOGAZ, 2019).

Major oil and gas companies have already set targets to reduce upstream leakage and this would account for 20% of these potential emission reductions (OGCI 2018). To promote emission reductions globally, the UNEP-led Climate and Clean Air Coalition's (CCAC's) Mineral Methane Initiative (MMI) initiated OGMP2.0 (Oil and Gas Methane Partnership, https://www.ccacoalition.org/en/resources/oil-and-gas-methane-partnership-ogmp-20-framework). Here, companies record efforts for emission reduction with high credibility and align to best practices. The OGMP relies on progress in the CCAC's Methane Science Studies, to improve techniques for emission reduction and emission estimation.

Natural gas can limit climate impacts by producing reduced CO_2 emissions during its combustion by up to 60% compared to other fossil fuels (Allen, 2014; Bell et al., 2017). As a potential transition fuel between coal and renewable technologies (e.g. solar thermal), its global demand is projected to grow to approximately 4500 billion cubic meters in 2030 and 5100 billion cubic meters in 2050 (IEA, 2021). Although the combustion of natural gas releases less CO_2 per unit of energy produced than other fossil fuels, methane (a key constituent of natural gas) emissions in leaks, venting,

and other parts associated with the supply chain can erode climate benefits and advantages of natural gas as a transition energy (Waxman et al., 2020; Zimmerle et al., 2020).

Improving CH_4 emission estimates across the natural gas supply chain is critical to better understanding and quantifying the implications of switching to natural gas. As discussed in Chapter 1, with the development of atmospheric measurement techniques, promising measurement systems are emerging to detect and quantify anthropogenic methane emissions in the natural gas supply chain ranging from facility to local (site) scales. Regulatory compliance and climate mitigation strategies currently rely essentially on standards based on activity data and emission factors. This is highly imprecise as it does not describe specific pieces of equipment or industry practices. Methods to independently monitor emissions, and verify emission reduction strategies, are still under development. Generally, the strategy is to measure directly the dispersion of methane in the atmosphere in the vicinity of industry assets. Current strategies typically target emission "hotspots" or super-emitters. These assets generate significant enhancements in atmospheric CH_4, that can be measured either using in situ measurements or ground-based or air-borne remote sensing. With recent development, satellite measurements may also play a role for identifying and estimating superemitters sources (i.e. sites with flow rate higher than 100 kg h^{-1}) or catastrophic accidental releases. In order to evaluate the ability of such measurement systems to trigger efficient mitigation actions, controlled release experiments with known emitting locations and emission rates and inter-comparison studies have been conducted in recent years (Feitz et al., 2018; Bell et al., 2020; Ravikumar et al., 2019; Kumar et al., 2022). Current studies raise contrasting or similar conclusions depending on the specific experimental set-up or the specific mobile of fixed platforms, sensors, sampling strategies and models. With the regular improvement of instruments and techniques, new inter-comparisons based on controlled releases and involving a wide range of techniques and instruments are regularly needed.

Therefore, this chapter investigates the ability of a wide range of state-of-art techniques to quantify fugitive emissions in a series of blind-controlled release experiments to provide an update on the current capabilities and fulfill the requirements discussed above. The controlled releases are performed at an inert compressor station. They cover a wide range of

situations such as different flow rates ranging from 0.01 kg h^{-1} to 50 kg h^{-1}, release heights ranging from 1 m to 28 m and different gas outlet. The range of emissions and the configuration of exhaust points aimed to reproduce realistic situations occurring in the midstream natural gas industry, including transmission pipelines, pumps, compressors stations, and storage facilities used to connect upstream extraction and production to downstream distribution and end users. Ten groups with different measurement systems participated in this one-week campaign after a pre-selection procedure to compare and evaluate a wide range of measurement systems, including mobile, ground-based, and handheld measurement platforms. All systems are dedicated to quantifying methane emissions at the industrial site level. Their respective strength, weaknesses, and potential complementarity depending on the emission and atmospheric conditions are evaluated in this study. More details of these measurement systems refer to the next subsection.

As a normalized performance indicator, the absolute value of the relative error (absolute error, $|(E_{estimate}-E_{real})/E_{real}|$) was computed for each release and each system. The ten measurement systems are named in this chapter as Lidar 1, Lidar 2, Drone 1, Drone 2, Tracer, Fixed 1, Fixed 2, OGI 1, OGI 2 and Hi-Flow. There is a large spread of typical errors in the results from one participant to the other, with average absolute errors per participant ranging from 19% (for Tracer) to 239% (for Drone 2). It is suggested in this study that the quantification lower limit for most of these systems lies between 0.01 kg h^{-1} and 0.1 kg h^{-1}. It highlights that some systems provide results with occasional discrepancies of more than one order of magnitude (OGIs). Additionally, five single-node releases have been performed and help refine the analysis of method performances. The mean absolute error for single-node release from node 1, node 3, node 4 and node 5 are 68%, 102%, 113%, and 172%, respectively. Single-node release at node 5 bear larger absolute errors than those with other nodes. This might be explained by the proximity of node 5 to the ground and hence a more complicated dispersion to capture.

Overall the results show that commercially available systems provide the ability to quantify fugitive emission rates at a reasonable level of precision (within an order of magnitude). The limited number of controlled releases implemented did not let significant impacts emerge from environmental parameters (e.g. wind speed), node shape and positions. More test scenarios are needed to acquire more statistics, and test dependence on wind

conditions. It is imperative in the near future to determine how these systems can be applied together to reconcile source-level and site-level quantification. The following subsection briefly introduces test scenarios, measurement systems, analysis and results.

3.2 PAPER TO BE SUBMITED: INTERCOMPARISON OF CURRENT METHANE EMISSIONS QUANTIFICATION TECHNIQUES FOR NATURAL GAS MIDSTREAM APPLICATIONS

Intercomparison of current methane emissions quantification techniques for natural gas midstream applications

Abstract

Fugitive emissions from natural gas systems are increasingly scrutinized, and accurate reporting requires site- and source-level measurement-based quantification. We evaluate the performance of available, state-of-the-art CH_4 emission quantification approaches against blind controlled release experiment. Ten different groups participated with their quantification systems in the experiment at an inert natural gas compressor station in 2021. The experiment consisted of 17 blind, 2-hour source releases at single or multiple simultaneous exhaust points. The controlled releases covered a range of flow rates from 0.01 kg h^{-1} to 50 kg h^{-1}. Measurement platforms included airborne, ground-based mobile and fixed atmospheric measurements, as well as handheld systems. Herewith, we compare their respective strengths, weaknesses, and potential complementarity depending on the emission and atmospheric conditions. Most systems accurately quantify the releases within an order of magnitude. The level of errors from the different systems was not significantly influenced by release rates larger than 0.1 kg h^{-1}. However, they were poorer for the 0.01 kg h^{-1} release. It was found that the so-called "source-level" systems (close to single leak) generally underestimated the emissions. In contrast, the "site-level" systems (integrating emissions for the site), relying on atmospheric dispersion, tended to overestimate the emission rates slightly. We assess the dependence of the emission quantification performance against key drivers such as wind speed, deployment constraints and temporal sampling. Although the experiments did not reveal a significant dependence to wind speed, the ability to quantify individual sources is degraded during multiple-

source releases. Compliance with the Oil and Gas Methane Partnership (OGMP2.0) highest level of reporting may require a combination of the specific advantages of each measurement technique along a continuum from source-level to site-level quantifications and will depend on reconciliation approaches.

Section 1: Introduction

Methane, a key constituent of natural gas, is a powerful short-lived (9 years) greenhouse gas and has about 28 times the global warming potential of CO_2 on a 100-year horizon (IPCC, 2018). Natural gas consumption has increased by 2.2% over the last decade to reach 4307.5 billion m^3, with the existing reserves reaching 188.1 trillion m^3 in 2021 (BP, 2022). Global demand for natural gas is projected to grow to approximately 4500 billion m^3 in 2030 and 5100 billion m^3 in 2050 (IEA, 2021). Although the combustion of natural gas release less CO_2 per unit of energy produced than other fossil fuels, methane emissions in leaks, venting and other parts associated with the supply chain erode the climatic advantage of natural gas as a transition energy (Balcombe et al., 2017; Cooper et al., 2021; Zimmerle et al., 2020). Improving CH_4 emission reporting across the natural gas value chain is thus critical to understanding the climate implications of a large-scale transition to natural gas.

Intensive research has recently focused on quantifying CH_4 emissions from different sectors of the natural gas supply chain (Roscioli et al., 2015; Crow et al., 2019; Duren et al., 2019; Bell et al., 2020; Defratyka et al., 2021b). To continuously improve reporting through better quantification of emissions in natural gas production, different atmospheric measurement systems have been developed and applied in the field during the past decade (Thorpe et al., 2016; Ars et al., 2017; Johnson et al., 2021; Morales et al., 2021). In most cases, at basin scale, CH_4 emissions estimated from atmospheric measurements were larger than the values reported in inventories at the basin scale (Harriss et al., 2015; Alvarez et al., 2018; Rutherford et al., 2021; Foulds et al., 2022), although overestimation might not be systematic in poorly constrained production regions such as the Western Russian Arctic or Arabian Gulf gas fields (Petäjä et al., 2020; Paris et al., 2021). Overestimation has been attributed to a variety of potential reasons: reporting based on assumptions of past years' activity while activity increases; lack of accounting for all sources in emission inventories;

lack of accounting for specific and time-limited venting operations; challenging spatial or temporal aggregation of activities or missing specific super-emitters.

Facing this challenge of reconciling inventories with atmospheric measurements and in order to monitor progress in emission reduction policies, the Oil and Gas Methane Partnership (OGMP2.0; https://www.ogmpartnership.com) voluntary initiative encourages reporting of site-level emissions by oil and gas operators as a complement to emission factor-based reporting. This approach is relevant to bridge the gap between the source-level bottom-up approach industry practice, and site-scale atmospheric measurements (Allen et al., 2014; Olczak et al., 2022). However, measuring site scale emissions relies on a range of atmospheric measurement systems, which have highly variable performances at this scale.

Controlled release experiments and intercomparison studies have been used to improve and evaluate the performances of methane emission measurement systems (e.g. Albertson et al., 2016; Ars et al., 2017; Feitz et al., 2018; Ravikumar et al., 2019). Ravikumar et al. (2019) reported the evaluation of the results from 10 vehicle, drone, and plane-based mobile CH_4 leak detection and quantification technologies through single-blind controlled release tests. They found that 6 of the 10 technologies could correctly detect over 90% of the test scenarios and correctly assign a leak to a specific equipment in at least 50% of test scenarios. Bell et al. (2020) assessed 12 CH_4 emission measurement technologies. They found that localization by handheld and mobile technologies is more accurate than continuous monitoring systems. However, Kumar et al. (2022) showed 20%-30% precision for the estimate of controlled CH_4 release rates when relying on either mobile or fixed station networks. Their localization of the releases was better when relying on fixed stations. With the rapid development of current technology, Sherwin et al. (2021) have shown that an airplane-based hyperspectral imaging CH_4 emission detection system can detect and quantify over 50% of total emissions from super-emitting sources.

Moreover, the airborne CH_4 measurement technology reported by Johnson et al. (2021) can detect, locate and quantify individual sources at or below the magnitudes of recently regulated venting limits with ± 31%-68% quantification uncertainties. These various studies propose conclusions that

strongly depend on the specific experimental set-up, mobile of fixed platforms, sensors, sampling strategies and models they use. With the regular improvement of instruments and techniques, new intercomparisons based on controlled releases and involving a wide range of technologies are regularly needed. Our study aims at providing an update on the current capabilities and at fulfilling this requirement.

Here, we investigate the performances of various available technologies to quantify fugitive emissions in a blind-controlled release experiment. The experiment was held at an inert compressor station. It was organized by the European Gas Research Group (GERG) in 2021. The range of emissions and the configuration of exhaust points aimed to reproduce reasonably realistic situations occurring in the midstream natural gas industry, including transmission pipelines, pumps, compressors stations and storage facilities that connect upstream exaction and production to downstream distribution and end users (GIE and MARCOGAZ, 2019). The experiment included 17 blind-controlled releases with 2-hour single or multiple emission sources. The controlled releases covered a wide range of situations, such as different flow rates (from 0.01 kg h^{-1} to 50 kg h^{-1}), release heights (ranging from 1 m to 28 m), and gas outlets. Ten groups with different promising measurement systems were selected to participate in this one-week campaign by GERG. The aim is to compare and evaluate these measurement systems (including mobile, ground-based, and handheld measurement platforms) to quantify CH_4 emissions at the industrial site level and analyze their respective strength, weaknesses, and potential complementarity depending on the emission and atmospheric conditions. The study focuses on quantifying emissions from single or multiple leak points. The detection and identification of those leaks are a prerequisite to this quantification but they are not evaluated here.

Section 2: Methodology

Site description

An idle compressor station was setected as the experiment site. The compressor station, located in Spain, has various compression equipment for injecting and treating gas extracted from nearby underground gas storage (Fig.3.1). It is no longer in operation and is completely inert, with no significant natural or anthropogenic sources of methane identified in the area. The site is surrounded by flat roads from the outside and inside,

making it suitable for vehicle-based mobile measurements.

There are five gas outlet points, called nodes hereafter, embedded in the site infrastructure. The nodes are split into two areas: Area A includes Node 1, and Area B includes Nodes 2-5 (Fig. 1). Node 1 is located at the top of the vent stack of the site, at a height of 28 m. In this case, the type of exit chosen is open-end to simulate the emission conditions in the vent stack. Node 2 is 9 m above ground level with an open-end exit. Node 3 is 4 m high with a ring-shaped opening. Node 4 is a linear tube three meters long with holes along it at 1.5 m height. Node 5 is an open outlet at 1.5 m height, dedicated exclusively to the tests with the lowest emission rates.

Figure 3.1 Aerial view of the Enagas site in Spain and node placement (white circles). The controlled release facility is indicated by a white disk marked “CRF”.

Controlled release facility

The controlled release facility (CRF) is a portable flow control system purposefully designed and configured to create ‘real-world’ gaseous emission scenarios. A detailed description can be found in Gardiner et al. (2017). The system (Fig. 3.2) enables the operator to replicate a variety of gaseous emissions at comparable scales in a range of industrial settings to validate emissions monitoring methodologies under the conditions in the field. The facility is computer-controlled and monitored, allowing for the execution of pre-written operational programs and the analysis of flow data post-test. Communication to the instrument is made via a low-voltage umbilical cable, allowing the operator to control the system from a distance

of up to 50 m from the gas blending equipment. The uncertainty of the CRF is dominated by the calibration uncertainty. The MidiCRF was used when the flow was below 1.2 kg h^{-1} (Node 5). Its principle derives from a simplified version of CRF.

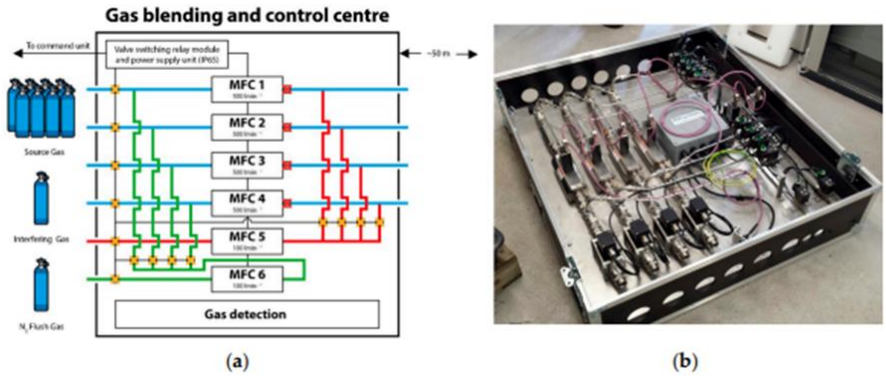

Figure 3.2 (a) the Controlled Release Facility Schematic and (b) photograph of the flow control system (Gardiner et al., 2017).

Test scenarios and organization of the experiment

The 17 controlled releases were performed from October 4 to October 8, 2021. They covered a range of situations combining different flow rates (0.01 kg h^{-1} - 50 kg h^{-1}), across single or multiple nodes. This approach aims to simulate a variety of fugitive emissions and venting conditions in natural gas midstream sites.

All the releases were made from single or multiple nodes with a constant emission rate over 2 hours. The releases were “blind”, i.e. the release rates were not known by the participants. The series of release rates were established in advance and ordered randomly within the range of 0.01 kg h^{-1} to 50 kg h^{-1} to prevent participants from guessing these rates (Table 3.1). Two releases took place in Area A only, 14 in Area B only, and one in both Areas A and B. The participants knew the areas of emission (A and/or B) but not the exact emitting node(s) in the case of Area B. Participants also knew the range of total emission rates and the timing of releases. Participants ignored each others’ results until after all participants blindly uploaded their results to an ‘upload only’ server, 3 weeks after the end of the experiment.

The lowest release rates (below 0.5 kg h^{-1}) were dedicated to evaluate the quantification limit, defined here as the lower limit below which a technique does not provide relevant emission estimates.

Due to the linearity of the CH_4 atmospheric dispersion, the releases correspond to either a “low concentration regime” where measured concentrations are commensurate with instrumental precision or a “high concentration regime” where instrumental precision is not expected to play a significant role. In a low-concentration regime, the uncertainties in emission rate estimates are expected to decrease with increasing release rates. The quantification limit should thus correspond to the emission threshold above which the signal-to-noise ratios of the different sensors are sufficiently high so that the uncertainty in the result does not depend on the release rates. We used a relatively uniform sampling of the emission rates within the range of 0.01 kg h^{-1} to 50 kg h^{-1} to infer it.

Within each 2 h release, the series of measurements by the different participants was sequenced to minimize the impact of a specific quantification system on others. For example, drones flew sequentially to avoid any collision risk. The helicopter flew over the site only at the very end of the releases to avoid disturbing plume dispersion for other groups. The drones generate turbulences that can influence the structures of the plume measured by other platforms (in particular by Lidar 2), which can perturb the corresponding emission computation. An initial organizational briefing ensured the alignment of all technology providers and a smooth succession of releases and measurements. During the campaign week, permanent coordination by radio was applied between site coordinators and all involved groups. Experiment details and sequencing technologies were shared with all participants through a paperboard on the site. The different quantification systems relied on different measurement durations to provide release estimates due to this organization but also because they follow different operating protocols.

A sonic anemometer (Vaisala WXT530) attached to a mast was located between Areas A and B at 5 m height to perform wind measurements during the campaign. Low wind speed (below 1 m s^{-1}-2 m s^{-1}) can be challenging for most participants relying on atmospheric dispersion (Wilson et al., 1976).

The Drone 2 group performed daily background measurements prior to any release (using drone-based optical CH_4 measurements). The background was reported only over a wide interval. It was found to be constant within this range (i.e., morning daily concentrations remained within 2.2 ppm-2.5 ppm). These background measurements indicated no large, local CH_4 sources near the site. Therefore, it is unlikely that any significant CH_4 enhancement from outside the site may have influenced the release experiment.

Table 3.1 Test scenarios with detail of emission rates per node (unit in kg h^{-1}). The uncertainties account for ± 95% confidence intervals.

Test	Total emission rate	Node1 MFC2	Node2 MFC3	Node3 MFC4	Node4 MFC1	Node5 MFC 9 or 10
1	2.6±1.8			2.6±1.8		
2	5.7±0.7	5.7±0.7				
3	1.2±0.01					1.2±0.01
4	22.7±2.2		9.7±0.5	3.1±1.8	10.0±1.2	
5	5.7±1.3		2.0±0.5		3.6±1.2	
6	22.4±2.2		9.8±0.5	2.7±1.8	10.0±1.2	
7	18.9±0.7	18.9±0.7				
8	46.4±2.3	11.0±0.7	15.2±0.5	9.0±1.8	11.1±1.2	
9	0.1±0.0001					0.1±0.0001
10	5.1±1.2				5.1±1.2	
11	8.1±1.2				8.1±1.2	
12	32.5±2.2		16.7±0.5	5.9±1.8	9.9±1.2	
13	0.5±0.01					0.5±0.01
14	7.03±1.31		2.5±0.5		4.5±1.2	
15	0.01±0.0001					0.01±0.0001
16	3.8±1.2				3.8±1.2	
17	14.6±2.2		2.3±0.5	9.8±1.8	2.5±1.2	

Participants and measurement systems

Twelve quantification systems were selected based on an internal review by the GERG consortium (https://www.gerg.eu/). The ability to detect leaks was not part of the criteria, as this study focuses on quantification. Besides the performances of each measurement system, the criteria included sufficiently high Technology Readiness Level (TRL), demonstrated ability to perform such measurements on-site, and the possibility for the service to be performed commercially by an independent operator. Table 3.2 summarizes the main characteristics of these systems. These quantification systems combine measurement platforms, instruments, and post-processing algorithms to derive emission rates. The systems are based on handheld, vehicle, drone, and airborne mobile platforms and ground-based fixed measurements. The devices include optical gas imaging cameras, lidar, off-axis integrated cavity output spectroscopy, and tunable diode laser spectrometry.

Different methods such as inverse dispersion modeling, proprietary data algorithms, and their developed quantification software were applied to derive CH_4 emission rates, and six of them provided their diagnostics of uncertainties in the estimates (hereafter, all uncertainties are provided in terms of 1-sigma values). Most participants provided estimates of their uncertainties

along with their release rate estimates. The reporting of the emission rate was done according to a specific template. The reporting of uncertainties, however, was not specified and was reported on a free basis.

A group operating two systems decided to provide no quantification data on their quality control after the experiment. It concluded that their measurement technology was to be optimized.

Table 3.2 A summary of the systems participating in the campaign.

Name	Platform	Sensor	Quantification algorithm	Assessment type
Drone 1	Matrice 300 RTK from DJI	Tunable Diode Laser Spectrometry	Inverse dispersion modelling, considering the location of the plume, sensor measurements and local weather data	Site-level
Lidar 1	Helicopter (AirLloyd)	LiDAR DIAL	Direct estimation by multiplying the integrated gas concentration, the respective wind speed and the sine of the angle between fence line and wind direction	Site-level
Tracer	Van	Off-axis integrated cavity output spectroscopy	Calculated as the integrated signal of CH_4 concentration relative to the integrated signal of tracer gas concentration	Site-level
Lidar 2	Truck	Differential absorption lidar	Determined by combining the concentration map with wind speed and direction	Site-level
Drone 2	DJI M300 UAS	An in-situ tunable diode laser absorption spectrometer	Proprietary data algorithms based on an engineering control volume model	Site-level
Fixed 1	Ground	Laser dispersion spectroscopy operating in the midIR region	The algorithm combines gas concentration data of each retroreflector with meteorological data	Source-level
Fixed 2	Unmanned carmers	Two OGI cameras: an uncooled LWIR detector and a cooled MWIR de-	Depends on three variables: thermal contrast between the plume and the background; column density; absorp-	Source-level

		tector	tion peak of the target gas	
Hi-Flow	Handheld	A venture tube supplied by a compressed air cylinder	Determined by the gas concentration and the suction flow rate of the venture	Source-level
OGI 1	A handed camera	Optical gas imaging camera	EyeCSite 2.0 quantification software	Source-level
OGI 2	A handed camera	OGI camera	Determined by the QL320 tablet	Source-level

Section 3: Data collection and analysis

The primary purpose of the experiment was to assess the ability to infer the total emission rates during each release. Therefore, the reporting focused on providing a total emission estimate for each release. During multiple node releases, we also considered detailed reported estimates for individual nodes when available from the participants. The ability to provide estimates per individual source during a multiple release was considered a desirable feature of site-level quantification techniques.

As a normalized performance indicator, the absolute value of the relative error (called hereafter "absolute error", $|(E_{estimate}-E_{real})/E_{real}|$) was computed for each release and each provider. $E_{estimate}$ is the estimate provided by a given participant (in kg h^{-1}), and E_{real} is the actual emission rate. The distributions of absolute error are analyzed per release (considering each provider as a single realization) or per provider (considering each release as a different realization).

Table 3.3 gives an overview of the results provided by each participant after the experiment. It indicates, for each experiment, whether a given participant provided the estimate for the total emission rate, partial emission rate estimates where one or several nodes may be missing, or no valid estimate. Overall, no single release was reported by all participants, and no system could report fully on all releases; the number of total emission estimates is between 5 and 9 for a given release, and between 5 and 16 for a given system. The amount of data reported directly constrained our ability to identify robust statistical relationships between the errors in the release rate es-

timates and potential drivers of the quantification skill such as the meteorological conditions or the type of CH_4 releases.

Each participant followed their selection process to quality-control and validate their estimates. Some participants excluded data points considered poor and provided reduced coverage of the releases to maintain a lower uncertainty, while others provided extensive coverage, potentially at the cost of slightly higher uncertainty. Each data provider relied on its judgment and procedures to balance the quantity and quality of the estimates. This balance is essential to consider when evaluating the respective merits of each system as a high overall precision may be a trade-off with a high "coverage" of the release rates. The uncertainties provided by the participants are reported as 1-sigma. Each provider reported specific limitations and challenges explaining the coverage of the releases after the campaign.

Table 3.3 Overview of valid emission estimates for each release. The letter indicates the availability of estimation. T: total emissions were captured; P: partial emission rate, one or several nodes may be missing from the total; 0: no estimate or value considered invalid by the provider.

Release ID	1	2	3	4	5	6	7	8	9	10	11	12	13	14	15	16	17	Nb full	% Full
Drone 1	0	T	T	T	T	0	T	T	T	T	T	0	T	0	T	T	0	12	71%
Lidar 1	T	T	0	T	T	0	T	T	T	T	T	T	T	T	T	T	T	15	88%
Tracer	T	0	T	T	T	T	T	T	T	T	T	0	T	T	0	T	T	14	82%
Hi-Flow	0	0	T	P	P	P	0	0	T	0	0	0	T	P	T	T	0	5	29%
Flixed 1	T	0	T	T	T	T	0	P	T	T	T	T	T	T	T	T	T	14	82%
Lidar 2	0	T	0	0	T	T	T	P	0	0	0	0	T	T	0	0	T	7	41%
OGI 1	T	T	T	T	T	T	T	T	T	T	T	T	T	T	T	T	P	16	94%
Drone 2	T	T	T	T	P	T	T	T	T	T	T	T	T	T	T	T	T	16	94%
Fixed 2	T	T	0	P	P	T	T	P	0	T	T	T	0	P	0	T	T	9	53%
OGI 2	T	T	T	P	T	P	T	P	T	T	T	T	T	T	T	T	T	14	82%
Nb full estimates	7	7	7	6	8	6	8	5	8	8	8	6	9	7	7	9	7		

Section 4: Results and discussion

Qualitative assessment of the total emission estimates per participant

Figure 3 compares the total emission estimates provided by each participant with actual total emission rates. It displays linear regressions between the estimated and actual emission rates (without weighting the estimates based on the diagnostics of uncertainties). However, as discussed in the previous section, in the "high concentration regime" (for release rates

above the quantification limit), we expect correlations between the errors in the estimates or the diagnostics of uncertainties in these estimates. Results indicate that for almost all of the quantification systems, the quantification limit is relatively low. Therefore, the "linearity" between the estimated and actual release rates across the full range of estimates is not used as a criterion for assessing the quantification systems.

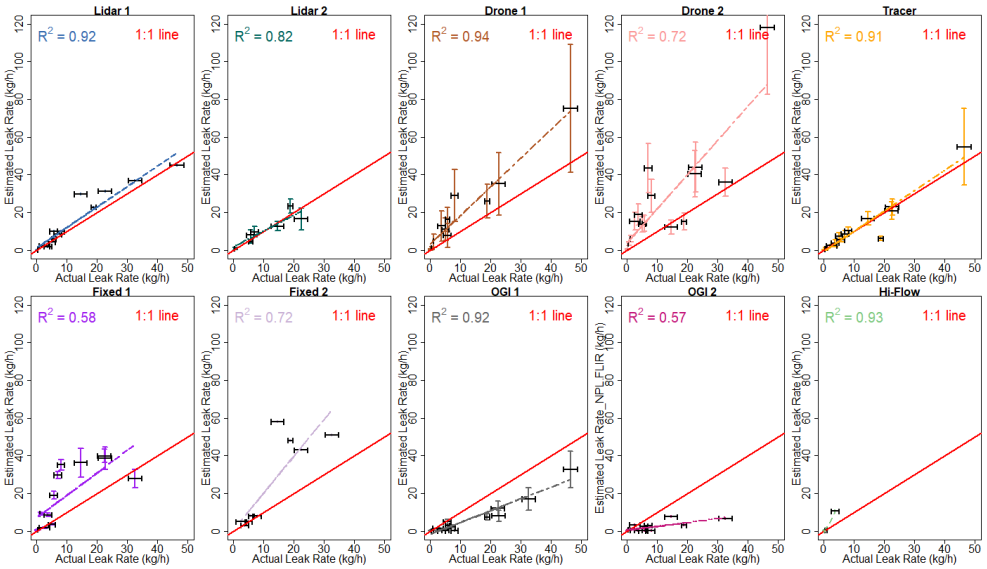

Figure 3.3 Scatter plot of estimated and actual rates for the releases for each participant. Linear regression (dashed line) and the 1:1 line (red) are shown for reference. The horizontal uncertainty bars are the 1-sigma uncertainties of the controlled release facility. The vertical error bars are 1-sigma uncertainties provided by the participant.

Lidar 1 slightly overestimated the emission rates, especially in the middle range of release rates. There is no significant bias in the release estimates from Lidar 2. Drone 1 and Drone 2 tend to overestimate the emission rates. All estimates but one from Tracer bear errors that fit in the 1-sigma uncertainty diagnosed by this system. Fixed 1 tends to overestimate the emission rates from 5 kg h^{-1} to 30 kg h^{-1}. For Fixed 2, the performance is better for lower emissions (below 10 kg h^{-1}) and tends to overestimate the emission rates above 10 kg h^{-1}. By contrast, OGI 1 and OGI 2 tend to underestimate the emission rates. There is no obvious bias for Hi-Flow, but it provides only three estimates.

In summary, the quantification systems of Lidar 1, drones and both fixed sensors generally overestimate the emission rates, and the systems of handheld OGI generally underestimate them. However, two site-level systems do not follow this tendency. The estimates from Tracer are close to the actual rates.

Total release emission estimates: quantitative synthesis

Figure 3.4 provides the distribution of absolute error for the series of estimates from each participant, excluding the results for the two smallest releases of 0.01 kg h^{-1} and 0.1 kg h^{-1}, whose specific goal was to support the assessment of the quantification limits.

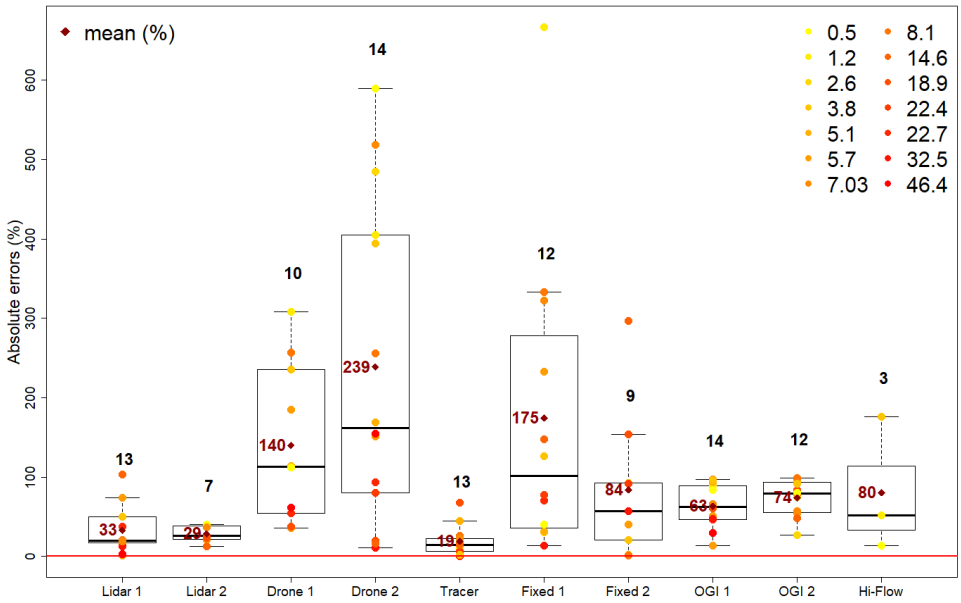

Figure 3.4 Absolute errors for each system, in percent. The color scale corresponds to the actual rates of the different releases, given in the top right corner (kg h^{-1}). Whisker plots indicate the median, interquartile range, min, and max (excluding outliers) of the distributions. The means are also indicated (dark red dot, %). The number of points accounted for in the statistical distribution is indicated on top of each whisker plot. The techniques are ordered arbitrarily from site-level systems on the left to source-level systems on the right.

The absolute errors range from 0% to 600%, even when excluding the releases below 0.5 kg h^{-1}. There is a large spread of typical errors in the results from one participant to the other, with average absolute errors per par-

ticipant ranging from 19% (for Tracer) to 239% (for Drone 2). Among the site-level quantification systems, Lidar and Tracer provide estimates with absolute errors typically smaller than 50%, while estimates from drones generally bear more than 100% errors. Fixed sensors provide intermediate performances, with an average absolute error of 84% to 175%. The different source-level quantification systems provide relatively consistent performances with 63% to 80% average absolute errors and absolute errors for any release that generally lie below 100%. Hi-Flow, which relies on a particular sampling principle, provides good performances among the source-level measurements but is based on 3 complete release estimates only, while OGI 1 and OGI 2 provide. 14 and 12 estimates, respectively.

Table 3.4 shows how often the estimates from a system fall within a multiplicative range of the actual values, either between half and twice the actual value or within the order of magnitude of the actual value. Notably, it highlights that some systems provide results with occasional discrepancies of more than one order of magnitude (OGI). The table excludes the releases of 0.01 kg h^{-1} and 0.1 kg/h. The only system that limits 100% of its discrepancies within a factor of 2 (range 0.5 - 2) has the second-lowest coverage rate (Lidar 2). Conversely, OGI 1 and Drone 2 provide the best coverage but are only within the factor 2 range for 36% of the releases.

Table 3.4 Fraction of provided release estimates within a particular multiplicative range of the true value. “0.5-2x”: fraction of occurrences of total reported estimate falling between half the true value and twice the true value. “0.1-10x”: fraction of occurrences within an order of magnitude of the true values. The last column indicates the percentage of total releases each participant provided for total emission estimates.

Estimated/Actual	Discrepancy within a particular range of true release rate (% of provided total estimates)		% releases covered
	0.5-2x*	0.1-10x*	
Drone 1	40	100	71 %
Lidar 1	92	100	88%
Tracer	92	100	82 %
Hi-Flow	33	100	29 %
Fixed 1	50	100	82 %
Lidar 2	100	100	41%
OGI 1	36	79	94%
Drone 2	36	100	94%
Fixed 2	78	100	53%

OGI 2	25	69	82%

Parameters influencing total release estimates

Role of measurement duration

The errors are not correlated with the time used by the different participants to make measurements. Both fixed sensors (Fixed 1 and Fixed 2) integrate measurements over two hours, while Lidar 1 relies on nearly instantaneous images of the concentration field. Tracer is among the mobile techniques relying on the longest records of measurements (over 45 min on average). Future experiments should support the investigation of how the performance of some techniques relying on integration over measurement durations that can vary would improve with increasing duration. However, the lack of required information during this experiment does not allow for such an analysis.

Dependence of error on emission rate

Figure 3.5 shows the relation of absolute errors with the total emission rate. The estimates of the 0.01 kg h^{-1} bear errors systematically larger than 100% for all participants' systems and often reach more than 500%. The wind conditions during this smallest release did not appear to be more challenging than during the other releases (wind speed was 2.6 m s^{-1}). Therefore, the low amplitude of this release challenged all types of systems. This shows that this leak rate is below the quantification limit for most techniques. Besides this case, and even considering the 0.1 kg h^{-1} release, the range of errors does not appear to decrease with increasing release rates, consistent with expectations in a high-concentration regime. Thus, the quantification limit for most of the systems appears to lie between 0.01 kg h^{-1} and 0.1 kg h^{-1}.

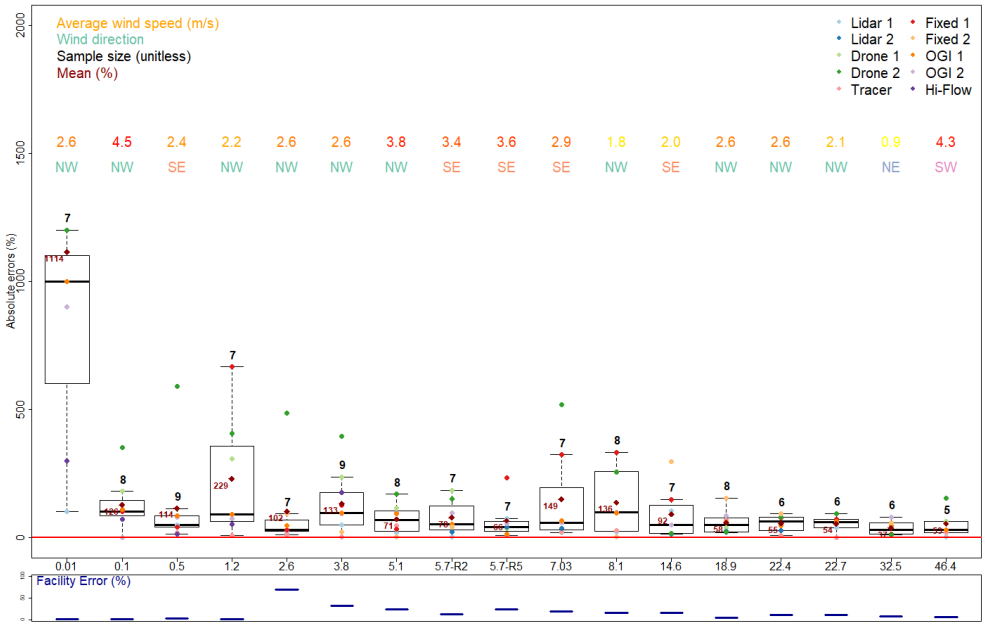

Figure 3.5 Aggregated absolute errors as a function of total release rate. Dot colors correspond to individual participants (top right legend). Whisker plots indicate the median, interquartile range, min, and max (excluding outliers) for each release. The means are also indicated. Average wind speed and direction per release are provided in the upper part of the top panel. The lower panel shows the uncertainty in the CRF rate for each release, with the same scale as the top panel.

Role of wind

The amplitude of the signal and the accuracy of the modeling frameworks are expected to depend strongly on the wind and turbulence conditions, primarily on the wind speed. The wind direction likely plays a role since the positioning of the sensors is constrained by logistical issues due to the potential overlapping or divergence of plumes from different nodes and since some directions drive the plume against or close to obstacles impacting the atmospheric flows. Low wind speed values (below 1 m s^{-1}-2 m s^{-1}) and specific wind direction sectors prevented some participants from providing valid estimates during specific releases. However, once considering the valid estimates, the results do not reveal any clear relationship between the wind speed or direction and the errors. Among the releases for which the errors were significantly larger than for the others is that of 1.2 kg h^{-1} from Node 5 only and that of 8.1 kg h^{-1} from Node 4 only. In these cases the average wind speeds were relatively small and the wind

was blowing from the NW. But better performances were reported for other releases, which were conducted under weaker and/or NW wind. A more thorough examination of individual releases with a high spread in performance is required. Overall, it is likely that improving wind measurement protocols may lead to enhanced accuracy for the leak rate estimates.

Sensitivity to the different types of nodes

In this section, we investigate the influence of specific nodes (with a specific shape, configuration and/or location; see Section 2.1) on the relative errors. Mean absolute errors for single node releases from Node 1, Node 3, Node 4 and Node 5 are 68%, 102%, 113% and 172% respectively (Table 3.5). There was no single release from Node 2 only. Node 5 bears larger absolute errors than other nodes. This might be explained by the dedication of Node 5 to the lowest rates and its proximity to the ground. This position may induce a dispersion that is more complicated to capture.

Some nodes may raise specific issues during multiple node releases e.g. because they are away from the others and thus require extensive sampling (which is notably the case for Node 1). However, we have only seven multiple-node releases, which systematically include Nodes 2 and 4 and exclude Node 5. This limits our ability to get robust conclusion regarding the impact of the presence of specific nodes during multiple node releases.

Table 3.5 Distributions of the mean absolute errors (%) across the available, total release estimates from the different measurement systems for each release.

Nodes	Emission rate (kg/h)	Release ID	Mean absolute errors (participants)
1	5.7	2	78 (7)
1	18.9	7	58 (8)
3	2.6	1	102 (7)
4	3.8	16	133 (9)
4	5.1	10	71 (8)
4	8.1	11	136 (8)
5	0.5	13	114 (9)
5	1.2	3	229 (7)
2&4	5.7	5	66 (7)
2&4	7.03	14	148 (7)
2&3&4	14.6	17	92 (7)

2&3&4	22.4	6	55 (6)
2&3&4	22.7	4	54 (6)
2&3&4	32.5	12	37 (6)
1&2&3&4	46.7	8	53 (5)

Node 1 (the vent stack) is away from the other nodes and raises specific challenges for some systems. In particular, Fixed 1 and Hi-Flow were unable to measure Node 1 due to the low accessibility. Statistics for single-node releases (Table 3.5) showed that the results for releases from Node 1 are better than for other single-node releases. Table 3.6 details the results per measurement system for the releases with emissions from Node 1 only. For those releases, Lidar 1 and Lidar 2 provide estimates with less than 25% absolute errors and other systems can yield more than 50% absolute errors.

Figure 3.6 is similar to Fig. 3.4 but it excludes all releases including Node 1 (i.e. excluding releases #2, #7 and #8). Removing releases including Node 1, increases the range of errors in the available estimates. These results confirm that emissions from Node 1 do not represent a particular challenge for most systems compared to emissions from the other nodes.

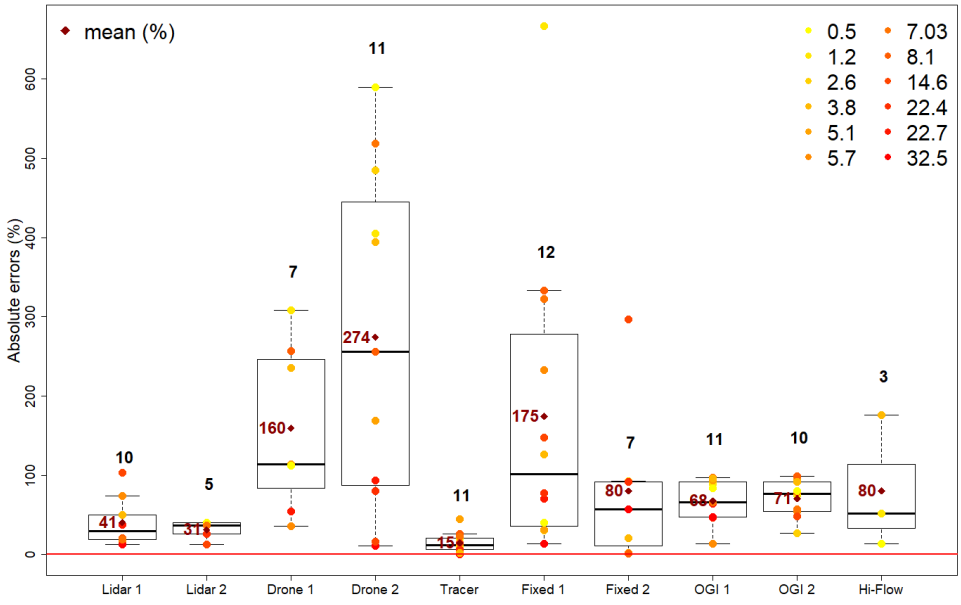

Figure 3.6 Same as Figure 3.4 but excluding vent stack emissions.

Table 3.6 Absolute errors (%) for releases from Node 1 (the vent stack).

Release ID	R2 (5.7 kg h^{-1})	R7 (18.9 kg h^{-1})
Lidar 1	2	20

Lidar 2	21	23
Drone 1	303	94
Drone 2	151	20
Fixed 2	40	154
OGI 1	51	61
OGI 2	95	84
Mean (%)	95	65

Are site-level performances better during single releases compared to multiple releases?

If ignoring the releases of 0.01 kg h^{-1} and 0.1 kg h^{-1}, we have eight single-node releases and seven multiple nodes releases, as shown in Table 1. In general, most measurement systems' total estimates of multiple node releases are better than their estimates of single node releases (6 out of 9 systems, by 70% on average, as shown in Table 3.7). This result is unexpected since, in principle, it is more challenging to sample and properly analyze information on multiple plumes more or less overlapping and arising from more or less distant sources rather than to sample and analyze a single plume from a single source. It is unclear whether this result is statistically robust because of the limited number of data points. For some specific techniques (Lidars and Fixed 2), the opposite is true: single node estimates are more accurate than their total estimates for multiple-node releases.

Table 3.7 Distributions of the mean absolute errors (%) of each measurement system of single-node releases, multiple-node releases, and all releases according to the estimates provided by each participant.

Release Type	Single-node	Number	Multi-node	Number	ALL
Lidar 1	26	7	42	6	33
Lidar 2	28	3	29	4	29
Drone 1	178	7	51	3	140
Drone 2	309	8	146	6	239
Tracer	26	7	11	6	19
Fixed 1	205	6	144	6	175
Fixed 2	52	6	149	2	84
OGI 1	77	8	45	6	63
OGI 2	81	8	60	4	74

Hi-Flow	80	3	NA	NA	80
Mean (%)	106	N/A	75	NA	94

From site level to source level: Node-level performances

This section aims at assessing the potential for mapping and attributing the site-level emissions to different sources (in complement to quantifying the total emissions) in an industrial site, focusing on individual nodes. Such single-node estimates were optionally provided during multiple-node releases by some of the measurement systems, which have the capability to distinguish the signal from the different nodes. In principle, this is a defining feature of source-level systems. However, most site-level techniques had this ability as well. The accessibility of nodes and their location nearby other leaks have conditioned the provision of valid data by participants.

Figure 3.7 compares the collective performance of all techniques at the single node level during single and multiple node releases for all the measurement systems. Multiple-node releases were available for all nodes excluding Node 5. Single node releases were unavailable from Node 2. The quantification systems perform better on average when no other node emits. Node 3 is quantified with a 51% mean error when emitting alone, against 127% when part of a multiple node release. Similarly for Node 4 the mean error during the single releases is 100%, increasing to 124% during multiple node releases. This effect is less obvious for Node 1 (comparing 67% and 71% errors). The generally better performance in quantifying individual nodes when no other node emits is likely linked to the influence of the signal from other emissions in quantifying the individual node. Source-level techniques perform equally well for individual nodes during multiple and single releases. This highlight that good performance in site-level emission quantification does not necessarily imply good performances in individual source-level quantification. This suggests that requirements for leak quantification need to be carefully specified prior to selecting a particular technique.

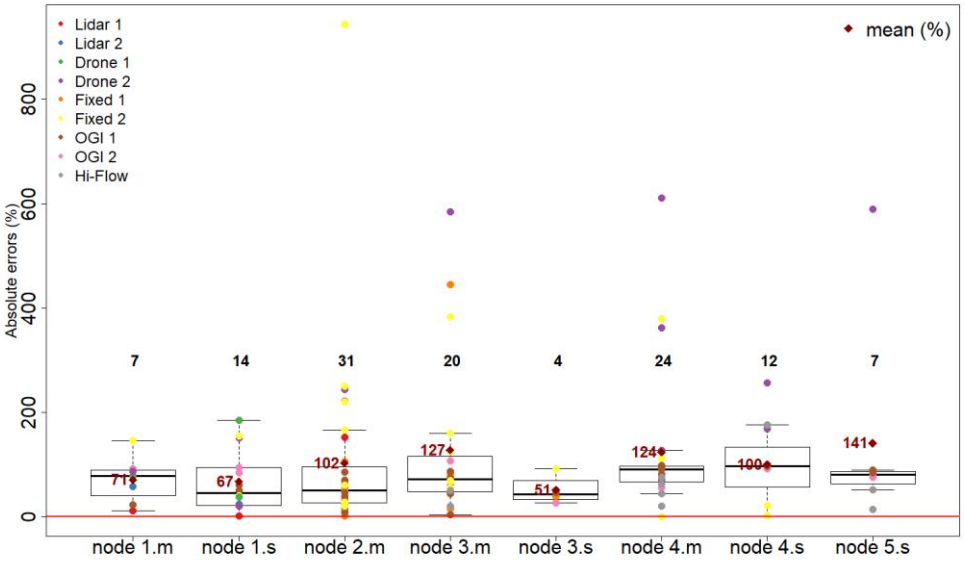

Figure 3.7 Comparison of absolute errors for single node releases (".s") and multiple node releases (".m"). Excluding the releases of 0.1 kg h^{-1} or less. Each point is a participant's node-level estimate.

Focusing now only on single-node estimates during multiple-node releases, absolute errors on individual Nodes 1-4 are 71%, 102%, 127% and 124% respectively. These significantly higher uncertainties for Nodes 2-4 are linked to the fact that they are located in Area B, embedded in a large structure and with a close location of nodes. This directly impacts Nodes 2-4 uncertainties, with the possibility to have influence of the same building structure combined with a possible overlap in plumes dispersion if wind runs parallel to the alignment of these nodes.

Differences in node-level errors during multiple releases across Nodes 2-4 are not statistically significant. There is therefore no obvious detectable influence of the node shape on the performances in the context of multiple releases.

Each technique had specific performances for specific combinations of nodes. Fixed 2 showed relatively larger absolute errors for Area A, and Drone 2 showed relatively larger absolute errors for Area B. OGI measurement systems showed relatively stable and smaller absolute errors than other systems during multiple node releases.

On a more general level, the distinction between source-level and site-level techniques, and their respective advantages appears partially obscured by two elements in our study. Firstly, source-level techniques are not sys-

tematically able to capture all emissions during multiple-node releases due to constraints such as the node configuration and wind speed and wind direction. Secondly, source-level techniques do not perform systematically better than site level techniques even for single nodes. They cannot access some of the nodes (e.g. Node 1, given its position at height). Therefore, this distinction is only moderately able to inform the choice of technology for a given need. Overall, this suggests that combining different source- and site-level techniques might be a useful pathway for a detailed and robust assessment of emissions.

Section 5: Conclusions and implications

We compared performances of currently available quantification systems for midstream industrial fugitive emissions, based on 17 blind controlled release experiments. The controlled releases covered a wide range of situations, such as different flow rates (from 0.01 kg h^{-1} to 50 kg h^{-1}), release heights (ranging from 1 m to 28 m), and different types of the gas outlet (e.g. open-end, ring-shaped and linear). The analysis attempts to identify environmental and configuration factors limiting performances. Although the measurement was conducted under partially controlled conditions, low wind speed and unavoidable interferences between measurement systems have been identified.

Table 3.8 represents a summary of the findings from this study. Most systems have been reportedly correct within an order of magnitude of the controlled release rate. Lidar 2 and Tracer have demonstrated average absolute errors below 50% on more than two-thirds of releases. The best performers are also associated with deployment constraints. Lidar 1 requires the deployment of a helicopter. The mobile ground measurements (e.g. Tracer and Lidar 2) may have difficulties getting access to areas downwind of source emissions based on meteorological and road conditions. Tracer performs well if the acetylene release is well-collocated next to pre-identified leak areas and roads available downwind. Lidar 2, while having minor typical minor errors, had challenges in positioning the truck-based platform under certain wind conditions, and could cover a few releases. The ground-based measurements such as Fixed 1, Fixed 2, and OGI have limited detection distances. Overall, our results show that commercially available systems do provide the ability to quantify fugitive emission rates at a reasonable level of precision. However, there is yet no current possibility of

determining a working standard for quantification since measurement systems are permanently evolving along with estimation methodologies.

Table 3.8 A summary of findings from this study.

Systems	Absolute errors (%)	Provided uncertainty (%)	0.5-2x (%)	0.1-10x(%)	Release coverage (%)
Lidar 1	33	N/A	92	100	88
Lidar 2	29	17	100	100	41
Drone 1	140	55	40	100	71
Drone 2	239	29	36	100	94
Tracer	19	15	92	100	82
Fixed 1	175	13	50	100	82
Fixed 2	84	N/A	78	100	53
OGI 1	63	36	36	79	94
OGI 2	74	N/A	25	69	82
Hi-Flow	80	12	33	100	29

The limited number of releases (17) implemented did not let emerge significant influence from wind speed and node shape. Nodes clustered in Area B and its structure induced more challenging conditions for single node measurements during multiple node releases. More control release experiments are needed to acquire more statistics and test the dependence on a wider range of environmental parameters, especially wind conditions. Careful consideration of the integration of detection along with quantification would be valuable. Sensor precision may play a role in small release rates but likely has a limited influence on the releases above 0.1 kg h^{-1}. There is an apparent random character, mostly technique-dependent, not elucidated in the frame of this experiment, but that could likely be clarified with more data and comparing atmospheric turbulences and building configurations, and controlled gas temperature/injection speed and direction.

Additionally, this study demonstrated that Tracer and Lidar 1 could be independently used for monitoring and quantifying CH_4 emissions. Continuous monitoring and OGIs could be a good combination for continuous and exhaustive CH_4 emission measurement if the deployment of networks is sufficiently dense. Moreover, Lidars and Tracer show better estimates of the total emissions among site-level measurement systems, and OGIs show stable and better estimates of the individual nodes during multiple node releases compared with other source-level measurement systems. Therefore, Lidars/Tracer applied with OGIs together have the potential to obtain not only

accurate estimates of total emissions but also accurate estimates from each node. Further work is needed to determine how these systems can be applied together to reconcile source-level and site-level quantification.

Only Lidar 1 appears to combine the advantage of site-level techniques and source-level precision, albeit at the cost of deploying a helicopter. The distinction between source-level and site-level techniques appears to be mostly a functional one. Most techniques could be considered lying along a continuum between site and source levels, each with its respective merits toward fulfilling the two functions.

In our experiment, the site was positioned in an environment selected for its isolation from other methane sources. In a real-life context with nearby sources (e,g, industrial complex and proximity to agriculture), our assessment of node-level performances in multiple vs. single node releases (Section 4.4) suggests that most techniques would see their performances degraded to some extent, depending on the proximity of the other sources. How close exactly this statement would be true remains to be determined. With the influence of nearby sources, the distinction between low-concentration and high-concentration regimes might not hold. The sensor precision would then be expected to play a role in the ability to discern specific plumes of interest from other nearby sources.

The ambitious OGMP 2.0 Level 5 reporting requires using complementary site-level measurements such as the ones scrutinized in our study. Level 5 is the highest grade and elaborates on top of level 4, a source-level estimate of asset emission. The site selected for our study is considered an archetypal site of the natural gas midstream industry that would be using this reporting. Our study selected state-of-the-art systems currently available and able to perform measurements such as those required by OGMP 2.0 Level 5 reporting. In real-life applications, whether or not these techniques can fulfill the requirements of this reporting depends not only on individual performances, but also on the frequency of deployment and reconciliation methodology. However, we have shown that the definition of ‘site-level’ as considered in Level 5 reporting still represents a challenge for measurement techniques. Level 5 requires reconciliation with the source-level estimate, which should be investigated in future research.

YL performed data synthesis and data analysis, and wrote the manuscript.

The analysis conducted during this inter-comparison has shown that each measurement system has strengths and weaknesses to address different situations and scales. Therefore, relying on several measurement systems seems important while continuing to improve the different measurement systems, eventually extending the scale of relevance and reducing their uncertainties. In this context, it is important that all the relevant spatial scales for emissions can be covered by observation systems. Gaps still exist, requiring the extension of existing methods or the development of new methods. From point-to-site scales, unmanned aerial vehicles (UAV) can help mind the gap between vehicle and airborne measurements. In the following chapter, we present the development and first test of a compact and lightweight UAV system dedicated to atmospheric CO_2 measurements.

4 IMPROVEMENTS OF A LOW-COST CO_2 COMMERCIAL NDIR SENSOR FOR UAV ATMOSPHERIC MAPPING APPLICATIONS

4.1 OVERVIEW

Although systematic atmospheric CO_2 measurements started 60 years ago, contemporary atmospheric CO_2 trends are still under discussion (e.g. Le Quéré et al., 2013, 2018; Friedlingstein et al., 2022). So far, GHG observation networks have been widely set up worldwide including various measurement platforms and techniques, as discussed in the first chapter. Recently, mobile platforms have been developed to study specific emitters or sources (e.g. Chapter 3). A large part of anthropogenic CO_2 is emitted from point emission sources. To monitor CO_2 emissions at these smaller scale locations, such as industrial establishments and urban areas, an appropriate sensor for UAV platforms has the potential to provide independent CO_2 measurements across these source plumes to quantify emission rates (Pinty et al., 2017; Reuter et al., 2021; Kunz et al., 2018), bridging thus the gap between vehicle (car) and aircraft observations. However, until now, only a few calibrated CO_2 measurements have been reported in the literature, and more importantly, very few studies among them could reach a CO_2 measurement accuracy below 2 ppm with a payload below 2 kg on board UAVs (Kunz et al., 2018; Chiba et al., 2019; Reuter et al., 2021). In addition, it is still challenging to have stable and high-frequency measurements against rapid changes in pressure and temperature, which is also the main reason for limited UAV-CO_2 measurements.

As a part of this topic, a cost-effective, compact, light weight CO_2 measurement system has been developed. It runs at high frequency (1 Hz) with good accuracy (within 1 ppm) and can be widely applied on different UAVs. This chapter describes the integration and validation of this portable CO_2 sensor system. Before the integration, the accuracy and linearity of the low-cost commercial CO_2 sensor (Senseair AB, Sweden) based on nondispersive near-infrared (NDIR) were ensured with a series of laboratory tests. In the laboratory, a Picarro model G2401 instrument (Picarro, USA) based on cavity ring-down spectroscopy (CRDS) (Crosson, 2008) was used as a reference instrument. The laboratory tests included i) calibrations to

determine the sensors' stability, ii) calibration functions that link the measured values to assigned values, and iii) Allan deviation tests to determine sensors' precision for 1 Hz. The above process concluded that the precision of the CO_2 sensor remains within ±1 ppm (1σ) at 1 Hz.

Moreover, temperature and pressure sensitivity tests were performed in a closed automated climate chamber. The temperature ranged from 0 °C to 45 °C, and pressure ranged from 600 hPa to 1000 hPa. These tests determined the linear response of SaA and SaB sensors against temperature and pressure. As an outcome, it is highly recommended to characterize every individual sensor at least once before any use and repeat regularly (e.g. annually) these tests as sensor performance tends to change over time.

For the evaluation, the system was also installed into a manned aircraft to validate the system in ambient conditions. Direct comparison with a Picarro model G2401-m as a reference instrument onboard the same aircraft was performed. This experiment showed that the sensors' precision during the flights was within 2 ppm (1σ) at 1 Hz, a number larger than the precision calculated during the laboratory tests. This degradation was expected due to less optimal measurement conditions. Then the CO_2 sensor was integrated into a quad-rotor to evaluate and validate the sensor's performance on board UAVs. The CO_2 setup weighs 1058 g with dimensions of 15 cm × 9.5 cm× 11 cm, including the battery. The sampled air first passed through a 15 cm customized cartridge filled with magnesium perchlorate ($Mg(ClO_4)_2$), sufficient to dry air, and then through a membrane filter to remove particles. A diaphragm micro-pump drove the gas line to the CO_2 sensor. Temperature and relative humidity were continuously monitored via a Rotronic HC2-ROPCB sensor. A 12 V DC supply powered the integrated system. During the validation flights, a time-dependent correction, based on running time, was calculated and applied for calibration sequences. Practically, this correction was applied to obtain flight-specific calibration response curves according to the sensor running time and confirmed by the target linear drift.

As a proof of concept, intensive flights using the developed UAV CO_2 sensor system were performed in the urban area of Nicosia (Cyprus) and are presented here. The field campaign was performed from early morning 0600 local time to late afternoon 1730 local time. Mole fractions of CO_2 up to 440 ppm (20 ppm above the background levels) were detected during the morning traffic rush hour, attributed to emissions from a major road located

southwest of the flight path. In addition, the system also revealed its ability to capture the temporal variability of the vertical CO_2 gradient between the surface and the lower atmosphere. A detailed description of this field campaign is shown in the next subsection. It is also shown that the system is easily to be reproduced, enabling a wide range of field applications, such as urban and point-source emissions monitoring.

In conclusion, the designed system demonstrated its ability to measure fast CO_2 mole fraction changes and spatial gradients, to provide accurate plume dispersion maps. It proved to be a good complementary measurement tool to the in-situ observations performed at the surface. The targeted and potential applications include emissions estimates, stack emission factor measurements and mapping CO_2 distribution in mixed natural-urban environments.

This chapter has been published as Liu, Y., Paris, J.-D., Vrekoussis, M., Antoniou, P., Constantinides, C., Desservettaz, M., Keleshis, C., Laurent, O., Leonidou, A., Philippon, C., Vouterakos, P., Quéhé, P.-Y., Bousquet, P., and Sciare, J.: Improvements of a low-cost CO_2 commercial nondispersive near-infrared (NDIR) sensor for unmanned aerial vehicle (UAV) atmospheric mapping applications, Atmos. Meas. Tech., 15, 4431–4442, https://doi.org/10.5194/amt-15-4431-2022, 2022. The supplement related to this chapter refers to Appendix B.

4.2 PUBLICATION: IMPROVEMENTS OF A LOW-COST CO_2 COMMERCIAL NONDISPERSIVE NEAR-INFRARED (NDIR) SENSOR FOR UNMANNED AERIAL VEHICLE (UAV) ATMOSPHERIC MAPPING APPLICATIONS

Improvements of a low-cost CO_2 commercial NDIR sensor for UAV atmospheric mapping applications

Yunsong Liu[1,2], Jean-Daniel Paris[1,2], Mihalis Vrekoussis[2,3], Panayiota Antoniou[2], Christos Constantinides[2], Maximilien Desservettaz[2], Christos Keleshis[2], Olivier Laurent[1], Andreas Leonidou[2], Carole Philippon[1], Panagiotis Vouterakos[2], Pierre-Yves Quéhé[2], Philippe Bousquet[1], Jean Sciare[2]

[1]Laboratoire des Sciences du Climat et de l'Environnement, CEA-CNRS-UVSQ, UMR8212, IPSL, Gif sur Yvette, 91191, France
[2]Climate and Atmosphere Research Center (CARE-C), the Cyprus Institute, Nicosia, 2113, Cyprus
[3]Institute of Environmental Physics and Remote Sensing (IUP) & Center of Marine Environmental Sciences (MARUM), University of Bremen, Bremen, D-28359, Germany

Correspondence to: Yunsong Liu (yunsong.liu@lsce.ipsl.fr)

Abstract

Unmanned Aerial Vehicles (UAVs) provide a cost-effective way to fill in gaps between surface in-situ observations and remote-sensed data from space. In this study, a novel portable CO_2 measuring system suitable for operations on-board small-sized UAVs has been developed and validated. It is based on a low-cost commercial nondispersive near-infrared (NDIR) CO_2 sensor (Senseair AB, Sweden), with a total weight of 1058 g, including batteries. The system performs in situ measurements autonomously, allowing for its integration into various platforms. Accuracy and linearity tests in the lab showed that the precision remains within ±1 ppm (1σ) at 1 Hz. Corrections due to temperature and pressure changes were applied following environmental chamber experiments. The accuracy of the system in the field was validated against a reference instrument (Picarro, USA) onboard a piloted aircraft and it was found to be ±2 ppm (1σ) at 1 Hz and ±1 ppm (1σ) at 1 min. Due to its fast response, the system has the capability to measure CO_2 mole fraction changes at 1 Hz, thus allowing the monitoring of CO_2 emission plumes and the characteristic of their spatial and temporal distribution. Details of the measurement system and field implementations are described to support future UAV platform applications for atmospheric trace gas measurements.

Section 1: Introduction

According to the IPCC (2021), the global mean temperature will increase by at least 1.5 °C in the next 20 years relative to the pre-industrial period for all scenarios. This warming, attributed to human activities, is driven by the increased emissions of heat-trapping greenhouse gases (GHGs) in the atmosphere. Impacts of global warming, such as heatwaves, extreme precipitation events, sea-level rise and biodiversity loss are already visible, affecting human societies and natural ecosystems (IPCC 2018;

Khangaonkar et al., 2019). Because of its importance, global warming has become one of the most critical challenges of the 21st century from both a scientific and societal perspective. To tackle global warming, almost all members of the United Nations agreed to join forces to keep the warming below 2 °C (ideally 1.5 °C) under the Paris Agreement of 2015. This agreement intensifies the need to strengthen our capability of having high-quality and accurate observations of atmospheric GHG at all scales including local, regional and global measurements both at the surface and vertically resolved. Atmospheric concentration measurements from various platforms can therefore be used to estimate emissions at different scales.

Carbon dioxide (CO_2) is the most abundant, human-released GHG, in the atmosphere. Notably, the CO_2 mole fraction recently reached a new high in 2020 of 413.2 ± 0.2 μmol mol^{-1} (ppm), which is 49% over its pre-industrial level (WMO, 2021). About 90% of total CO_2 emissions emanate from fossil fuel combustion, with around 26% of it being taken up by the oceans and 30% by land surfaces (Friedlingstein et al., 2021).

Systematic in-situ ground-based measurements of CO_2 started in 1958 in Mauna Loa in Hawaii (Pales and Keeling, 1965). Since then, in-situ measurements at many locations but also from various mobile platforms (e.g., cars and ships) have significantly improved our knowledge of the CO_2 spatial and temporal distribution (Daube et al., 2002; Agustí-Panareda et al., 2014; Liu et al., 2018; Defratyka et al., 2021; Paris et al., 2021). Throughout time, in-situ measurements have been complemented by remote sensing providing space-based global observations of CO_2 column-averaged mole fraction data and ground-based remote sensing observations from various instruments (Bovensmann et al., 1999; Wunch et al., 2011; Turner et al., 2015; Jacob et al., 2016; Wunch et al., 2017; Frey et al., 2019; Suto et al., 2021). Meanwhile, CO_2 instrumentation onboard airborne platforms have been developed in the past 20 years (e.g. Watai et al., 2006; Sweeney et al., 2015). These measurements are meant to fill the gap between ground-based observations and remote sensing space-based observations to better represent CO_2 spatial distribution at large scales. However, manned (piloted) aircraft which can carry standard analyzers are costly and complex to organize, requiring frequent maintenance (Berman et al., 2012b; Bara Emran et al., 2017b). Furthermore, at smaller geographical scales (landscape, industrial assets, urban area), manned airborne platforms have strong limitations and cannot fly at low speed in all areas. UAVs have been

demonstrated to be useful to detect and map emission plumes of other trace gases because of their ability to operate at very low speed/altitude and with slow cruising speeds (e.g. Barchyn et al., 2017). Additionally, UAVs, unlike piloted aircraft, can operate over hazardous areas such as volcanic eruptions and forest wildfires. Actually, high-precision calibrated CO_2 instruments have been deployed in manned aircraft (e.g. Paris et al., 2008; Xueref-Remy, et al., 2011; O'Shea et al., 2014; Pitt et al., 2018; Barker et al., 2020), but they are too heavy, large and expensive for UAV applications. However, until now very few calibrated CO_2 measurements have been reported in the literature (Kunz et al., 2018) due to the challenge of measuring this species with sufficient precision.

A large part of the anthropogenic CO_2 originates from point emission sources such as power plants burning fossil fuels (Pinty et al., 2017; Reuter et al., 2021). An appropriate sensor for UAV platforms would have the potential to provide independent CO_2 measurements across these source plumes to verify mitigation strategies. Often the CO_2 signals of strong emitters can be mixed with strong biospheric signals even at local scales. In addition, the planetary boundary layer (PBL) dynamics can strongly influence atmospheric concentrations. It is therefore important to separate the influence of exogenic factors and isolate the contribution from targeted emission plumes. Another potential application of a UAV-CO_2 system is to document the spatial distribution of CO_2 around fixed observations. Watai et al. (2006) argued that UAVs have the potential to provide measurements close to the surface and inside the PBL complementary of data obtained from fixed observatories such as tall towers, and make frequent and simultaneous measurements in multiple locations at low cost. In this case, UAV measurements help separate signal variability into a large-scale footprint of ground stations and variability due to local influences. Despite these challenges, there have been ongoing efforts to develop compact, lightweight, and low-powered GHG sensors, able to be integrated into UAVs to address these needs. Berman et al. (2012b) developed a highly accurate UAV greenhouse gas system (but heavy: 19.5 kg) for measuring carbon dioxide (CO_2) and methane (CH_4) mole fraction. Malaver et al.(2015b) integrated a non-dispersive infrared (NDIR) sensor (3285 g) for CO_2 measurement into a solar-powered UAV for effective 3D monitoring. Kunz et al. (2018) reported the development of a high accuracy (±1.2 ppm) CO_2 instrumentation well-suited for UAVs. However, the commercial CO_2 sensor used in the study was disassembled and redesigned, making it

difficult to replicate widely. Allen et al (2019b) applied a UAV-CO_2 sensor system to infer a landfill gas plume. Chiba et al. (2019) developed a UAV system (2.7 kg) to measure regional CO_2 mole fraction and obtain vertical distributions within 1.75 ppm standard deviation over a farmland area and deduced vegetation sink distribution from their results. More recently, Reuter et al. (2021) developed a lightweight (about 1.2 kg) UAV system to quantify CO_2 emissions of point sources with a precision of 3 ppm at 0.5 Hz. Moreover, very high-precision and commercial sensors (<0.2 ppm 1σ at 1 Hz) for UAV applications are emerging currently such as the ABB light Micro-portable Greenhouse Gas Analyzer (pMGGA) (Shah et al., 2020). However, the weight (about 3 kg) is much larger and the price is more expensive compared to the NDIR sensors mentioned in the above literature.

These works have faced the difficulty to miniaturize high-precision, fast-response CO_2 sensors. Few studies among them could reach a CO_2 measurement accuracy below 2 ppm with light payload (2 kg) on board UAVs. It is also challenging to have stable and high-frequency measurements against rapid changes in pressure and temperature, which is also the main reason for UAV-CO_2 measurements not being widely applied. Therefore, this study aims to develop a cost-effective, compact, lightweight CO_2 measurement system with high frequency and accuracy that can be widely used in different UAV applications. Targeted applications include emission estimates from point sources, stack emission factor measurements, as well as mapping CO_2 distribution in mixed natural/urban environments.

Towards this goal, a portable CO_2 sensor system has been developed based on a low-cost commercial NDIR CO_2 sensor (Senseair AB, Sweden). Prior to integration, the accuracy and linearity of the instrument were ensured with a series of laboratory tests. The performance of the system was validated during laboratory (chamber) and ambient conditions. For the latter, the system was installed onboard a manned aircraft and unmanned aerial vehicle platforms. As a proof of concept, intensive flights of the developed UAV-CO_2 sensor system were presented in the urban area (Nicosia, Cyprus). It is shown that our system is easy to be reproduced, enabling a wide range of field applications, such as urban and point-source emissions monitoring. Moreover, the system developed in this study has the potential to accommodate other sensors to make stack emission ratio measurements.

Section 2: Methodology

2.1 CO_2 sensor

The sensor used in this study is a non-dispersive near-infrared (NDIR) sensor from SenseAir AB based on their High-Performance Platform (HPP) 3.2 version for sub-ppm gas detection. These sensors measure the molar fraction of CO_2 in the optical cell based on IR light absorption, based on the Beer-Lambert law (Barritault et al., 2013). The multi-pass cell of the sensor provides eight roundtrips of the beam with a total path length of 1.28 m. Temperature-controlled molded optics in the sensors are used to keep the temperature of the sensor cell constant to prevent condensation on the mirrors (Hummelga˚rd et al., 2015). This study involved two CO_2 sensor units using this technology (named SaA and SaB hereafter). More information on the sensor can be found in Arzoumanian et al. (2019).

2.2 Laboratory tests

The schematic diagram of the measurement setup used for laboratory testing is shown in Fig. 1. In this setup, the sampled air first passes through a 15 cm cartridge filled with magnesium perchlorate ($Mg(ClO_4)_2$), which is sufficient to dry air at a room temperature (24 ˚C) and a flow rate of 500 ml min-1 to a water mole fraction of 20 ppm for 2 h; and then through a 0.5 μm membrane filter to remove particles. A diaphragm micro-pump (GardnerDenverThomas, USA, Model 1410VD/1.5/E/BLDC/12V) drives the air through the gas line towards SaA and SaB. Temperature and relative humidity are continuously monitored via a SHT75 sensor placed between the micro-pump and the two sensors. Finally, a Raspberry Pi3 acquires the data from all the sensors. The integrated system is powered by a 12 V DC supply, isolated from the UAV power system. Parallel to the two sensors, a Picarro model G2401instrument (Picarro, USA) based on cavity ring-down spectroscopy (CRDS) (Crosson, 2008) served as a reference instrument in this setup (see Figure 4.1).

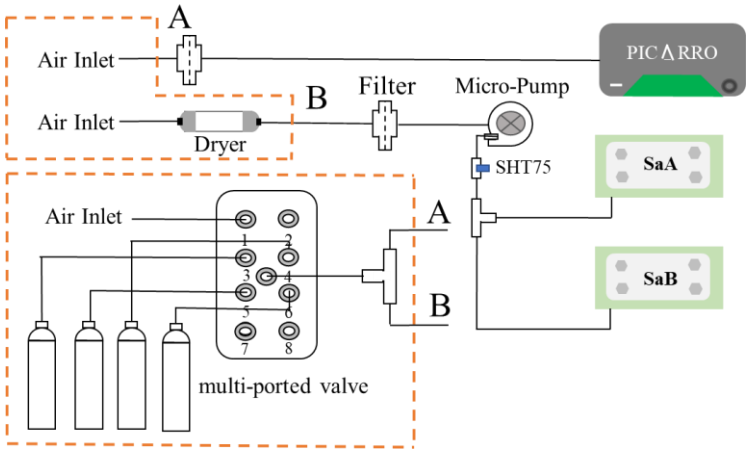

Figure 4.1 The schematic of the developed system for lab tests and field deployment (A and B represent air flows to G2401 and CO_2 sensors, respectively).

Figure 4.2 presents the data quality control procedure flow-chart. SaA and SaB were firstly tested in the metrology laboratory of the Integrated Carbon Observation System (ICOS) Atmosphere thematic center (ICOS ATC). Then the system was integrated into a manned aircraft and UAVs to be validated and evaluated under ambient conditions. Table 4.1 is a summary of all the laboratory and field tests performed for the system, and all results are presented in Section 3. In the laboratory, four calibration sequences were performed to determine the calibration function that linked the measured values to the assigned values (Yver Kwok et al., 2015a). Four high-pressure calibration standard gas cylinders with known amounts of CO_2, ranging from 380.096 ppm to 459.773 ppm, were used. The standard gases were calibrated using the international primary standard for GHG, maintained in NOAA CMDL, Boulder, Colorado, USA (www.esrl.noaa.gov/gmd/ccl/). To ensure stabilization after adequate flushing of each sensor's cell with CO_2, each standard gas ran for 30 min continuously and only the last 10 min of data were used. Then the calibration function using a linear fit was calculated for the sensors and the Picarro instrument. The cylinder with 459.773 ppm CO_2 was considered to resemble ambient atmospheric conditions. During the Allan Deviation test (Hummelga˚rd et al., 2015), the CO_2 sensors continuously measured a cylinder filled with dry air for 24 h.

Temperature (T) and pressure (P) sensitivity tests were performed in a closed automated climate chamber at the Observatoire de Versailles Saint-

Quentin-en-Yvelines (OVSQ) Guyancourt, France, using the Plateforme d'Integration et de Tests (PIT). The temperature (from -60 ˚C to 100 ˚C) and pressure (from 10 hPa to 1000 hPa) ranges inside the chamber can be controlled and supervised by the Spirale 2 software (https://www.ovsq.uvsq.fr/essais-thermiques). We implemented repeated sequences of variable temperature and pressure following (Arzoumanian et al., 2019). These tests allow determining the linear response of SaA and SaB sensors against temperature and pressure (as shown in Section 3.2).

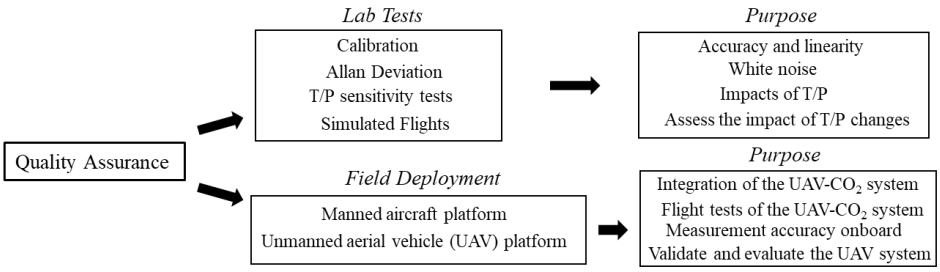

Figure 4.2 The flow chart of data quality control procedures.

Table 4.1 A summary of the laboratory tests and field deployment.

Code name	Name	Purpose	Parameters	Range of T (℃) and P (mbar)	Duration (h)	Sensors tested
CA	Calibration	Test calibration frequency and stability	CO_2	N/A	8	SaA, SaB
AD	Allan Deviation	Illustrate white noise, stability and detection limit	CO_2	N/A	24	SaA, SaB
PT1	Temperature and pressure sensitivity tests	Correlation between CO_2 and P/T	T, P	0-45 and 600-1000	72	SaA, SaB
PT2	Temperature and pressure sensitivity tests	Correlation between CO_2 and P/T	T, P	0-45 and 600-1000	72	SaB
SF1	Simulation flight	Estimate P/T impact	T, P	15-25 and 800-1000	4	SaB
SF2	Simulation flight	Estimate P/T impact	T, P	15-35 and 600-1000	10	SaB
Aircraft Test	Manned aircraft Test	Estimate precision onboard	T, P, CO_2	Real flight conditions	2.5	SaA, SaB
UAV Test	UAV Test	Test and evaluate the system on UAVs	T, P, CO_2	Real flight conditions	~0.3	SaB

2.3 Aircraft test

After a series of laboratory tests, the sensors were moved to a manned

aircraft together with a reference instrument Picarro G2401-m to test the performance of SaA and SaB under real atmospheric conditions.

SaA, SaB and a reference Picarro instrument G2401-m were flown onboard a manned aircraft on April 8, 2019 in the vicinity of Orleans forest (150 km south of Paris), France. All instruments were calibrated using standard cylinders from ICOS-ATC before and after the flight (Hazan et al., 2016). The setup used and the aircraft are shown in S1. These flights aimed to confirm the accuracy of SaA and SaB in real flight conditions.

2.4 Unmanned Aerial Vehicle (UAV) system integration

Then, for further validation the system was miniaturized and integrated into a small-size Unmanned Aerial System (UAS), developed at the Unmanned Systems Research Laboratory (USRL) of the Cyprus Institute (CyI) (https://usrl.cyi.ac.cy/). The components of the integrated system are shown in Fig.4.3a. The CO_2 sensor setup weighs 1058 g with dimensions of 15 cm × 9.5 cm × 11 cm, including the battery. A 15 cm customized cartridge replaced here to reduce volume and weight. The impact of water vapor dilution on dry CO_2 mole fraction is within 40 ppb by using the dryer. It does not depend on external systems, allowing for its integration into various small UAVs. The system was successfully integrated into the USRL small-sized quad-rotor UAS (Fig. 3b), optimally developed in terms of minimum size and maximum performance, to accomplish the desired CO_2 unmanned measurements. Multi-rotors allow vertical take-off and landing (VTOL) in urban and remote regions (Kezoudi et al., 2021). The UAS has up to 30 min flight endurance for atmospheric measurements with the selected sensor. In order to improve accuracy and response time for in-fight temperature measurements (critical for CO_2 correction), a Rotronic HC2-ROPCB sensor (Rotronic, Switzerland) replaced the SHT75 sensor. To validate the system on site, calibration sequences were performed before and after the flights in the laboratory. In addition, a target gas cylinder was performed for 20 min between each flight to determine and correct the instrument’s drift over time.

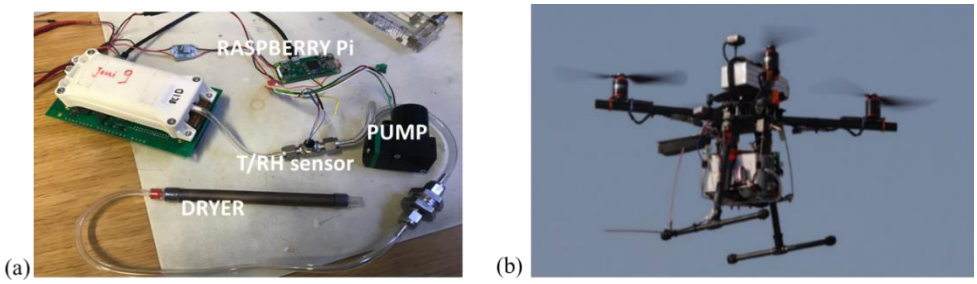

Figure 4.3 Components of the portable CO_2 sensor system setup (a) and the selected UAV (b).

Section 3: Results

3.1 Sensor calibration

The response curves obtained from the CO_2 calibration are shown in S2. The stability of successive CO_2 calibrations is shown in Fig.4.4, which presents the difference between CO_2 mole fraction measured by sensors and CO_2 mole fraction assigned to each calibration cylinder. The biases of SaA and SaB against the four calibration standards are negative and positive, respectively, during the calibration (Fig.4.4). Additionally, the biases increased by 0.2 ppm on average between calibration sequences (2 h of each sequence). This drift against sensors' running time is further investigated and validated in the field deployment (Section 3.4). The result of the Allan Deviation (AD) test is shown in S3. The plot shows the stability as a function of integration time (Hummelga˚rd et al., 2015). The unfiltered data were used from HPP data set. The precision improved by increasing the integration time. However, the sensors were intended for mobile platforms, their performance at 1 Hz was chosen as the most significant. The precision is respectively ± 0.36 ppm (1σ) and ± 0.85 ppm (1σ) for SaA and SaB at 1 Hz (S3), which shows the precision of the sensors in the laboratory is below 1 ppm (1σ) at 1 Hz.

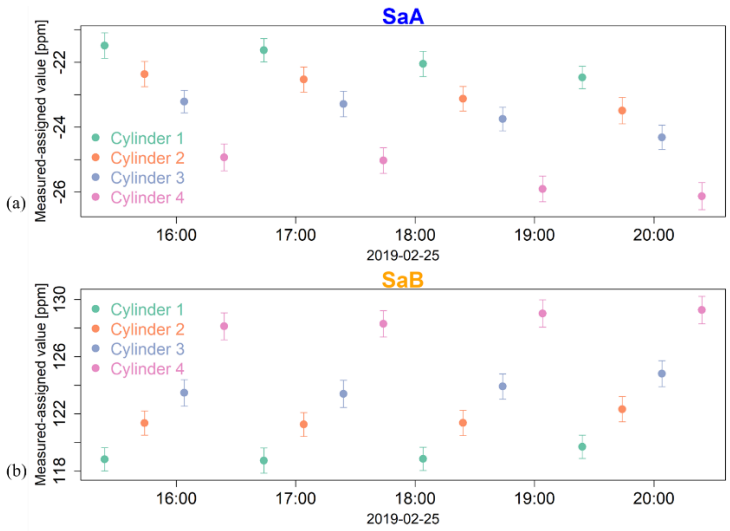

Figure 4.4 Stability of successive CO_2 calibrations for SaA (a) and SaB (b), the error bars represent the standard deviation of 2-second averages.

3.2 Temperature and pressure dependence

3.2.1 Temperature sensitivity test

During temperature sensitivity tests, the chamber pressure was kept constant at 950 hPa, while the temperature was gradually changed, as seen in S4. The temperature ranged between 0 ˚C and 45 ˚C, following 9 ˚C increment steps, lasting for 20 min. The sensors' cell temperature exhibited an unstable behavior for chamber temperatures below 25 ˚C, while it was stable, at approximate 57 ˚C, for chamber temperatures above 25 ˚C. However, SaA and SaB behaved oppositely when their cells' temperature changed. Therefore, two scenarios were considered for both sensors.

The first scenario is when the analyzer's cell temperature is stable while the ambient air temperature changes (above 25 ˚C). The trend coefficients of CO_2 mole fraction over ambient temperatures were -0.564 and -0.527 for SaA and SaB, respectively (shown in Fig.4.5a and Fig.4.5c). The second scenario is when both the analyzer's cell and ambient temperatures change simultaneously. In this case, the impact of ambient air temperature changes obtained from the first scenario has been corrected prior to considering the cell temperature changes. The trend coefficients of CO_2 mole fraction over cell temperatures were -0.979 and 0.378 for SaA and SaB, respectively (shown in Fig.4.5 b and d). Consequently, SaA performed better when applying the temperature sensitivity test (high R^2, lower standard error).

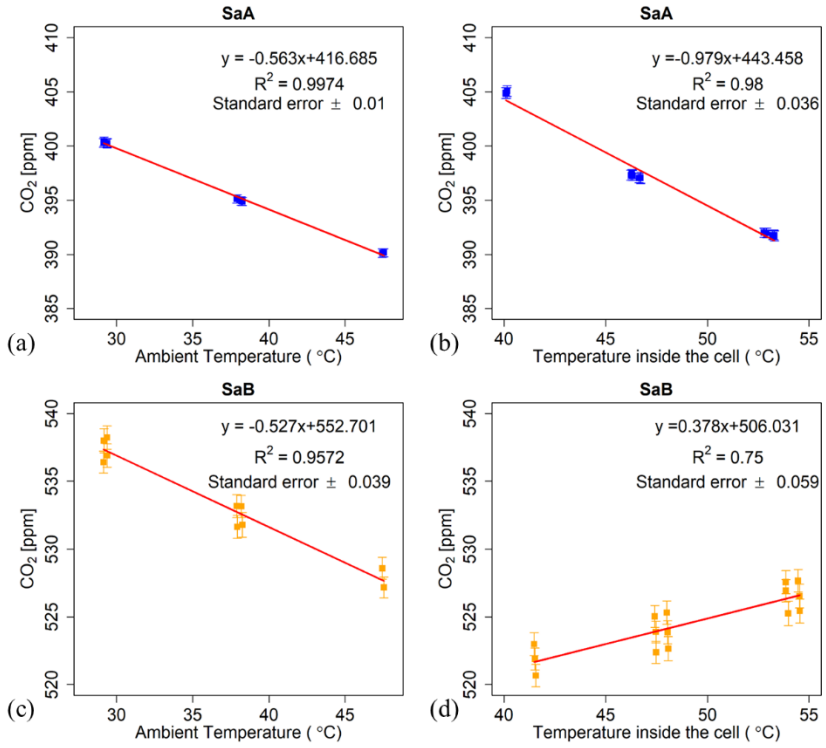

Figure 4.5 Temperature sensitivity tests in the environment chamber, (a) and (c) represent the first scenario, (b) and (d) represent the second scenario.

3.2.2 Pressure sensitivity test

During the pressure tests, the chamber temperature was maintained at 25˚C, and pressure ranged from 600 hPa corresponding to 3 km above sea level (ASL) to 1000 hPa in 100 hPa steps, repeated twice. SaA and SaB performed significantly differently in this test, with the SaB sensor showing increased sensitivity to pressure changes (Fig.4.6). Generally, the sensors have an internal pressure correction from the manufacturer and it is not implemented to SaB apparently. However, SaB performed better in the pressure sensitivity test, with tighter linearity (higher R^2) when both tests were accounted for.

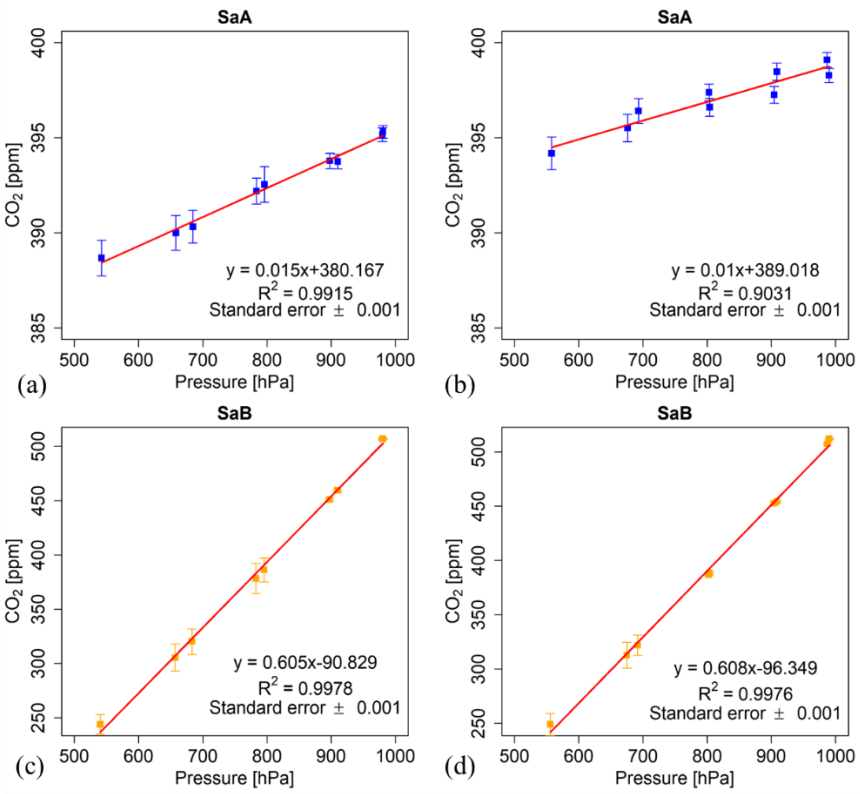

Figure 4.6 Pressure sensitivity tests in the environment chamber, (a) and (b) represent SaA results of the repeated pressure tests, (c) and (d) represent SaB results of the repeated pressure tests.

From the sensitivity tests presented above, we derived the following equations for both sensors:

SaA: $C_{cor}=C_{obs}+0.564\times(Ta-Ta_0)+0.979\times(Tc-Tc_0)-0.013\times(P-P_0)$ (Equation 1)

SaB: $C_{cor}=C_{obs}+0.527\times(Ta-Ta_0)-0.378\times(Tc-Tc_0)-0.607\times(P-P_0)$ (Equation 2)

Where C_{cor} is the mole fraction after corrected for P/T changes. C_{obs} is the observed mole fraction. Tc represents the analyzer's measurement cell temperature and Tc_0 is the original cell temperature at the start of the measurements. Ta represents the ambient temperature and Ta_0 is the ambient temperature at the start of the measurement. P represents the ambient pressure and P_0 is the ambient pressure at the start of the measurements. The equations are also applied for calibrations.

Replications of temperature and pressure sensitivity tests for SaB at a later stage showed high consistency with the initial results presented above. Both sensors have shown different responses in the tests. Therefore, it is essential to perform both temperature and pressure sensitivity tests for individual sensors to obtain their individual correction equations against temperature and pressure changes. Here, we highly recommend to characterize every individual sensor at least once before any use. We also recommend to repeat regularly (e.g. annually) these tests as sensor performances tend to change over time.

3.3 Mannued aircraft test results

SaA and SaB measured consistently with the Picarro G2401-m for atmospheric pressure above 800 hPa (equal to 1.5 km ASL) (see Fig.4.7a). Their precision was ±1.4 ppm (1σ) and ±1.7 ppm (1σ) at 1 Hz, 0.78 ppm (1σ) and ±1.1 ppm (1σ) with minute averaged data respectively (Fig.4.7b), larger than the precisions calculated during the laboratory tests. This degradation was expected due to less optimal measurement conditions. Therefore, the test on the piloted aircraft shows sensors' precision onboard under the real flight condition is within 2 ppm (1σ) at 1 Hz and improves to about 1 ppm (1σ) with minute averaged data.

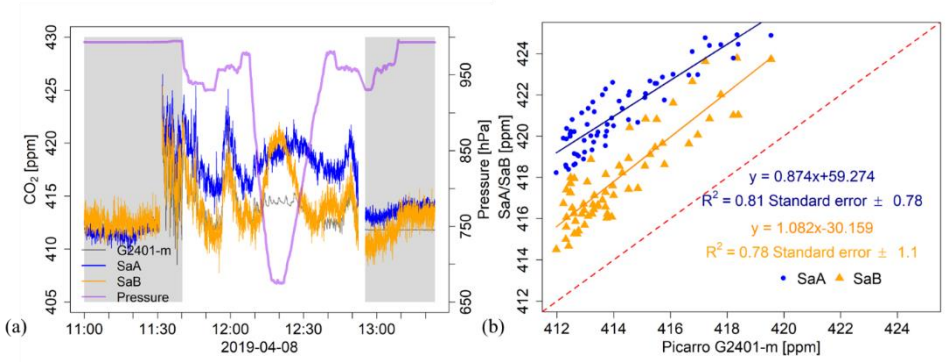

Figure 4.7 Manned aircraft results, (a) is the time series and the grey shaded parts present measurements on the ground and measurements of the gas cylinder; (b) is the correlation between CO_2 sensors and G2401-m.

3.4 Unmanned Aerial Vehicle (UAV) tests and validation

SaB was chosen for field deployments due to technical issues with SaA. SaB was integrated into a quad-rotor to evaluate and validate the performance of the sensor onboard a UAV platform during flights. The flight path was over the Athalassa National Forest Park (35.1294˚ N,

33.3916˚ E) in Nicosia, Cyprus (Fig.4.8). Four flights were performed on June 10, 2021 from 1500 to 1800 LT. The procedure was the following: calibration response curves were obtained before and after the flights. A target gas cylinder was measured for 20 min between each flight to characterize the instrument drift. The sensitivity correction Eq. (2) was then applied to the raw data. It was noted that the measured target gas mole fraction drifted linearly throughout the day (S5a). To account for that, a time-dependent correction, based on running time, was calculated and applied for calibration sequences (S5a). Practically, this correction was applied to obtain flight-specific calibration response curves according to the sensor running time and confirmed by the target linear drift (S5).

Reference CO_2 measurements were additionally conducted with another Picarro G2401 on the roof of the Novel Technologies Building (NTL) at the Cyprus Institute (CyI) (Fig.8), at 174 m ASL, 1.82 km northwest upwind from the UAV launching location (187 m ASL). Therefore, the flight path was downwind from the Picarro G2401. The residual values of CO_2 between Picarro and UAV-CO_2 systems varied from 0.2 ppm to 2.1 ppm (median =1.1 ppm) during the experiment.

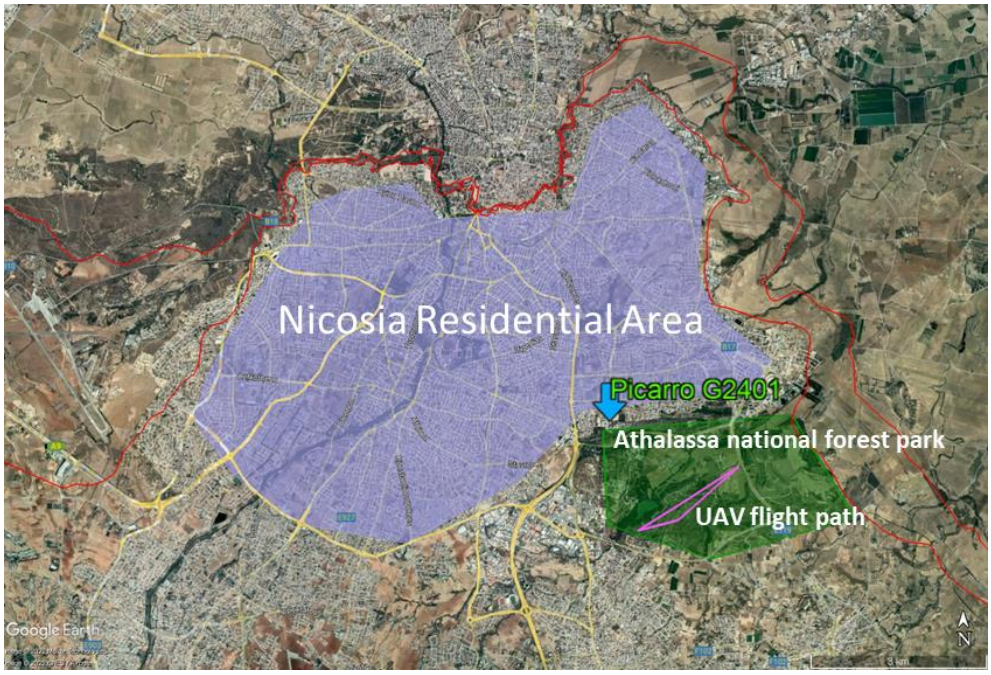

Figure 4.8 The map presents the locations of the Picarro G2401 at CyI, the UAV flight path, Athalassa National Forest Park and the residential area in Nicosia (© Google Earth 2022).

Section 4: Case study for CO_2 measurements in urban environment (Nicosia)

The field campaign to test operation in real conditions of our UAV CO_2 system was performed on May 14, 2021 from early morning 0600 (LT) to late afternoon 1730 (LT). It took place above the Athalassa National Forest Park located southeast of CyI in Nicosia, where 16 flights were performed. Each flight lasted approximately 15 min with most of the flight performed at a constant altitude of 50 m and 100 m above ground level (AGL) alternatively. The altitudes were determined following security rules. Firstly, the UAV had to maintain a safe distance above the treeline of the forest park. Therefore, the lowest safe altitude to fly the drone was 50 m AGL. Secondly, the ceiling of the UAV-CO_2 flights was decided to 100 m AGL, following the European regulations (2019/947 and 2019/945) for UAV operations in sparsely populated areas (open category A2), with flights permitted up to 120 m AGL. The two selected altitudes were used alternatively in order to obtain representative measurements for either horizontal "mapping" or vertical gradients. The vertical gradients were completed at lower altitudes by rooftop measurements in a nearby building. CO_2 mole fractions, as well as meteorological conditions, were measured during the flights on the roof of NTL at CyI. CO_2 measurements were done using a Picarro G2401 (174 m ASL, 16 m AGL, 35.141˚ N, 33.381˚ E); wind speed and wind direction were measured using a sonic anemometer Clima Sensor US model 4.920x.x0.00x with a resolution of wind speed 0.1 m s^{-1} and wind direction 1 ˚.

Each pair of 50 m and 100 m altitude flights lasted approximately 1 h (including flight time and the time needed to change the dryer and battery on the ground). The 15 cm cartridge filled with magnesium perchlorate ($Mg(ClO_4)_2$) was changed every two flights. The first six flights (three pairs) were performed continuously from 0600 to 0900 (LT), as well as the last six flights from 1500 to 1730 (LT). In between, four flights (two pairs) took place between 1000 and 1100 (LT) and between 1300 and 1400 (LT).

According to the meteorological station data, the wind direction in the morning (before 0800 LT) was from the northwest, with an average wind speed of 1.2 m s^{-1}. Then the wind direction shifted to northeast and southeast during the day before 1300 LT, with an average wind speed of 0.9 m s^{-1}. Afterwards, the wind shifted back to northwest, but with stronger

wind speeds (average of 5.3 m s^{-1}).

Figure 4.9a displays the measured CO_2 (ppm) time series from all UAV flights and the Picarro. The CO_2 mole fraction measured during the flights in the early morning and evening, when northwesterlies occurred, was consistent with that measured by the G2401. A CO_2 enhancement linked to morning traffic peak (from 0700 to 0800 LT) was detected at all altitudes. Interestingly, the two measurements eventually differed at 1000 LT, creating a vertical gradient: the CO_2 mole fraction measured onboard the UAV remained constant, whereas a decrease of about 5 ppm was measured by the G2401 on the ground.

During the day, with the surface wind direction shifting starting 0800 LT from northwest to northeast and then southeast, the Picarro G2401 progressively sampled air from the Athalassa National Forest Park. The park, with a total area of 8.4 km^2, is an oasis of greenery with many trees, shrubs and grasses located on the southeastern edge of Nicosia. Considering that the inlet of the G2401 is at the same altitude above sea level as the UAV launching location, the lower observed CO_2 mole fraction by the G2401 can most likely be attributed to the Athalassa National Forest Park acting as a surface sink taking up CO_2. The reduction of traffic after peak hour can also play a role in the first part of the day, when the air was blowing from the north. At 50 m or 100 m height, the constancy of CO_2 mole fractions during the day can suggest a different origin for the air sampled depending on the wind direction at these altitudes (wind was not measured onboard the UAV). Potential origins may include “regional” air moving above the surface layer or a plume of emissions from the city lofted at a few tens of meters with a stratified airmass above the park.

During the afternoon, the progressive convergence of surface and UAV observations, with a decrease of UAV-CO_2 values, suggest either a diffusion of the surface signals in altitude or an enhanced atmospheric mixing. This explanation could be supported using an anemometer integrated onboard the UAV to provide additional wind data at various heights. UAV-integrated wind measurements would have to be considered for future applications.

A CO_2 mapping during the traffic peak hour is shown in Fig.4.9c combined with the flight path at 100 m (the red dot represents the launching site). Figure 4.9b shows the corresponding CO_2 time series combined with

wind direction (arrow head) and wind speed (arrow length) information. The high mole fraction (20 ppm above background levels) probably originated from local traffic emissions from the main road south-west of the Athalassa National Forest Park (Fig.4.8). This finding highlights the capability of the developed UAV-CO_2 sensor system to detect fast mole fraction changes and the potential to provide useful insight into CO_2 emissions close to the ground in urban areas.

From the vertical profiles (Fig.4.10), the difference between the 0600 and 0700 LT profiles highlights the traffic peak hour. Additionally, we observed an increasing difference (about 3 ppm) between ground level and 50 m AGL, followed by a difference (about 0.5 ppm) between 50 m and 100 m AGL from 0800 to 1300 LT when the air mass came from the Athalassa National Forest Park with an average wind speed of 0.9 m s-1. This suggests that the CO_2 mole fraction measured by the G2401 and UAV-CO_2 system represents local CO_2 characteristics and that the Athalassa National Forest Park acted as a CO_2 sink. Later on, between 1500 and 1700 LT when the average wind speed increased (5.3 m s^{-1}), the CO_2 mole fraction at 50 m AGL and 100 m AGL converged towards surface values. This suggests that the observed wind speed enhancement enabled a better mixing of surface signals in altitude. However, the transport of well-mixed regional background air masses at the measurement area could also be an alternative explanation (background CO_2 mole fraction is 418.9 ppm). Although we demonstrated the usefulness of UAV measurements to capture horizontal and vertical CO_2 gradients in the planetary boundary layer in an urban or periurban environment, a definitive explanation of this particular observation would be beyond the scope of this paper.

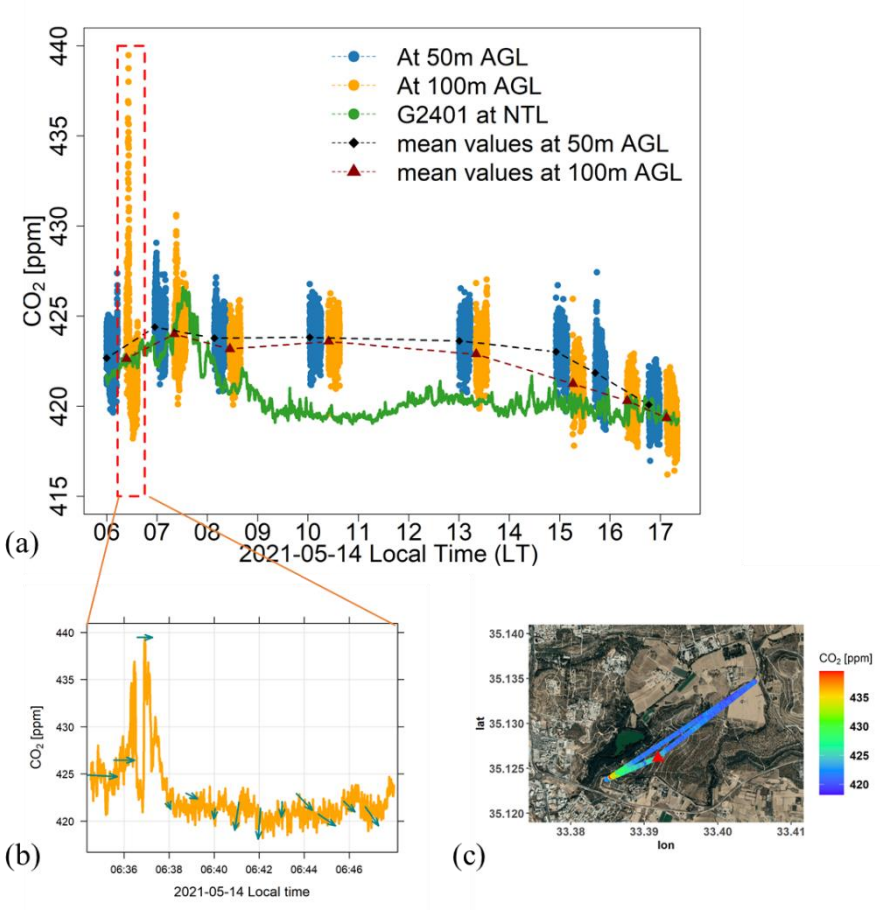

Figure 4.9 (a) time series of CO_2 mole fraction measured by the UAV CO_2 sensor (at 50 m in blue and 100 m AGL in orange) and by the Picarro G2401 at CyI (in green). The black dots represent the averaged CO_2 mole fraction measured by SaB during the flights at 50 m, and the dark red dots represent the averaged CO_2 mole fraction measured by SaB during the flight at 100 m. (b) the corresponding CO_2 time series combined with wind direction (arrow head) and wind speed (arrow length) information obtained from the nearby meteorological station, which is a zoom of the second flight marked in the red dashed box in (a). (c) presents the CO_2 mapping (the red dot represents the launching location) during the rush hour (Map data: © Google, Maxar Technologies).

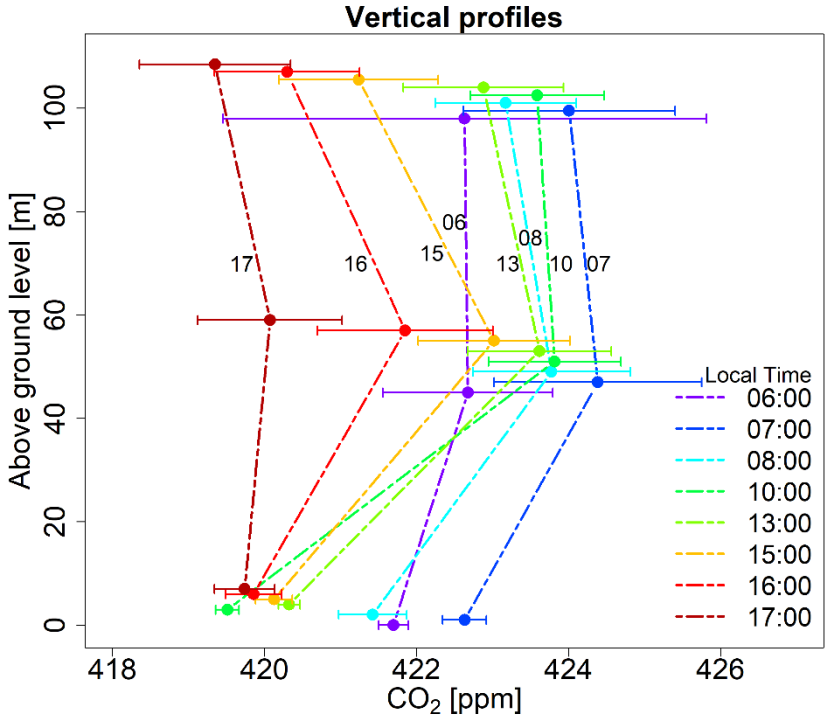

Figure 4.10 Vertical profiles from the eight pairs of flights. The ground level values are from the Picarro G2401 at CyI. CO_2 at 50 m and 100 m AGL are from the UAV-CO_2 sensor horizontal flights, the error bars represent the standard deviation of the duration of each flight.

Section 5: Conclusions

Following the integration of a NDIR CO_2 sensor, we developed and validated an autonomous system that can be regarded as a portable package (1058 g), suitable for CO_2 measurements on board small UAVs (or other platforms) with good field performance after applying calibration and data corrections (±1 ppm accuracy for 1 min averages). Prior to deployment, and in order to acquire high-quality observations, the sensor followed a series of quality control procedures. The laboratory tests indicated that the precision was within ±1 ppm (1σ) at 1 Hz. Two CO_2 sensors (SaA and SaB) were tested. It is essential to conduct calibrations before any measurements as shown in this study. NDIR CO_2 sensors should not be considered plug-and-play without conducting calibrations and bias correction prior to any measurement campaigns as measurement data would suffer from large, unknown biases without that important step. In general, we advocate that low- and mid-cost sensor units should systematically be characterized for their dependence to pressure and temperature, and their factory correction

and calibration verified. Strategies for field deployment should also take into account the significant drift that can be observed at the hourly scale. Using a single target gas between flights in sufficient to cope with this drift. Alternative strategies to correct the drift without using gas cylinders on the field remain to be explored, such as comparison against a high precision instrument at regular intervals during the deployment. Each sensor's performance is impacted by changes in pressure and temperature; therefore, it is necessary to perform pressure and temperature sensitivity tests before any field applications.

Further validation onboard a manned aircraft resulted in an estimated precision of ± 2 ppm (1σ) at 1 Hz and ±1 ppm (1σ) at 1 min time resolution. During the integration of our system onboard a small quad-copter, the calibration strategy has been extended to account for running-time-dependent instrumental drifts. Due to its simplicity, the developed system can be replicated easily for wider applications since it has compact, cost-effective and lightweight advantages. It is anticipated that the integrated portable package can be used in the investigation of emission ratios and fluxes, especially when combined with other sensors on board the UAV platform.

As a proof-of-concept, the developed system had been deployed in a UAV-based flight campaign, where several horizontal flights were performed near the ground and up to 100 m in height. Mole fraction of CO_2 up to 440 ppm (20 ppm above the background levels) was detected during the morning traffic rush hour, attributed to emission from a major road located on the southwest of the Athalassa National Forest Park. The CO_2 mole fraction measured by the UAV system was consistent with that measured by the Picarro G2401 at CyI when the flight path was downwind of CyI. The system also revealed its ability to capture the temporal variability of the vertical CO_2 gradient between the surface and the lower atmosphere. The observed CO_2 profiles depict the contribution of traffic emission in the morning from 0600 to 0800 LT, and also a probable sink due to the Athalassa National Forest Park during the course of the day from 0800 to 1300 LT. Furthermore, the measurement system captured the mole fraction drop from 1500 to 1700 LT observed at different height levels due to the intensification in the wind speed leading to more horizontal and vertical mixing. In conclusion, the designed system demonstrated its capability to measure fast mole fraction changes and spatial gradients, and

to provide accurate plume dispersion maps. It proved to be a good complementary measurement tool to the in-situ observations performed at the surface.

Data availability. The data presented in this study are based on many different experiments and given the fact that our experiments and field deployments were aimed at characterizing the two sensors used here. The data is not made publicly available in a repository, but can be requested from the corresponding author.

Author Contributions. YL contributed to lab experiments' design and setup, field deployments, data collection, data analysis and writing of the manuscript. JDP, MV, PB and JS contributed to project advising, reviewing, and editing the manuscript. PA, CC, CK, AL, PV contributed to the miniaturization, integration and evaluation of the UAV-CO_2 sensor system, UAS operations and data collection. OL and CP contributed to laboratory experiments' setup, design and advising. PYQ contributed to manned aircraft flight measurements, ground Picarro G2401 and meteorological station measurements and maintenance, data collection and providing supports during UAV-CO_2 flights. MD contributed to the review and editing of the manuscript.

Competing Interests. The authors declare that they have no conflict of interest.

Acknowledgements. We would like to thank ICOS teams at LSCE for supporting a series of laboratory tests and aircraft field deployment flights. We are grateful for all the efforts of the technicians, pilots and software developers from USRL/CARE-C at CyI for their support in the integration and field validation of the UAV-CO_2 sensor system.

Financial support. This research has been supported by the project Eastern Mediterranean Middle East-Climate & Atmosphere Research Center (EMME-CARE) which has received the funding from the European Union's Horizon 2020 research and innovation programme under grant agreement No. 856612 and the Cyprus Government, and the project Air Quality Services for clean air in Cyprus (AQ-SERVE) INTEGRATED/0916/0016 is co-financed by the European Regional Development Fund and the Republic of Cyprus through the Research and Innovation Foundation.

5 CONCLUSIONS AND OUTLOOKS

5.1 CONCLUSIONS

The research presented in this thesis aimed to characterize CH_4 and CO_2 emissions from the local to national scale using mobile measurements through variable platforms (vehicles, aircraft and drones). Part of a LSCE-Cyprus institute collaboration, my work found a very relevant "natural laboratory" in Cyprus with a significant but limited number of GHG points or city emissions and is rather isolated from other regional European emissions. Indeed, methane emissions from waste and agriculture are the key sources in Cyprus. To verify local and national methane emissions, car-based mobile measurements (24 survey days) of key landfills and cattle farm areas and airborne measurements (3 flights) were performed in Cyprus. Moreover, methane emission rates were estimated using the Gaussian plume model and mass balance approach. Then, the results were compared with the bottom-up national inventory of Cyprus (UNFCCC, 2021).

Further, the performance of a wide range of state-of-art commercial measurement systems was intercompared during a series of blind-controlled release experiments at an industrial site. To improve our current understanding of methane emissions across the natural gas supply chain.

Lastly, as a part of this study, an autonomous UAV-CO_2 sensor system was developed, suitable for CO_2 measurements with good field performance after applying calibration and data corrections.

The verification of Cyprus national methane emissions: Based on our car-based mobile surveys, the measured methane emissions from three hotspots accounted for about 28% of the total methane emissions in Cyprus according to the bottom-up inventory (UNFCCC, 2021). It was found that CH_4 emissions from solid waste disposal, were about 160% larger than that reported in the bottom-up inventory. The significant difference may result from i) obsolete inventory data, possibly due to empirical/regional/default input values based on limited and outdated research; ii) incorrect attribution of emissions from the closed landfill, which is unmanaged and did not meet the standards for landfills of European Union directives, iii) uncertainties in the top-down estimates, including country-scale extrapolation. Regarding

livestock methane emissions from enteric fermentation, it was estimated, using in-situ measurements, that they are 40% greater than the reported ones in the national inventory. The possible reasons for this difference include time variability in the number of animals, non-specific emission factors, diurnal variation in the strength of cattle enteric fermentation, and the possibility that measured emission rates contain a part of manure methane emissions. This study provides a method to quantify and extrapolate enteric methane emissions from cattle from the local to the national scale. As long as a 'representative' sampling of the emitting sectors can be achieved, this survey method can be applied to other regions or countries aiming to assess the methane emission structure independently from inventories and support policymakers in designing and implementing efficient mitigation actions. Applied elsewhere, the uncertainty of this method will also directly depend on how many cumulative emitters can be sampled with respect to total emissions. The bottom-up approach was completed with airborne measurements to assess total emissions from a mass balance perspective. However, flight constraints prevented a full closure of the upwind and downwind air masses and hence a top-down emission estimate. The aircraft data, analysed with a Lagrangian model, suggested nevertheless that the observed methane emissions emanated from local emissions in Cyprus, according to a preliminary analysis.

Methane controlled release experiments at an industrial station: This is a comprehensive study to compare the performance of several state-of-art methane quantification systems for midstream industrial fugitive emissions. Most systems have reportedly been correct within an order of magnitude of the controlled release rate. The best performers are also associated with deployment constraints. There is no current possibility to determine a standard for quantification since measurement systems are permanently evolving along with estimation methodologies. The limited number of releases (17) implemented did not let significant influence identified from wind speed (except very slow wind speed), node shape, and position. More control release experiments are needed to acquire robust statistics and test the dependence on a wider range of environmental parameters. Careful consideration of the integration of detection along with quantification would be valuable. Sensor precision may play a role in small release rates but has likely a limited influence on the releases above 0.1 kg h^{-1}. There is an apparent random character, mostly technique-dependent, not elucidated in the frame of this experiment, but that could likely be clarified with more

data and comparing atmospheric turbulences and building configurations, and controlled gas temperature/injection speed and direction. An initial idea was to check how to validate top-down (site-level) quantification from robust bottom-up measurements (source-level). It appeared that not only source-level measurements cannot achieve full coverage of emission types, but also that they have their own biases and unvertainties. Further work is needed to determine how estimates provided by these systems can be reconciled with real-life emissions from an industrial site with complex temporality in operations.

A developed UAV-CO_2 system for atmospheric mapping applications
This developed system is autonomous and suitable for CO_2 measurements on board small UAVs with good field performance after applying calibration and data corrections. In general, it is advocated that low- and mid-cost sensor units should systematically be characterized for their dependence on pressure and temperature and their factory correction and calibration verified. To obtain high-quality measurements, the sensor followed a series of quality control procedures as shown in Chapter 4. The laboratory tests indicated that the precision was within ± 1 ppm (1σ) at 1 Hz. The validation on board a manned aircraft indicated an estimated precision of ± 2 ppm (1σ) at 1 Hz and ± 1 ppm (1σ) at a 1 min time resolution. During system's deployment on board a small quadcopter, the calibration strategy was extended to account for running-time-dependent instrumental drifts. As a proof of concept, the developed system was deployed in a UAV-based flight campaign. The mole fraction of CO_2 up to 440 ppm (20 ppm above the background levels) was detected during the morning traffic rush hour, attributed to emissions from a major road located southwest of the flight path. It showed that the CO_2 mole fraction measured by the UAV system was consistent with that measured by a reference instrument Picarro G2401 when the flight path was downwind of the instrument. In addition, the system also revealed its ability to capture the temporal variability of the vertical CO_2 gradient between the surface and the lower atmosphere. Overall, the designed system demonstrated its capability to measure fast mole fraction changes and spatial gradients and to provide accurate plume dispersion maps. It proved to be a good complementary measurement tool to the in-situ observations performed at the surface.

5.2 OUTLOOKS

Reconciling top-down and bottom-up estimates at the national scale. It remains a key challenge in the MRV (monitoring, reporting, verification) paradigm to reconcile top-down and bottom-up estimates at the national scale. This study provides a method to quantify methane emissions, bridging the local (site) scale to the national scale and independent verification of the emission budgets with alternative methods such as mobile in-situ measurements through different platforms, modelling and inventories. Moreover, this survey method can be applied to other regions or countries to assess the methane emission structure independently from inventories and support policymakers in designing and implementing efficient mitigation actions. It is promising for developing countries with limited resources to develop atmospheric networks or sophisticated reporting and inventories. To improve the method used in this study for wider applications, the following suggestions can be considered in future research.

- **Including more species for mobile measurements**

In the future, additional instruments could be added to the current mobile setup for cars to include more species useful for source apportionment studies, such as ethane (C_2H_6) and methane isotopes. For instance, ethane is a co-emitter from thermogenic methane sources (Schwietzke et al., 2014), and methane isotopes can be used to distinguish thermogenic and biogenic methane sources (Defratyka et al., 2021). To quantify emissions originating from specific point sources or urban areas, complementary surveys with UAVs could be done, taking into account that drone measurements require careful wind measurements to yield relevant estimates. Indeed, for the case of multiple emission sources or overlapping sources, this improved configuration could quantify emissions for different categories or sub-categories and provide a more accurate and robust emission budget.

- **Refining modelling tools**

The dispersion model used in this study to convert atmospheric car-based GHG observations to emissions is a simple Gaussian plume model from the Polyphemus platform. The bias caused in calculating methane emission rates is attributed to input parameters (e.g. stability classes and wind conditions). In addition, Gaussian models do not consider topography, which can cause additional biases in the calculation, especially for ground-

level emission sources. For complex cases, as suggested in the study of Ars et al. (2017) and Kumar et al. (2022), tracer release techniques and near-field statistical atmospheric inversions allow for improvements in the computation. It is noted that locating the tracer gas as close as possible to methane emission sources could improve the estimate of emission rates by any modelling tools.

Supporting data for establishing effective policies and regulations of methane emissions in the oil and natural gas industry. Effective policies and regulations are essential to achieve methane abatement in the natural gas supply chain. This study provides an update on the capabilities and inter-comparisons of currently state-of-the-art measurement systems to methane emissions from the natural gas supply chain based on a series of blind-controlled release experiments. Methane emissions from this energy sector can be divided into fugitive, vented and incomplete combustion emissions. Normalizing the monitoring, reporting and verification of methane emissions across the entire natural gas production chain (including upstream, midstream and downstream) would enhance the value of these informations both for climate negotiators, policy makers and operators. Therefore, more work towards reconciling different technologies and methodologies used, reducing their uncertainties and extending their field of action is essential to unify and make more robust the reporting methods across companies and organizations.

Additionally, following reliable standards, guidelines and frameworks to assess methane emissions can ensure that the collected data are replicable and verifiable by a third party. To achieve this requirement, cost-effective methane analyzers and protocols are needed for broad measurements across the natural gas supply chain. With these efforts and more future work, the natural gas industry chain will continuously improve the management of methane emissions to achieve efficient mitigation.

Potential optimization and applications of the UAV system for GHG measurements and reporting data calibrated on the WMO scale, which is novel within current UAV CO_2 measurements. It is proven that the system has the capability to detect anthropogenic CO_2 emissions in urban areas and measure spatial gradients to provide accurate plume dispersion maps. Moreover, the system could be further applied for more applications after considering adding an anemometer and including other lightweight sensors.

- **Adding an anemometer**

The system has been used to capture the temporal variability of the vertical CO_2 gradient between the surface and the lower atmosphere. Since wind conditions could vary with the altitude, with an anemometer installed on board the drone, real-time wind speed and direction will be measured in parallel, which could be used to better locate and determine emission sources.

- **Including other small sensors**

The system weighs 1058 g, including the battery, which leaves the potential to add other small sensors on board the drone, depending on the allowed payload. Then, the enhanced system could be used for wider applications, such as the determination of emission factors and the investigation of emission rates. Emission factors as an emission indicator are generally calculated as the amount of a pollutant emitted per unit mass of fuel burned. They can be used to develop emission inventories when quantities of the fuels consumed are known. In addition, the UAV measurement is also a cost-effective solution. For instance, recently, Vernooij et al. (2022) have built a UAV sampling system with lightweight sensors on board to measure biomass burning emission factors for CO_2, CO, CH_4, N_2O, $PM_{2.5}$ and equivalent black carbon in fresh biomass smoke. Smoke stack emission factor quantification would also meet an important demand. Thanks to the rapid development of UAV payloads and lightweight sensors, there is still much room to improve this application in the near future.

- **Indicating anthropogenic emissions from point sources**

It is known that a large part of the anthropogenic CO_2 and CH_4 originates from point emission sources such as power plants burning fossil fuels (Pinty et al., 2017). A targeted application of the developed system is to estimate emissions from point sources in the future, as suggested in the study of Reuter et al. (2021). Also, modelling tools such as the Gaussian plume model and statistical atmospheric inversions could be included to estimate emission fluxes at the local scale.

- **Develop a methane version**

Besides CO_2, high accurate UAV-CH_4 measurements are now emerging

with the development of lightweight sensors and measurement systems. For instance, Tuzson et al. (2020) developed a compact and lightweight mid-infrared laser absorption spectrometer for high-precision atmospheric CH_4 measurements on UAVs at 1 Hz. They proved its capability to capture fast and subtle changes in atmospheric CH_4 mole fractions. More recently, Gålfalk et al. (2021) developed a drone system to map CH4 concentrations with a precision of 0.84 ppb s^{-1} and 0.1 m s^{-1}. Vinković et al. (2022) calculated CH_4 emission rates at the farm scale using the UAV-based (with an active AirCore system on board) mass balance approach. Indeed, high precision and acquisition frequency UAV-CH_4 measurements are required and attractive to quantify emissions at site scales.

- **Integrate mobile platform measurements into the urban observation network**

During the past decade, research teams have put a good amount of efforts into establishing urban GHG monitoring networks to determine city emissions using ground-based in situ measurements (e.g. sensors) and column measurements (e.g. solar-tracking Fourier transform spectrometer EM27/SUN) (Mitchell et al., 2022; Dietrich et al., 2021; Bares et al., 2019; Gordon and Johnson, 2018). Integrating UAV mobile platforms into the current urban GHG monitoring network has the advantage providing extra emission information. It fills in the gap between existing ground-based and column network measurements.

Collaboration and co-construction with local stakeholders. Mobile measurement surveys through various platforms could be more efficient by collaborating with local government departments and local industrials as they are more familiar with local situations and emissions and may have more specific emission factors than the national inventories. They are important sources of active data in the bottom-up inventory. For instance, the characteristics of landfills (e.g. age and waste type and amount) and type of cattle farms (e.g. dairy cattle or non-dairy cattle) could be verified and modified if necessary in analysis such as those presented in this Ph.D. Moreover, the collaboration with local authorities provides a bridge with local operator companies allowing the comparison of emission factors estimated by top-down and bottom-up approaches to update the current emission factors used in the inventory (e.g. power plants).

This Ph.D. initiated a large collaboration between LSCE and CyI and is a part of a few first studies on GHG emissions in Cyprus and the EMME region. The results showed a high value of mobile measurement methods to determine GHG emissions from site scale to national scale. Moreover, this study developed methods that would be easily duplicated and applicable to other regions and emission sectors.

LIST OF ABBREVIATIONS

AD – Allan Deviation

AGL – Above Ground Level

ASL – Above Sea Level

CO – Carbon Monoxide

CO_2 – Carbon Dioxide

CH_4 – Methane

C_2H_6 – Ethane

CRDS – Cavity ring-down spectroscopy

CRF – Controlled release facility

COCCON – Collaborative Carbon Column Observing Network

CARE-C – Climate and Atmosphere Research Center

CyI – The Cyprus Institute

^1D – excited atomic oxygen O

DOC – Degradable Organic Carbon

EDGAR – Emissions Database for Global Atmospheric Research

EMME – Eastern Mediterranean and Middle East

F – atomic fluorine

FOD – First-Order Degradation

FTIR – Fourier transform infrared

FTS – Fourier transform spectrometer

GERG – European Gas Research Group

GHG – Greenhouse Gas

GHGSat – Greenhouse Gas Satellite

GOSAT – Greenhouse Gases Observing Satellite

HPP – High Performance Platform

IASI – Infrared Atmospheric Sounding Interferometer

ICOS-ATC – Integrated Carbon Observation System-Atmosphere Thematic Center

IPCC – International Panel of Climate Change

LSCE – Laboratoire des sciences du climat et de l'environnement

LT – Local Time

$Mg(ClO_4)_2$ – Magnesium perchlorate

MOX – Metal oxide resistive sensor

MRV – Monitoring, Reporting, Verification

NDIR – non-dispersive infrared

NGO – non-governmental organizations

N_2O – Nitrous oxide

NOAA CMDL – National Oceanic and Atmospheric Administration Climate Monitoring and Diagnostics Laboratory

NO_x – Nitrogen oxides

OCO-2 – Orbiting Carbon Observatory-2

OGI – Optical gas imaging

OH – Hydroxide

OVSQ – Observatoire de Versailles Saint-Quentin-en-Yvelines

P – Pressure

pMGGA – light Micro-portable Greenhouse Gas Analyzer

SO_2 – Sulfur dioxide

T – Temperature

TanSat – Carbon Dioxide Observation Satellite

TCCON – Total Carbon Column Observing Network

TRL – Technology Readiness Level

TROPOMI – TROPOspheric Monitoring Instrument

UAV – Unmanned Aerial Vehicle

UAS – Unmanned Aerial System

UNFCCC – United Nations Framework Convention on Climate Change

USRL – Unmanned

WMO/GAW – World Meteorological Organization Global Atmosphere Watch Programme

X_{CO2} – column-averaged dry air CO_2 mole fraction

REFERENCES

Alberti, C., Hase, F., Frey, M., Dubravica, D., Blumenstock, T., Dehn, A., Castracane, P., Surawicz, G., Harig, R., Baier, B. C., Bès, C., Bi, J., Boesch, H., Butz, A., Cai, Z., Chen, J., Crowell, S. M., Deutscher, N. M., Ene, D., Franklin, J. E., García, O., Griffith, D., Grouiez, B., Grutter, M., Hamdouni, A., Houweling, S., Humpage, N., Jacobs, N., Jeong, S., Joly, L., Jones, N. B., Jouglet, D., Kivi, R., Kleinschek, R., Lopez, M., Medeiros, D. J., Morino, I., Mostafavipak, N., Müller, A., Ohyama, H., Palmer, P. I., Pathakoti, M., Pollard, D. F., Raffalski, U., Ramonet, M., Ramsay, R., Sha, M. K., Shiomi, K., Simpson, W., Stremme, W., Sun, Y., Tanimoto, H., Té, Y., Tsidu, G. M., Velazco, V. A., Vogel, F., Watanabe, M., Wei, C., Wunch, D., Yamasoe, M., Zhang, L., and Orphal, J.: Improved calibration procedures for the EM27/SUN spectrometers of the COllaborative Carbon Column Observing Network (COCCON), Atmos. Meas. Tech., 15, 2433–2463, https://doi.org/10.5194/amt-15-2433-2022, 2022.

Albertson, John. D., Harvey, T., Foderaro, G., Zhu, P., Zhou, X., Ferrari, S., Amin, M. S., Modrak, M., Brantley, H., and Thoma, E. D.: A Mobile Sensing Approach for Regional Surveillance of Fugitive Methane Emissions in Oil and Gas Production, Environ. Sci. Technol., 50, 2487–2497, https://doi.org/10.1021/acs.est.5b05059, 2016.

Allen, D. T.: Methane emissions from natural gas production and use: reconciling bottom-up and top-down measurements, Current Opinion in Chemical Engineering, 5, 78–83, https://doi.org/10.1016/j.coche.2014.05.004, 2014.

Allen, D. T., Torres, V. M., Thomas, J., Sullivan, D. W., Harrison, M., Hendler, A., Herndon, S. C., Kolb, C. E., Fraser, M. P., Hill, A. D., Lamb, B. K., Miskimins, J., Sawyer, R. F., and Seinfeld, J. H.: Measurements of methane emissions at natural gas production sites in the United States, Proceedings of the National Academy of Sciences, 110, 17768–17773, https://doi.org/10.1073/pnas.1304880110, 2013.

Allen, G., Hollingsworth, P., Kabbabe, K., Pitt, J. R., Mead, M. I., Illingworth, S., Roberts, G., Bourn, M., Shallcross, D. E., and Percival, C. J.: The development and trial of an unmanned aerial system for the measurement of

methane flux from landfill and greenhouse gas emission hotspots, Waste Management, 87, 883–892, https://doi.org/10.1016/j.wasman.2017.12.024, 2019.

Alvarez, R. A., Zavala-Araiza, D., Lyon, D. R., Allen, D. T., Barkley, Z. R., Brandt, A. R., Davis, K. J., Herndon, S. C., Jacob, D. J., Karion, A., Kort, E. A., Lamb, B. K., Lauvaux, T., Maasakkers, J. D., Marchese, A. J., Omara, M., Pacala, S. W., Peischl, J., Robinson, A. L., Shepson, P. B., Sweeney, C., Townsend-Small, A., Wofsy, S. C., and Hamburg, S. P.: Assessment of methane emissions from the U.S. oil and gas supply chain, Science, eaar7204, https://doi.org/10.1126/science.aar7204, 2018.

Amini, S., Kuwayama, T., Gong, L., Falk, M., Chen, Y., Mitloehner, Q., Weller, S., Mitloehner, F. M., Patteson, D., Conley, S. A., Scheehle, E., and FitzGibbon, M.: Evaluating California dairy methane emission factors using short-term ground-level and airborne measurements, Atmospheric Environment: X, 14, 100171, https://doi.org/10.1016/j.aeaoa.2022.100171, 2022.

Ars, S., Broquet, G., Yver Kwok, C., Roustan, Y., Wu, L., Arzoumanian, E., and Bousquet, P.: Statistical atmospheric inversion of local gas emissions by coupling the tracer release technique and local-scale transport modelling: a test case with controlled methane emissions, Atmos. Meas. Tech., 10, 5017–5037, https://doi.org/10.5194/amt-10-5017-2017, 2017.

Arzoumanian, E., Vogel, F. R., Bastos, A., Gaynullin, B., Laurent, O., Ramonet, M., and Ciais, P.: Characterization of a commercial lower-cost medium-precision non-dispersive infrared sensor for atmospheric CO_2 monitoring in urban areas, Atmos. Meas. Tech., 12, 2665–2677, https://doi.org/10.5194/amt-12-2665-2019, 2019.

Atherton, E., Risk, D., Fougère, C., Lavoie, M., Marshall, A., Werring, J., Williams, J. P., and Minions, C.: Mobile measurement of methane emissions from natural gas developments in northeastern British Columbia, Canada, Atmos. Chem. Phys., 17, 12405–12420, https://doi.org/10.5194/acp-17-12405-2017, 2017.

Bakkaloglu, S., Lowry, D., Fisher, R. E., France, J. L., Brunner, D., Chen, H., and Nisbet, E. G.: Quantification of methane emissions from UK biogas plants, Waste Management, 124, 82–93, https://doi.org/10.1016/j.wasman.2021.01.011, 2021.

Balcombe, P., Anderson, K., Speirs, J., Brandon, N., and Hawkes, A.: The Natural Gas Supply Chain: The Importance of Methane and Carbon Dioxide Emissions, ACS Sustainable Chem. Eng., 5, 3–20, https://doi.org/10.1021/acssuschemeng.6b00144, 2017.

Bannink, A., van Schijndel, M. W., and Dijkstra, J.: A model of enteric fermentation in dairy cows to estimate methane emission for the Dutch National Inventory Report using the IPCC Tier 3 approach, Animal Feed Science and Technology, 166–167, 603–618, https://doi.org/10.1016/j.anifeedsci.2011.04.043, 2011.

Bara Emran, Dwayne Tannant, and Homayoun Najjaran: Low-Altitude Aerial Methane Concentration Mapping, Remote Sensing, 9, 823, https://doi.org/10.3390/rs9080823, 2017.

Barchyn, T., Hugenholtz, C. H., Myshak, S., and Bauer, J.: A UAV-based system for detecting natural gas leaks, J. Unmanned Veh. Sys., juvs-2017-0018, https://doi.org/10.1139/juvs-2017-0018, 2017.

Bares, R., Mitchell, L., Fasoli, B., Bowling, D. R., Catharine, D., Garcia, M., Eng, B., Ehleringer, J., and Lin, J. C.: The Utah urban carbon dioxide (UUCON) and Uintah Basin greenhouse gas networks: instrumentation, data, and measurement uncertainty, 18, 2019.

Barker, P. A., Allen, G., Gallagher, M., Pitt, J. R., Fisher, R. E., Bannan, T., Nisbet, E. G., Bauguitte, S. J.-B., Pasternak, D., Cliff, S., Schimpf, M. B., Mehra, A., Bower, K. N., Lee, J. D., Coe, H., and Percival, C. J.: Airborne measurements of fire emission factors for African biomass burning sampled during the MOYA campaign, Atmos. Chem. Phys., 20, 15443–15459, https://doi.org/10.5194/acp-20-15443-2020, 2020.

Barritault, P., Brun, M., Lartigue, O., Willemin, J., Ouvrier-Buffet, J.-L., Pocas, S., and Nicoletti, S.: Low power CO_2 NDIR sensing using a microbolometer detector and a micro-hotplate IR-source, Sensors and Actuators B: Chemical, 182, 565–570, https://doi.org/10.1016/j.snb.2013.03.048, 2013.

Bell, C. S., Vaughn, T. L., Zimmerle, D., Herndon, S. C., Yacovitch, T. I., Heath, G. A., Pétron, G., Edie, R., Field, R. A., Murphy, S. M., Robertson, A. M., and Soltis, J.: Comparison of methane emission estimates from mul-

tiple measurement techniques at natural gas production pads, Elementa: Science of the Anthropocene, 5, 79, https://doi.org/10.1525/elementa.266, 2017.

Bell, C. S., Vaughn, T., and Zimmerle, D.: Evaluation of next generation emission measurement technologies under repeatable test protocols, Elementa: Science of the Anthropocene, 8, 32, https://doi.org/10.1525/elementa.426, 2020.

Berchet, A., Pison, I., Crill, P. M., Thornton, B., Bousquet, P., Thonat, T., Hocking, T., Thanwerdas, J., Paris, J.-D., and Saunois, M.: Using shipborne observations of methane isotopic ratio in the Arctic Ocean to understand methane sources in the Arctic, Atmos. Chem. Phys., 20, 3987–3998, https://doi.org/10.5194/acp-20-3987-2020, 2020.

Bergamaschi, P., Krol, M., Meirink, J. F., Dentener, F., Segers, A., van Aardenne, J., Monni, S., Vermeulen, A. T., Schmidt, M., Ramonet, M., Yver, C., Meinhardt, F., Nisbet, E. G., Fisher, R. E., O'Doherty, S., and Dlugokencky, E. J.: Inverse modeling of European CH_4 emissions 2001–2006, J. Geophys. Res., 115, D22309, https://doi.org/10.1029/2010JD014180, 2010.

Bergamaschi, P., Corazza, M., Karstens, U., Athanassiadou, M., Thompson, R. L., Pison, I., Manning, A. J., Bousquet, P., Segers, A., Vermeulen, A. T., Janssens-Maenhout, G., Schmidt, M., Ramonet, M., Meinhardt, F., Aalto, T., Haszpra, L., Moncrieff, J., Popa, M. E., Lowry, D., Steinbacher, M., Jordan, A., O'Doherty, S., Piacentino, S., and Dlugokencky, E.: Top-down estimates of European CH_4 and N_2O emissions based on four different inverse models, Atmos. Chem. Phys., 15, 715–736, https://doi.org/10.5194/acp-15-715-2015, 2015.

Berman, E. S. F., Fladeland, M., Liem, J., Kolyer, R., and Gupta, M.: Greenhouse gas analyzer for measurements of carbon dioxide, methane, and water vapor aboard an unmanned aerial vehicle, Sensors and Actuators B: Chemical, 169, 128–135, https://doi.org/10.1016/j.snb.2012.04.036, 2012.

Blake, D. R., Mayer, E. W., Tyler, S. C., Makide, Y., Montague, D. C., and Rowland, F. S.: Global Increase in Atmospheric Methane Concentrations between 1978 and 1980, Geophys. Res. Lett., 9, 477–480, 1982.

Bovensmann, H., Burrows, J. P., Buchwitz, M., Frerick, J., Noël, S., Rozanov, V. V., Chance, K. V., and Goede, A. P. H.: SCIAMACHY: Mission Objectives and Measurement Modes, J. Atmos. Sci., 56, 127–150, https://doi.org/10.1175/1520-0469(1999)056<0127:SMOAMM>2.0.CO;2, 1999.

BP Statistical Review of World Energy 2022, https://www.bp.com/content/dam/bp/bussiness-sites/en/global/corporate/pdfs/energy-economics/statistics/statistical-review/bp-stats-review-2022-full-report.pdf, last access 29 September 2022, 2022.

Brantley, H. L., Thoma, E. D., Squier, W. C., Guven, B. B., and Lyon, D.: Assessment of Methane Emissions from Oil and Gas Production Pads using Mobile Measurements, Environ. Sci. Technol., 48, 14508–14515, https://doi.org/10.1021/es503070q, 2014.

Briggs, G., 1971: Some recent analyses of plume rise observations. Second International Clean Air Congress, H. M. Englund and W. T. Berry, Eds., Academic Press, 1029–1032.

Buchwitz, M., Dils, B., Boesch, H., Crevoisier, C., Detmers, R., Frankenberg, C., Hasekamp, O., Hewson, W., Laeng, A., Noel, S., Nothold, J., Parker, R., Reuter, M., and Schneising, O.: Product Validation and Intercomparison Report (PVIR) for the Essential Climate Variable (ECV) Greenhouse Gases (GHG), ESA Climate Change Initiative (CCI), report version 4, available at: http://cci.esa.int/sites/default/files/PVIR-GHG-CCI-v5_final. pdf (last acess: 22 September), 2022.

Bukosa, B., Deutscher, N. M., Fisher, J. A., Kubistin, D., Paton-Walsh, C., and Griffith, D. W. T.: Simultaneous shipborne measurements of CO_2, CH_4 and CO and their application to improving greenhouse-gas flux estimates in Australia, Atmos. Chem. Phys., 19, 7055–7072, https://doi.org/10.5194/acp-19-7055-2019, 2019.

Cai, B., Cui, C., Zhang, D., Cao, L., Wu, P., Pang, L., Zhang, J., and Dai, C.: China city-level greenhouse gas emissions inventory in 2015 and uncertainty analysis, Applied Energy, 253, 113579, https://doi.org/10.1016/j.apenergy.2019.113579, 2019.

Caulton, D. R., Li, Q., Bou-Zeid, E., Fitts, J. P., Golston, L. M., Pan, D., Lu, J., Lane, H. M., Buchholz, B., Guo, X., McSpiritt, J., Wendt, L., and Zondlo, M. A.: Quantifying uncertainties from mobile-laboratory-derived emissions of well pads using inverse Gaussian methods, Atmos. Chem. Phys., 18, 15145–15168, https://doi.org/10.5194/acp-18-15145-2018, 2018.

Chang, R. Y.-W., Miller, C. E., Dinardo, S. J., Karion, A., Sweeney, C., Daube, B. C., Henderson, J. M., Mountain, M. E., Eluszkiewicz, J., Miller, J. B., Bruhwiler, L. M. P., and Wofsy, S. C.: Methane emissions from Alaska in 2012 from CARVE airborne observations, Proc Natl Acad Sci USA, 111, 16694–16699, https://doi.org/10.1073/pnas.1412953111, 2014.

Cheewaphongphan, P., Chatani, S., and Saigusa, N.: Exploring Gaps between Bottom-Up and Top-Down Emission Estimates Based on Uncertainties in Multiple Emission Inventories: A Case Study on CH4 Emissions in China, Sustainability, 11, 2054, https://doi.org/10.3390/su11072054, 2019.

Chen, Z., Jacob, D., Nesser, H., Sulprizio, M., Lorente, A., Varon, D., Lu, X., Shen, L., Qu, Z., Penn, E., and Yu, X.: Methane emissions from China: a high-resolution inversion of TROPOMI satellite observations, Gases/Atmospheric Modelling/Troposphere/Physics (physical properties and processes), https://doi.org/10.5194/acp-2022-303, 2022.

Chevallier, F., Remaud, M., O'Dell, C. W., Baker, D., Peylin, P., and Cozic, A.: Objective evaluation of surface- and satellite-driven carbon dioxide atmospheric inversions, Atmos. Chem. Phys., 19, 14233–14251, https://doi.org/10.5194/acp-19-14233-2019, 2019.

Chiba, T., Haga, Y., Inoue, M., Kiguchi, O., Nagayoshi, T., Madokoro, H., and Morino, I.: Measuring Regional Atmospheric CO_2 Concentrations in the Lower Troposphere with a Non-Dispersive Infrared Analyzer Mounted on a UAV, Ogata Village, Akita, Japan, Atmosphere, 10, 487, https://doi.org/10.3390/atmos10090487, 2019.

Ciais, P., Sabine, C., Govindasamy, B., Bopp, L., Brovkin, V., Canadell, J., Chhabra, A., DeFries, R., Galloway, J., Heimann, M., Jones, C., Le Quéré, C., Myneni, R., Piao, S., and Thornton, P.: section

6: Carbon and Other Biogeochemical Cycles, in: Climate Change 2013 The Physical Science Basis, edited by: Stocker, T., Qin, D., and Platner, G.-K.,

Cambridge University Press, Cambridge, 2013.

Collins, M., Knutti, R., Arblaster, J., Dufresne, J.-L., Fichefet, T., Friedlingstein, P., Gao, X., Gutowski, W. J., Johns, T., Krinner, G., Shongwe, M., Tebaldi, C., Weaver, A. J., and Wehner, M.: Long-term Climate Change: Projections, Commitments and Irreversibility, in: Climate Change 2013: The Physical Science Basis, Contribution of Working Group I to the Fifth Assessment Report of the Intergovernmental Panel on Climate Change, edited by: Stocker, T. F., Qin, D., Plattner, G.-K., Tignor, M., Allen, S. K., Boschung, J., Nauels, A., Xia, Y., Bex, V., and Midgley, P. M., Cambridge University Press, Cambridge, UK, New York, NY, USA, 2013.

Cooper, J., Balcombe, P., and Hawkes, A.: The quantification of methane emissions and assessment of emissions data for the largest natural gas supply chains, Journal of Cleaner Production, 320, 128856, https://doi.org/10.1016/j.jclepro.2021.128856, 2021.

Crevoisier, C., Nobileau, D., Armante, R., Crépeau, L., Machida, T., Sawa, Y., Matsueda, H., Schuck, T., Thonat, T., Pernin, J., Scott, N. A., and Chédin, A.: The 2007–2011 evolution of tropical methane in the mid-troposphere as seen from space by MetOp-A/IASI, Atmos. Chem. Phys., 13, 4279–4289, https://doi.org/10.5194/acp-13-4279-2013, 2013.

Crosson, E. R.: A cavity ring-down analyzer for measuring atmospheric levels of methane, carbon dioxide, and water vapor, Appl. Phys. B, 92, 403–408, https://doi.org/10.1007/s00340-008-3135-y, 2008.

Crow, D. J. G., Balcombe, P., Brandon, N., and Hawkes, A. D.: Assessing the impact of future greenhouse gas emissions from natural gas production, Science of The Total Environment, 668, 1242–1258, https://doi.org/10.1016/j.scitotenv.2019.03.048, 2019.

Davis, K. J., Bakwin, P. S., Yi, C. X., Berger, B. W., Zhao, C. L., Teclaw, R. M., and Isebrands, J. G.: The annual cycles of CO_2 and H_2O exchange over a northern mixed forest as observed from a very tall tower, Global Change Biol., 9, 12781293, doi:10.1046/j.1365-2486.2003.00672.x, 2003.

De Wachter, E., Kumps, N., Vandaele, A. C., Langerock, B., and De Mazière, M.: Retrieval and validation of MetOp/IASI methane, Atmos.

Meas. Tech., 10, 4623–4638, https://doi.org/10.5194/amt-10-4623-2017, 2017.

Defratyka, S. M., Paris, J.-D., Yver-Kwok, C., Loeb, D., France, J., Helmore, J., Yarrow, N., Gros, V., and Bousquet, P.: Ethane measurement by Picarro CRDS G2201-i in laboratory and field conditions: potential and limitations, Gases/In Situ Measurement/Instruments and Platforms, https://doi.org/10.5194/amt-2020-410, 2020.

Defratyka, S. M., Paris, J.-D., Yver-Kwok, C., Loeb, D., France, J., Helmore, J., Yarrow, N., Gros, V., and Bousquet, P.: Ethane measurement by Picarro CRDS G2201-i in laboratory and field conditions: potential and limitations, Atmos. Meas. Tech., 14, 5049–5069, https://doi.org/10.5194/amt-14-5049-2021, 2021a.

Defratyka, S. M., Paris, J.-D., Yver-Kwok, C., Fernandez, J. M., Korben, P., and Bousquet, P.: Mapping Urban Methane Sources in Paris, France, Environ. Sci. Technol., 55, 8583–8591, https://doi.org/10.1021/acs.est.1c00859, 2021b.

Deng, Z., Ciais, P., Tzompa-Sosa, Z. A., Saunois, M., Qiu, C., Tan, C., Sun, T., Ke, P., Cui, Y., Tanaka, K., Lin, X., Thompson, R. L., Tian, H., Yao, Y., Huang, Y., Lauerwald, R., Jain, A. K., Xu, X., Bastos, A., Sitch, S., Palmer, P. I., Lauvaux, T., d'Aspremont, A., Giron, C., Benoit, A., Poulter, B., Chang, J., Petrescu, A. M. R., Davis, S. J., Liu, Z., Grassi, G., Albergel, C., Tubiello, F. N., Perugini, L., Peters, W., and Chevallier, F.: Comparing national greenhouse gas budgets reported in UNFCCC inventories against atmospheric inversions, Earth Syst. Sci. Data, 14, 1639–1675, https://doi.org/10.5194/essd-14-1639-2022, 2022.

Department of Environment, Ministry of Agriculture, Rural Development and Environment, 2021. Cyprus National Greenhouse Gas Inventory 2021. April, 2021. https://unfccc.int/documents/271515. Accessed 29 September 2022.

Desjardins, R. L., Worth, D. E., Pattey, E., VanderZaag, A., Srinivasan, R., Mauder, M., Worthy, D., Sweeney, C., and Metzger, S.: The challenge of reconciling bottom-up agricultural methane emissions inventories with top-down measurements, Agricultural and Forest Meteorology, 248, 48–59, https://doi.org/10.1016/j.agrformet.2017.09.003, 2018.

DeVries, T., Quéré, C. L., Andrews, O., Berthet, S., Hauck, J., Ilyina, T., Landschützer, P., Lenton, A., Lima, I. D., Nowicki, M., Schwinger, J., and Séférian, R.: Decadal trends in the ocean carbon sink, P. Natl. Acad. Sci. USA, 116, 11646–11651, https://doi.org/10.1073/pnas.1900371116, 2019.

Dietrich, F., Chen, J., Voggenreiter, B., Aigner, P., Nachtigall, N., and Reger, B.: MUCCnet: Munich Urban Carbon Column network, Atmos. Meas. Tech., 14, 1111–1126, https://doi.org/10.5194/amt-14-1111-2021, 2021.

Dlugokencky, E. and Tans, P.: Trends in atmospheric carbon dioxide, National Oceanic and Atmospheric Administration, Earth System Research Laboratory, http://www.esrl. noaa.gov/gmd/ccgg/trends/global.html, last access: 29 September 2022.

Doury, A.: Une methode de calcul pratique et generale pour la prevision numerique des pollutions vehiculees par l'atmosphere Tech. Rep. 4280, CEA, France, 1976.

Duren, R. M., Thorpe, A. K., Foster, K. T., Rafiq, T., Hopkins, F. M., Yadav, V., Bue, B. D., Thompson, D. R., Conley, S., Colombi, N. K., Frankenberg, C., McCubbin, I. B., Eastwood, M. L., Falk, M., Herner, J. D., Croes, B. E., Green, R. O., and Miller, C. E.: California's methane super-emitters, Nature, 575, 180–184, https://doi.org/10.1038/s41586-019-1720-3, 2019.

EDGAR: Emissions Database for global atmospheric research, https://data.jrc.ec.europa.eu/collection/edgar, last access: 29 September 2022.

Edie, R., Robertson, A.M., Field, R.A., Soltis, J., Snare, D.A., Zimmerle, D., Bell, C.S., Vaughn, T.L. and Murphy, S.M.: Constraining the accuracy of flux estimates using OTM 33A. Atmospheric Measurement Techniques, 13(1), 341–353. https://doi.org/ 10.5194/amt-13-341-2020.

European Union Aviation Safety Agency (EASA) Easy Access Rules for Unmanned Aircraft Systems (Regulation (EU) 2019/947 and Regulation (EU) 2019/945): https://www.easa.europa.eu/document-library/easy-access-rules/easy-access-rules-unmanned-aircraft-systems-regulation-eu, last access: 29 September 2022.

Feitz, A., Schroder, I., Phillips, F., Coates, T., Negandhi, K., Day, S., Luhar, A., Bhatia, S., Edwards, G., Hrabar, S., Hernandez, E., Wood, B., Naylor, T., Kennedy, M., Hamilton, M., Hatch, M., Malos, J., Kochanek, M., Reid, P., Wilson, J., Deutscher, N., Zegelin, S., Vincent, R., White, S., Ong, C., George, S., Maas, P., Towner, S., Wokker, N., and Griffith, D.: The Ginninderra CH_4 and CO_2 release experiment: An evaluation of gas detection and quantification techniques, International Journal of Greenhouse Gas Control, 70, 202–224, https://doi.org/10.1016/j.ijggc.2017.11.018, 2018.

Feng, L., Palmer, P. I., Yang, Y., Yantosca, R. M., Kawa, S. R., Paris, J.-D., Matsueda, H., and Machida, T.: Evaluating a 3-D transport model of atmospheric CO_2 using ground-based, aircraft, and space-borne data, Atmos. Chem. Phys., 11, 2789–2803, https://doi.org/10.5194/acp-11-2789-2011, 2011.

Filges, A., Gerbig, C., Chen, H., Franke, H., Klaus, C., and Jordan, A.: The IAGOS-core greenhouse gas package: a measurement system for continuous airborne observations of CO_2 , CH_4 , H_2O and CO, Tellus B: Chemical and Physical Meteorology, 67, 27989, https://doi.org/10.3402/tellusb.v67.27989, 2015.

Foulds, A., Allen, G., Shaw, J. T., Bateson, P., Barker, P. A., Huang, L., Pitt, J. R., Lee, J. D., Wilde, S. E., Dominutti, P., Purvis, R. M., Lowry, D., France, J. L., Fisher, R. E., Fiehn, A., Pühl, M., Bauguitte, S. J. B., Conley, S. A., Smith, M. L., Lachlan-Cope, T., Pisso, I., and Schwietzke, S.: Quantification and assessment of methane emissions from offshore oil and gas facilities on the Norwegian continental shelf, Atmos. Chem. Phys., 22, 4303–4322, https://doi.org/10.5194/acp-22-4303-2022, 2022.

Frankenberg, C., Meirink, J. F., Bergamaschi, P., Goede, A. P. H., Heimann, M., Körner, S., Platt, U., van Weele, M., and Wagner, T.: Satellite chartography of atmospheric methane from SCIAMACHY on board ENVISAT: Analysis of the years 2003 and 2004, J. Geophys. Res., 111, D07303, https://doi.org/10.1029/2005JD006235, 2006.

Fraser, A., Palmer, P. I., Feng, L., Boesch, H., Cogan, A., Parker, R., Dlugokencky, E. J., Fraser, P. J., Krummel, P. B., Langenfelds, R. L., O'Doherty, S., Prinn, R. G., Steele, L. P., van der Schoot, M., and Weiss, R. F.: Estimating regional methane surface fluxes: the relative importance of surface and GOSAT mole fraction measurements, Atmos. Chem. Phys., 13,

5697–5713, https://doi.org/10.5194/acp-13-5697-2013, 2013.

Friedlingstein, P., O'Sullivan, M., Jones, M. W., Andrew, R. M., Hauck, J., Olsen, A., Peters, G. P., Peters, W., Pongratz, J., Sitch, S., Le Quéré, C., Canadell, J. G., Ciais, P., Jackson, R. B., Alin, S., Aragão, L. E. O. C., Arneth, A., Arora, V., Bates, N. R., Becker, M., Benoit-Cattin, A., Bittig, H. C., Bopp, L., Bultan, S., Chandra, N., Chevallier, F., Chini, L. P., Evans, W., Florentie, L., Forster, P. M., Gasser, T., Gehlen, M., Gilfillan, D., Gkritzalis, T., Gregor, L., Gruber, N., Harris, I., Hartung, K., Haverd, V., Houghton, R. A., Ilyina, T., Jain, A. K., Joetzjer, E., Kadono, K., Kato, E., Kitidis, V., Korsbakken, J. I., Landschützer, P., Lefèvre, N., Lenton, A., Lienert, S., Liu, Z., Lombardozzi, D., Marland, G., Metzl, N., Munro, D. R., Nabel, J. E. M. S., Nakaoka, S.-I., Niwa, Y., O'Brien, K., Ono, T., Palmer, P. I., Pierrot, D., Poulter, B., Resplandy, L., Robertson, E., Rödenbeck, C., Schwinger, J., Séférian, R., Skjelvan, I., Smith, A. J. P., Sutton, A. J., Tanhua, T., Tans, P. P., Tian, H., Tilbrook, B., van der Werf, G., Vuichard, N., Walker, A. P., Wanninkhof, R., Watson, A. J., Willis, D., Wiltshire, A. J., Yuan, W., Yue, X., and Zaehle, S.: Global Carbon Budget 2020, Earth Syst. Sci. Data, 12, 3269–3340, https://doi.org/10.5194/essd-12-3269-2020, 2020.

Friedlingstein, P., Jones, M. W., O'Sullivan, M., Andrew, R. M., Bakker, D. C. E., Hauck, J., Le Quéré, C., Peters, G. P., Peters, W., Pongratz, J., Sitch, S., Canadell, J. G., Ciais, P., Jackson, R. B., Alin, S. R., Anthoni, P., Bates, N. R., Becker, M., Bellouin, N., Bopp, L., Chau, T. T. T., Chevallier, F., Chini, L. P., Cronin, M., Currie, K. I., Decharme, B., Djeutchouang, L., Dou, X., Evans, W., Feely, R. A., Feng, L., Gasser, T., Gilfillan, D., Gkritzalis, T., Grassi, G., Gregor, L., Gruber, N., Gürses, Ö., Harris, I., Houghton, R. A., Hurtt, G. C., Iida, Y., Ilyina, T., Luijkx, I. T., Jain, A. K., Jones, S. D., Kato, E., Kennedy, D., Klein Goldewijk, K., Knauer, J., Korsbakken, J. I., Körtzinger, A., Landschützer, P., Lauvset, S. K., Lefèvre, N., Lienert, S., Liu, J., Marland, G., McGuire, P. C., Melton, J. R., Munro, D. R., Nabel, J. E. M. S., Nakaoka, S.-I., Niwa, Y., Ono, T., Pierrot, D., Poulter, B., Rehder, G., Resplandy, L., Robertson, E., Rödenbeck, C., Rosan, T. M., Schwinger, J., Schwingshackl, C., Séférian, R., Sutton, A. J., Sweeney, C., Tanhua, T., Tans, P. P., Tian, H., Tilbrook, B., Tubiello, F., van der Werf, G., Vuichard, N., Wada, C., Wanninkhof, R., Watson, A., Willis, D., Wiltshire, A. J., Yuan, W., Yue, C., Yue, X., Zaehle, S., and Zeng, J.: Global Carbon Budget 2021, Antroposphere – Energy and Emissions, https://doi.org/10.5194/essd-2021-386, 2021.

Friedlingstein, P., Jones, M. W., O'Sullivan, M., Andrew, R. M., Bakker, D. C. E., Hauck, J., Le Quéré, C., Peters, G. P., Peters, W., Pongratz, J., Sitch, S., Canadell, J. G., Ciais, P., Jackson, R. B., Alin, S. R., Anthoni, P., Bates, N. R., Becker, M., Bellouin, N., Bopp, L., Chau, T. T. T., Chevallier, F., Chini, L. P., Cronin, M., Currie, K. I., Decharme, B., Djeutchouang, L. M., Dou, X., Evans, W., Feely, R. A., Feng, L., Gasser, T., Gilfillan, D., Gkritzalis, T., Grassi, G., Gregor, L., Gruber, N., Gürses, Ö., Harris, I., Houghton, R. A., Hurtt, G. C., Iida, Y., Ilyina, T., Luijkx, I. T., Jain, A., Jones, S. D., Kato, E., Kennedy, D., Klein Goldewijk, K., Knauer, J., Korsbakken, J. I., Körtzinger, A., Landschützer, P., Lauvset, S. K., Lefèvre, N., Lienert, S., Liu, J., Marland, G., McGuire, P. C., Melton, J. R., Munro, D. R., Nabel, J. E. M. S., Nakaoka, S.-I., Niwa, Y., Ono, T., Pierrot, D., Poulter, B., Rehder, G., Resplandy, L., Robertson, E., Rödenbeck, C., Rosan, T. M., Schwinger, J., Schwingshackl, C., Séférian, R., Sutton, A. J., Sweeney, C., Tanhua, T., Tans, P. P., Tian, H., Tilbrook, B., Tubiello, F., van der Werf, G. R., Vuichard, N., Wada, C., Wanninkhof, R., Watson, A. J., Willis, D., Wiltshire, A. J., Yuan, W., Yue, C., Yue, X., Zaehle, S., and Zeng, J.: Global Carbon Budget 2021, Earth Syst. Sci. Data, 14, 1917–2005, https://doi.org/10.5194/essd-14-1917-2022, 2022.

Frish, M. B., Wainner, R. T., Laderer, M. C., Allen, M. G., Rutherford, J., Wehnert, P., Dey, S., Gilchrist, J., Corbi, R., Picciaia, D., Andreussi, P., and Furry, D.: Low-cost lightweight airborne laser-based sensors for pipeline leak detection and reporting, SPIE Defense, Security, and Sensing, Baltimore, Maryland, USA, 87260C, https://doi.org/10.1117/12.2015813, 2013.

Gålfalk, M., Olofsson, G., Crill, P., and Bastviken, D.: Making methane visible, Nature Clim Change, 6, 426–430, https://doi.org/10.1038/nclimate2877, 2016.

Gålfalk, M., Påledal, S. N., and Bastviken, D.: Sensitive drone mapping of methane emissions without the need of supplementary ground-based measurements, ACS Earth and Space Chemistry, 5, 2668-2678, https://doi.org/10.1021/acsearthspacechem.1c00106, 2021.

Gao, Z., Desjardins, R. L., and Flesch, T. K.: Comparison of a simplified micrometeorological mass difference technique and an inverse dispersion technique for estimating methane emissions from small area sources, Agr. Forest Meteorol., 149, 891–898, https://doi.org/10.1016/j.agrformet.2008.11.005, 2009.

Gardiner, T., Helmore, J., Innocenti, F., and Robinson, R.: Field Validation of Remote Sensing Methane Emission Measurements, 10, 2017.

Gas Infrastructure Europe (GIE) and MARCOGAZ 2019: Potential ways the gas industry can contribute to the reduction of methane emissions, https://ec.europa.eu/info/sites/default/files/gie-marcogaz_-_report_-_reduction_of_methane_emissions.pdf, last access: 13 October 2022.

Gasser, T., Crepin, L., Quilcaille, Y., Houghton, R. A., Ciais, P., and Obersteiner, M.: Historical CO_2 emissions from land use and land cover change and their uncertainty, Biogeosciences, 17, 4075–4101, https://doi.org/10.5194/bg-17-4075-2020, 2020.

Giannakopoulos, C., Hadjinicolaou, P., Kostopoulou, E., Varotsos, K. V., and Zerefos, C.: Precipitation and temperature regime over Cyprus as a result of global climate change, Adv. Geosci., 23, 17–24, https://doi.org/10.5194/adgeo-23-17-2010, 2010.

Giorgi, F.: Climate change hot-spots, Geophys. Res. Lett., 33, L08707, https://doi.org/10.1029/2006GL025734, 2006.

Golston, L., Aubut, N., Frish, M., Yang, S., Talbot, R., Gretencord, C., McSpiritt, J., and Zondlo, M.: Natural Gas Fugitive Leak Detection Using an Unmanned Aerial Vehicle: Localization and Quantification of Emission Rate, Atmosphere, 9, 333, https://doi.org/10.3390/atmos9090333, 2018.

Golston, L. M., Pan, D., Sun, K., Tao, L., Zondlo, M. A., Eilerman, S. J., Peischl, J., Neuman, J. A., and Floerchinger, C.: Variability of Ammonia and Methane Emissions from Animal Feeding Operations in Northeastern Colorado, Environ. Sci. Technol., 54, 11015–11024, https://doi.org/10.1021/acs.est.0c00301, 2020.

Gordon, D. J. and Johnson, C. A.: City-networks, global climate governance, and the road to 1.5 °C, Current Opinion in Environmental Sustainability, 30, 35–41, https://doi.org/10.1016/j.cosust.2018.02.011, 2018.

Gordon, M., Li, S.-M., Staebler, R., Darlington, A., Hayden, K., O'Brien, J., and Wolde, M.: Determining air pollutant emission rates based on mass balance using airborne measurement data over the Alberta oil sands operations, Atmos. Meas. Tech., 8, 3745–3765, https://doi.org/10.5194/amt-8-3745-2015, 2015.

Goyal, A., Small, M. J., von Stackelberg, K., Burmistrov, D., and Jones, N.: Estimation of Fugitive Lead Emission Rates from Secondary Lead Facilities using Hierarchical Bayesian Models, Environ. Sci. Technol., 39, 4929–4937, https://doi.org/10.1021/es035465e, 2005.

Guha, A., Newman, S., Fairley, D., Dinh, T. M., Duca, L., Conley, S. C., Smith, M. L., Thorpe, A. K., Duren, R. M., Cusworth, D. H., Foster, K. T., Fischer, M. L., Jeong, S., Yesiller, N., Hanson, J. L., and Martien, P. T.: Assessment of Regional Methane Emission Inventories through Airborne Quantification in the San Francisco Bay Area, Environ. Sci. Technol., 54, 9254–9264, https://doi.org/10.1021/acs.est.0c01212, 2020.

Harriss, R., Alvarez, R. A., Lyon, D., Zavala-Araiza, D., Nelson, D., and Hamburg, S. P.: Using Multi-Scale Measurements to Improve Methane Emission Estimates from Oil and Gas Operations in the Barnett Shale Region, Texas, Environ. Sci. Technol., 49, 7524–7526, https://doi.org/10.1021/acs.est.5b02305, 2015.

Hanna, S., White, J., Trolier, J., Vernot, R., Brown, M., Gowardhan, A., Kaplan, H., Alexander, Y., Moussafir, J., Wang, Y., Williamson, C., Hannan, J., and Hendrick, E.: Comparisons of JU2003 observations with four diagnostic urban wind flow and Lagrangian particle dispersion models, Atmos. Environ., 45, 4073–4081, https://doi.org/10.1016/j.atmosenv.2011.03.058, 2011.

Hauck, J., Zeising, M., Le Quéré, C., Gruber, N., Bakker, D. C. E., Bopp, L., Chau, T. T. T., Gürses, Ö., Ilyina, T., Landschützer, P., Lenton, A., Resplandy, L., Rödenbeck, C., Schwinger, J., and Séférian, R.: Consistency and Challenges in the Ocean Carbon Sink Estimate for the Global Carbon Budget, Front. Mar. Sci., 7, 571720, https://doi.org/10.3389/fmars.2020.571720, 2020.

Hazan, L., Tarniewicz, J., Ramonet, M., Laurent, O., and Abbaris, A.: Automatic processing of atmospheric CO_2 and CH_4 mole fractions atthe ICOS Atmosphere Thematic Centre, Atmos. Meas. Tech., 9, 4719–4736, https://doi.org/10.5194/amt-9-4719-2016, 2016.

Helfter, C., Mullinger, N., Vieno, M., O'Doherty, S., Ramonet, M., Palmer, P. I., and Nemitz, E.: Country-scale greenhouse gas budgets using shipborne

measurements: a case study for the UK and Ireland, Atmos. Chem. Phys., 19, 3043–3063, https://doi.org/10.5194/acp-19-3043-2019, 2019.

Hiller, R. V., Neininger, B., Brunner, D., Gerbig, C., Bretscher, D., Künzle, T., Buchmann, N., and Eugster, W.: Aircraft-based CH_4 flux estimates for validation of emissions from an agriculturally dominated area in Switzerland, J. Geophys. Res. Atmos., 119, 4874–4887, https://doi.org/10.1002/2013JD020918, 2014.

Houweling, S., Krol, M., Bergamaschi, P., Frankenberg, C., Dlugokencky, E. J., Morino, I., Notholt, J., Sherlock, V., Wunch, D., Beck, V., Gerbig, C., Chen, H., Kort, E. A., Röckmann, T., and Aben, I.: A multi-year methane inversion using SCIAMACHY, accounting for systematic errors using TCCON measurements, Atmos. Chem. Phys., 14, 3991–4012, https://doi.org/10.5194/acp-14-3991-2014, 2014.

Hristov, A. N., Harper, M., Meinen, R., Day, R., Lopes, J., Ott, T., Venkatesh, A., and Randles, C. A.: Discrepancies and Uncertainties in Bottom-up Gridded Inventories of Livestock Methane Emissions for the Contiguous United States, Environ. Sci. Technol., 51, 13668–13677, https://doi.org/10.1021/acs.est.7b03332, 2017.

Hsu, Y.-K., VanCuren, T., Park, S., Jakober, C., Herner, J., FitzGibbon, M., Blake, D. R., and Parrish, D. D.: Methane emissions inventory verification in southern California, Atmospheric Environment, 44, 1–7, https://doi.org/10.1016/j.atmosenv.2009.10.002, 2010.

Hummelga˚rd, C., Bryntse, I., Bryzgalov, M., Henning, J.-A., Martin, H., Norén, M., and Rödjega˚rd, H.: Low-cost NDIR based sensor platform for sub-ppm gas detection, Urban Climate, 14, 342–350, https://doi.org/10.1016/j.uclim.2014.09.001, 2015.

IEA: International Energy Agency: Global Energy Review, https://www.iea.org/reports/global-energy-review-2021 (last access: 22 September 2022), 2021.

Integrated Non-CO_2 Observing System (INGOS): Ambient atmospheric methane observations from the ICOS/InGOS network 2000–2015, https://doi.org/10.18160/P7E9-EKEA, 2018.

IPCC: IPCC Guidelines for National Greenhouse Gas Inventories, The National Greenhouse Gas Inventories Programme, edited by: Eggleston, H. S., Buendia, L., Miwa, K., Ngara, T., and Tanabe, K., The Intergovernmental Panel on Climate Change, IPCC TSU NGGIP, IGES, Institute for Global Environmental Strategy, Hayama, Kanagawa, Japan, available at: http://www. ipcc-nggip.iges.or.jp/support/Primer_2006GLs.pdf (last access: 29 September 2022), 2006.

IPCC, 2013: Climate Change 2013: The Physical Science Basis. Contribution of Working Group I to the Fifth Assessment Report of the Intergovernmental Panel on Climate Change [Stocker, T.F., D. Qin, G.-K. Plattner, M. Tignor, S.K. Allen, J. Boschung, A. Nauels, Y. Xia, V. Bex and P.M. Midgley (eds.)]. Cambridge University Press, Cambridge, United Kingdom and New York, NY, USA, 1535 pp.

IPCC, 2018: Global Warming of 1.5°C. An IPCC Special Report on the impacts of global warming of 1.5°C above pre-industrial levels and related global greenhouse gas emission pathways, in the context of strengthening the global response to the threat of climate change, sustainable development, and efforts to eradicate poverty [Masson-Delmotte, V., P. Zhai, H.-O. Pörtner, D. Roberts, J. Skea, P.R. Shukla, A. Pirani, W. Moufouma-Okia, C. Péan, R. Pidcock, S. Connors, J.B.R. Matthews, Y. Chen, X. Zhou, M.I. Gomis, E. Lonnoy, T. Maycock, M. Tignor, and T. Waterfield (eds.)], Cambridge University Press, Cambridge.

IPCC, 2019: Climate Change and Land: an IPCC special report on climate change, desertification, land degradation, sustainable land management, food security, and greenhouse gas fluxes in terrestrial ecosystems [P.R. Shukla, J. Skea, E. Calvo Buendia, V. Masson-Delmotte, H.-O. Pörtner, D. C. Roberts, P. Zhai, R. Slade, S. Connors, R. van Diemen, M. Ferrat, E. Haughey, S. Luz, S. Neogi, M. Pathak, J. Petzold, J. Portugal Pereira, P. Vyas, E. Huntley, K. Kissick, M. Belkacemi, J. Malley, (eds.)]. ambridge University Press, Cambridge.

IPCC, 2021: Climate Change 2021: The Physical Science Basis. Contribution of Working Group I to the Sixth Assessment Report of the Intergovernmental Panel on Climate Change[Masson-Delmotte, V., P. Zhai, A. Pirani, S.L. Connors, C. Péan, S. Berger, N. Caud, Y. Chen, L. Goldfarb, M.I. Gomis, M. Huang, K. Leitzell, E. Lonnoy, J.B.R. Matthews, T.K.

Maycock, T. Waterfield, O. Yelekçi, R. Yu, and B. Zhou (eds.)]. Cambridge University Press, Cambridge, United Kingdom and New York, NY, USA.

Jacob, D. J., Turner, A. J., Maasakkers, J. D., Sheng, J., Sun, K., Liu, X., Chance, K., Aben, I., McKeever, J., and Frankenberg, C.: Satellite observations of atmospheric methane and their value for quantifying methane emissions, Atmos. Chem. Phys., 16, 14371–14396, https://doi.org/10.5194/acp-16-14371-2016, 2016.

Johnson, M. R., Tyner, D. R., Conley, S., Schwietzke, S., and Zavala-Araiza, D.: Comparisons of Airborne Measurements and Inventory Estimates of Methane Emissions in the Alberta Upstream Oil and Gas Sector, Environ. Sci. Technol., 51, 13008–13017, https://doi.org/10.1021/acs.est.7b03525, 2017.

Johnson, M. R., Tyner, D. R., and Szekeres, A. J.: Blinded evaluation of airborne methane source detection using Bridger Photonics LiDAR, Remote Sensing of Environment, 259, 112418, https://doi.org/10.1016/j.rse.2021.112418, 2021.

Jr, B. C. D., Boering, K. A., Andrews, A. E., and Wofsy, S. C.: A High-Precision Fast-Response Airborne CO_2 Analyzer for In Situ Sampling from the Surface to the Middle Stratosphere, JOURNAL OF ATMOSPHERIC AND OCEANIC TECHNOLOGY, 19, 12, 2002.

Karion, A., Sweeney, C., Tans, P., and Newberger, T.: AirCore: An Innovative Atmospheric Sampling System, Journal of Atmospheric and Oceanic Technology, 27, 1839–1853, https://doi.org/10.1175/2010JTECHA1448.1, 2010.

Karion, A., Sweeney, C., Kort, E. A., Shepson, P. B., Brewer, A., Cambaliza, M., Conley, S. A., Davis, K., Deng, A., Hardesty, M., Herndon, S. C., Lauvaux, T., Lavoie, T., Lyon, D., Newberger, T., Pétron, G., Rella, C., Smith, M., Wolter, S., Yacovitch, T. I., and Tans, P.: Aircraft-Based Estimate of Total Methane Emissions from the Barnett Shale Region, Environ. Sci. Technol., 49, 8124–8131, https://doi.org/10.1021/acs.est.5b00217, 2015a.

Kezoudi, M., Keleshis, C., Antoniou, P., Biskos, G., Bronz, M., Constantinides, C., Desservettaz, M., Gao, R.-S., Girdwood, J., Harnetiaux, J., Kan-

dler, K., Leonidou, A., Liu, Y., Lelieveld, J., Marenco, F., Mihalopoulos, N., Močnik, G., Neitola, K., Paris, J.-D., Pikridas, M., Sarda-Esteve, R., Stopford, C., Unga, F., Vrekoussis, M., and Sciare, J.: The Unmanned Systems Research Laboratory (USRL): A New Facility for UAV-Based Atmospheric Observations, Atmosphere, 12, 1042, https://doi.org/10.3390/atmos12081042, 2021.

Khan, A., Schaefer, D., Tao, L., Miller, D. J., Sun, K., Zondlo, M. A., Harrison, W. A., Roscoe, B., and Lary, D. J.: Low Power Greenhouse Gas Sensors for Unmanned Aerial Vehicles, Remote Sensing, 4, 1355–1368, https://doi.org/10.3390/rs4051355, 2012.

Kjeldsen, P.: Landfill gas migration in soil. In: Christensen, T.H., Cossu, R., Stegmann, R., (Eds.), Landfilling of waste: Biogas,. E. & FN Spon. London, GB. pp. 87–132, 1996.

Klappenbach, F., Bertleff, M., Kostinek, J., Hase, F., Blumenstock, T., Agusti-Panareda, A., Razinger, M., and Butz, A.: Accurate mobile remote sensing of X_{CO2} and X_{CH4} latitudinal transects from aboard a research vessel, Atmos. Meas. Tech., 8, 5023–5038, https://doi.org/10.5194/amt-8-5023-2015, 2015.

Klausner, T.: Urban greenhouse gas emissions from the Berlin area: A case study using airborne CO_2 and CH_4 in situ observations in summer 2018, 24, n.d.

Knapp, M., Kleinschek, R., Hase, F., Agustí-Panareda, A., Inness, A., Barré, J., Landgraf, J., Borsdorff, T., Kinne, S., and Butz, A.: Shipborne measurements of X_{CO2}, X_{CH4}, and X_{CO} above the Pacific Ocean and comparison to CAMS atmospheric analyses and S5P/TROPOMI, Earth Syst. Sci. Data, 13, 199–211, https://doi.org/10.5194/essd-13-199-2021, 2021.

Kondo, M., Ichii, K., Takagi, H., and Sasakawa, M.: Comparison of the data-driven top-down and bottom-up global terrestrial CO_2 exchanges: GOSAT CO_2 inversion and empirical eddy flux upscaling, Journal of Geophysical Research: Biogeosciences, 120, 1226–1245, https://doi.org/10.1002/2014JG002866, 2015.

Korsakissok, I. and Mallet, V.: Comparative Study of Gaussian Dispersion Formulas within the Polyphemus Platform: Evaluation with Prairie Grass

and Kincaid Experiments, Journal of Applied Meteorology and Climatology, 48, 2459–2473, https://doi.org/10.1175/2009JAMC2160.1, 2009.

Krautwurst, S., Gerilowski, K., Jonsson, H. H., Thompson, D. R., Kolyer, R. W., Iraci, L. T., Thorpe, A. K., Horstjann, M., Eastwood, M., Leifer, I., Vigil, S. A., Krings, T., Borchardt, J., Buchwitz, M., Fladeland, M. M., Burrows, J. P., and Bovensmann, H.: Methane emissions from a Californian landfill, determined from airborne remote sensing and in situ measurements, Atmos. Meas. Tech., 10, 3429–3452, https://doi.org/10.5194/amt-10-3429-2017, 2017.

Kumar, P., Broquet, G., Yver-Kwok, C., Laurent, O., Gichuki, S., Caldow, C., Cropley, F., Lauvaux, T., Ramonet, M., Berthe, G., Martin, F., Duclaux, O., Juery, C., Bouchet, C., and Ciais, P.: Mobile atmospheric measurements and local-scale inverse estimation of the location and rates of brief CH_4 and CO_2 releases from point sources, Atmos. Meas. Tech., 14, 5987–6003, https://doi.org/10.5194/amt-14-5987-2021, 2021.

Kumar, P., Broquet, G., Caldow, C., Laurent, O., Gichuki, S., Cropley, F., Yver-Kwok, C., Fontanier, B., Lauvaux, T., Ramonet, M., Shah, A., Berthe, G., Martin, F., Duclaux, O., Juery, C., Bouchet, C., Pitt, J., and Ciais, P.: Near-field atmospheric inversions for the localization and quantification of controlled methane releases using stationary and mobile measurements, Quarterly Journal of the Royal Meteorological Society, 148, 1886–1912, https://doi.org/10.1002/qj.4283, 2022.

Kunz, M., Lavric, J. V., Gerbig, C., Tans, P., Neff, D., Hummelgård, C., Martin, H., Rödjegård, H., Wrenger, B., and Heimann, M.: COCAP: a carbon dioxide analyser for small unmanned aircraft systems, Atmos. Meas. Tech., 11, 1833–1849, https://doi.org/10.5194/amt-11-1833-2018, 2018.

Kuze, A., Suto, H., Shiomi, K., Kawakami, S., Tanaka, M., Ueda, Y., Deguchi, A., Yoshida, J., Yamamoto, Y., Kataoka, F., Taylor, T. E., and Buijs, H. L.: Update on GOSAT TANSO-FTS performance, operations, and data products after more than 6 years in space, Atmos. Meas. Tech., 9, 2445–2461, https://doi.org/10.5194/amt-9-2445-2016, 2016.

Lamb, B. K., McManus, J. B., Shorter, J. H., Kolb, C. E., Mosher, B., Harriss, R. C., Allwine, E., Blaha, D., Howard, T., Guenther, A., Lott, R. A., Siverson, R., Westburg, H., and Zimmerman, P.: Development of

Atmospheric Tracer Methods To Measure Methane Emissions from Natural Gas Facilities and Urban Areas, Environ. Sci. Technol., 29, 1468–1479, https://doi.org/10.1021/es00006a007, 1995.

Lamb, B. K., Cambaliza, M. O. L., Davis, K. J., Edburg, S. L., Ferrara, T. W., Floerchinger, C., Heimburger, A. M. F., Herndon, S., Lauvaux, T., Lavoie, T., Lyon, D. R., Miles, N., Prasad, K. R., Richardson, S., Roscioli, J. R., Salmon, O. E., Shepson, P. B., Stirm, B. H., and Whetstone, J.: Direct and Indirect Measurements and Modeling of Methane Emissions in Indianapolis, Indiana, Environ. Sci. Technol., 50, 8910–8917, https://doi.org/10.1021/acs.est.6b01198, 2016.

Lan, X., Talbot, R., Laine, P., and Torres, A.: Characterizing Fugitive Methane Emissions in the Barnett Shale Area Using a Mobile Laboratory, Environ. Sci. Technol., 49, 8139–8146, https://doi.org/10.1021/es5063055, 2015.

Lauvaux, T., Miles, N. L., Deng, A., Richardson, S. J., Cambaliza, M. O., Davis, K. J., Gaudet, B., Gurney, K. R., Huang, J., O'Keefe, D., Song, Y., Karion, A., Oda, T., Patarasuk, R., Razlivanov, I., Sarmiento, D., Shepson, P., Sweeney, C., Turnbull, J., and Wu, K.: High-resolution atmospheric inversion of urban CO_2 emissions during the dormant season of the Indianapolis Flux Experiment (INFLUX), Journal of Geophysical Research: Atmospheres, 121, 5213–5236, https://doi.org/10.1002/2015JD024473, 2016.

Lelieveld, J., Lechtenbohmer, S., Assonov, S. S., Brenninkmeijer, C. A. M., Dienst, C., Fischedick, M., and Hanke, T.: Greenhouse gases: Low methane leakage from gas pipelines, Nature, 434, 841–842, https://doi.org/10.1038/434841a, 2005.

Le Quéré, C., Andres, R. J., Boden, T., Conway, T., Houghton, R. A., House, J. I., Marland, G., Peters, G. P., van der Werf, G. R., Ahlström, A., Andrew, R. M., Bopp, L., Canadell, J. G., Ciais, P., Doney, S. C., Enright, C., Friedlingstein, P., Huntingford, C., Jain, A. K., Jourdain, C., Kato, E., Keeling, R. F., Klein Goldewijk, K., Levis, S., Levy, P., Lomas, M., Poulter, B., Raupach, M. R., Schwinger, J., Sitch, S., Stocker, B. D., Viovy, N., Zaehle, S., and Zeng, N.: The global carbon budget 1959–2011, Earth Syst. Sci. Data, 5, 165–185, https://doi.org/10.5194/essd-5-165-2013, 2013.

Le Quéré, C., Andrew, R. M., Friedlingstein, P., Sitch, S., Hauck, J., Pongratz, J., Pickers, P. A., Korsbakken, J. I., Peters, G. P., Canadell, J. G., Arneth, A., Arora, V. K., Barbero, L., Bastos, A., Bopp, L., Chevallier, F., Chini, L. P., Ciais, P., Doney, S. C., Gkritzalis, T., Goll, D. S., Harris, I., Haverd, V., Hoffman, F. M., Hoppema, M., Houghton, R. A., Hurtt, G., Ilyina, T., Jain, A. K., Johannessen, T., Jones, C. D., Kato, E., Keeling, R. F., Goldewijk, K. K., Landschützer, P., Lefèvre, N., Lienert, S., Liu, Z., Lombardozzi, D., Metzl, N., Munro, D. R., Nabel, J. E. M. S., Nakaoka, S., Neill, C., Olsen, A., Ono, T., Patra, P., Peregon, A., Peters, W., Peylin, P., Pfeil, B., Pierrot, D., Poulter, B., Rehder, G., Resplandy, L., Robertson, E., Rocher, M., Rödenbeck, C., Schuster, U., Schwinger, J., Séférian, R., Skjelvan, I., Steinhoff, T., Sutton, A., Tans, P. P., Tian, H., Tilbrook, B., Tubiello, F. N., van der Laan-Luijkx, I. T., van der Werf, G. R., Viovy, N., Walker, A. P., Wiltshire, A. J., Wright, R., Zaehle, S., and Zheng, B.: Global Carbon Budget 2018, Earth Syst. Sci. Data, 10, 2141–2194, https://doi.org/10.5194/essd-10-2141-2018, 2018.

Lelieveld, J., Hadjinicolaou, P., Kostopoulou, E., Chenoweth, J., El Maayar, M., Giannakopoulos, C., Hannides, C., Lange, M. A., Tanarhte, M., Tyrlis, E., and Xoplaki, E.: Climate change and impacts in the Eastern Mediterranean and the Middle East, Climatic Change, 114, 667–687, https://doi.org/10.1007/s10584-012-0418-4, 2012.

Lelieveld, J., Hadjinicolaou, P., Kostopoulou, E., Giannakopoulos, C., Pozzer, A., Tanarhte, M., and Tyrlis, E.: Model projected heat extremes and air pollution in the eastern Mediterranean and Middle East in the twenty-first century, Reg Environ Change, 14, 1937–1949, https://doi.org/10.1007/s10113-013-0444-4, 2014.

Liu, Y., Zhou, L., Tans, P. P., Zang, K., and Cheng, S.: Ratios of greenhouse gas emissions observed over the Yellow Sea and the East China Sea, Science of The Total Environment, 633, 1022–1031, https://doi.org/10.1016/j.scitotenv.2018.03.250, 2018.

Lorente, A., Borsdorff, T., Butz, A., Hasekamp, O., aan de Brugh, J., Schneider, A., Wu, L., Hase, F., Kivi, R., Wunch, D., Pollard, D. F., Shiomi, K., Deutscher, N. M., Velazco, V. A., Roehl, C. M., Wennberg, P. O., Warneke, T., and Landgraf, J.: Methane retrieved from TROPOMI: improvement of the data product and validation of the first 2 years of meas-

urements, Atmos. Meas. Tech., 14, 665–684, https://doi.org/10.5194/amt-14-665-2021, 2021.

Lowry, D., Fisher, R. E., France, J. L., Coleman, M., Lanoisellé, M., Zazzeri, G., Nisbet, E. G., Shaw, J. T., Allen, G., Pitt, J., and Ward, R. S.: Environmental baseline monitoring for shale gas development in the UK: Identification and geochemical characterisation of local source emissions of methane to atmosphere, Science of The Total Environment, 708, 134600, https://doi.org/10.1016/j.scitotenv.2019.134600, 2020a.

Lu, X., Jacob, D. J., Wang, H., Maasakkers, J. D., Zhang, Y., Scarpelli, T. R., Shen, L., Qu, Z., Sulprizio, M. P., Nesser, H., Bloom, A. A., Ma, S., Worden, J. R., Fan, S., Parker, R. J., Boesch, H., Gautam, R., Gordon, D., Moran, M. D., Reuland, F., Villasana, C. A. O., and Andrews, A.: Methane emissions in the United States, Canada, and Mexico: evaluation of national methane emission inventories and 2010–2017 sectoral trends by inverse analysis of in situ (GLOBALVIEWplus CH_4 ObsPack) and satellite (GOSAT) atmospheric observations, Atmos. Chem. Phys., 22, 395–418, https://doi.org/10.5194/acp-22-395-2022, 2022.

Lyon, D. R., Zavala-Araiza, D., Alvarez, R. A., Harriss, R., Palacios, V., Lan, X., Talbot, R., Lavoie, T., Shepson, P., Yacovitch, T. I., Herndon, S. C., Marchese, A. J., Zimmerle, D., Robinson, A. L., and Hamburg, S. P.: Constructing a Spatially Resolved Methane Emission Inventory for the Barnett Shale Region, Environ. Sci. Technol., 49, 8147–8157, https://doi.org/10.1021/es506359c, 2015.

Maazallahi, H., Fernandez, J. M., Menoud, M., Zavala-Araiza, D., Weller, Z. D., Schwietzke, S., von Fischer, J. C., Denier van der Gon, H., and Röckmann, T.: Methane mapping, emission quantification, and attribution in two European cities: Utrecht (NL) and Hamburg (DE), Atmos. Chem. Phys., 20, 14717–14740, https://doi.org/10.5194/acp-20-14717-2020, 2020.

Malaver, A., Motta, N., Corke, P., and Gonzalez, F.: Development and Integration of a Solar Powered Unmanned Aerial Vehicle and a Wireless Sensor Network to Monitor Greenhouse Gases, Sensors, 15, 4072–4096, https://doi.org/10.3390/s150204072, 2015.

Mallet, V., Quelo, D., Sportisse, B., de Biasi, M. A., Debry, E., Korsakissok, I., Wu, L., Roustan, Y., Sartelet, K., Tombette, M., and Foudhil, H.: Tech-

nical Note: The air quality modeling system Polyphemus, Atmos. Chem. Phys., 9, 2007.

McKain, K., Down, A., Raciti, S. M., Budney, J., Hutyra, L. R., Floerchinger, C., Herndon, S. C., Nehrkorn, T., Zahniser, M. S., Jackson, R. B., Phillips, N., and Wofsy, S. C.: Methane emissions from natural gas infrastructure and use in the urban region of Boston, Massachusetts, Proc Natl Acad Sci USA, 112, 1941–1946, https://doi.org/10.1073/pnas.1416261112, 2015.

McNorton, J., Wilson, C., Gloor, M., Parker, R. J., Boesch, H., Feng, W., Hossaini, R., and Chipperfield, M. P.: Attribution of recent increases in atmospheric methane through 3-D inverse modelling, Atmos. Chem. Phys., 18, 18149–18168, https://doi.org/10.5194/acp-18-18149-2018, 2018.

Millar, R. J., Fuglestvedt, J. S., Friedlingstein, P., Rogelj, J., Grubb, M. J., Matthews, H. D., Skeie, R. B., Forster, P. M., Frame, D. J., and Allen, M. R.: Emission budgets and pathways consistent with limiting warming to 1.5˚ C, Nat. Geosci., 10, 741–747, https://doi.org/10.1038/ngeo3031, 2017.

Miller, S. M. and Michalak, A. M.: Constraining sector-specific CO_2 and CH_4 emissions in the US, Atmos. Chem. Phys., 17, 3963–3985, https://doi.org/10.5194/acp-17-3963-2017, 2017.

Million, T., Kefale, G., and Ulfina, G.: Estimation of enteric methane emission factor in cattle species in Ethiopia using IPCC tier 2 methodology, Ann Environ Sci Toxicol, 6, 013–018, https://doi.org/10.17352/aest.000047, 2022.

Mitchell, L. E., Lin, J. C., Hutyra, L. R., Bowling, D. R., Cohen, R. C., Davis, K. J., DiGangi, E., Duren, R. M., Ehleringer, J. R., Fain, C., Falk, M., Guha, A., Karion, A., Keeling, R. F., Kim, J., Miles, N. L., Miller, C. E., Newman, S., Pataki, D. E., Prinzivalli, S., Ren, X., Rice, A., Richardson, S. J., Sargent, M., Stephens, B. B., Turnbull, J. C., Verhulst, K. R., Vogel, F., Weiss, R. F., Whetstone, J., and Wofsy, S. C.: A multi-city urban atmospheric greenhouse gas measurement data synthesis, Sci Data, 9, 361, https://doi.org/10.1038/s41597-022-01467-3, 2022.

Mønster, J., Kjeldsen, P., and Scheutz, C.: Methodologies for measuring fugitive methane emissions from landfills – A review, Waste Management, 87, 835–859, https://doi.org/10.1016/j.wasman.2018.12.047, 2019.

Morales, R., Ravelid, J., Vinkovic, K., Korbeń, P., Tuzson, B., Emmenegger, L., Chen, H., Schmidt, M., Humbel, S., and Brunner, D.: A tracer release experiment to investigate uncertainties in drone-based emission quantification for methane point sources, Gases/In Situ Measurement/Validation and Intercomparisons, https://doi.org/10.5194/amt-2021-314, 2021.

Moran, D., Pichler, P.-P., Zheng, H., Muri, H., Klenner, J., Kramel, D., Többen, J., Weisz, H., Wiedmann, T., Wyckmans, A., Strømman, A. H., and Gurney, K. R.: Estimating CO_2 Emissions for 108,000 European Cities, Antroposphere – Energy and Emissions, https://doi.org/10.5194/essd-2021-299, 2021.

Mueller, K., Yadav, V., Lopez-Coto, I., Karion, A., Gourdji, S., Martin, C., and Whetstone, J.: Siting Background Towers to Characterize Incoming Air for Urban Greenhouse Gas Estimation: A Case Study in the Washington, DC/Baltimore Area, Journal of Geophysical Research: Atmospheres, 123, 2910–2926, https://doi.org/10.1002/2017JD027364, 2018.

Müller, M., Graf, P., Meyer, J., Pentina, A., Brunner, D., Perez-Cruz, F., Hüglin, C., and Emmenegger, L.: Integration and calibration of non-dispersive infrared (NDIR) CO_2 low-cost sensors and their operation in a sensor network covering Switzerland, Atmos. Meas. Tech., 13, 3815–3834, https://doi.org/10.5194/amt-13-3815-2020, 2020.

Nathan, B. J., Golston, L. M., O'Brien, A. S., Ross, K., Harrison, W. A., Tao, L., Lary, D. J., Johnson, D. R., Covington, A. N., Clark, N. N., and Zondlo, M. A.: Near-Field Characterization of Methane Emission Variability from a Compressor Station Using a Model Aircraft, Environ. Sci. Technol., 49, 7896–7903, https://doi.org/10.1021/acs.est.5b00705, 2015.

Neininger, B. G., Kelly, B. F. J., Hacker, J. M., Lu, X., and Schwietzke, S.: Coal seam gas industry methane emissions in the Surat Basin, Australia: comparing airborne measurements with inventories, Phil. Trans. R. Soc. A., 379, 20200458, https://doi.org/10.1098/rsta.2020.0458, 2021.

Nisbet, E. G., Manning, M. R., Dlugokencky, E. J., Fisher, R. E., Lowry, D., Michel, S. E., Myhre, C. L., Platt, S. M., Allen, G., Bousquet, P., Brownlow, R., Cain, M., France, J. L., Hermansen, O., Hossaini, R., Jones, A. E., Levin, I., Manning, A. C., Myhre, G., Pyle, J. A., Vaughn, B., Warwick, N. J., and White, J. W. C.: Very strong atmospheric methane growth in the four years

20142017: Implications for the Paris Agreement, Global Biogeochem. Cy., 33, 318–342, https://doi.org/10.1029/2018GB006009, 2019.

Nisbet, E. G., Fisher, R. E., Lowry, D., France, J. L., Allen, G., Bakkaloglu, S., Broderick, T. J., Cain, M., Coleman, M., Fernandez, J., Forster, G., Griffiths, P. T., Iverach, C. P., Kelly, B. F. J., Manning, M. R., Nisbet-Jones, P. B. R., Pyle, J. A., Townsend-Small, A., al-Shalaan, A., Warwick, N., and Zazzeri, G.: Methane Mitigation: Methods to Reduce Emissions, on the Path to the Paris Agreement, Rev. Geophys., 58, https://doi.org/10.1029/2019RG000675, 2020.

Oil and Gas Climate Initiative report 2018, https://www.ogci.com/wp-content/uploads/2018/09/OGCI_Report_2018.pdf, last access: 13 October 2022.

Oil & Gas Methane Partnership 2.0, https://www.ogmpartnership.com/, last access: 29 September 2022.

OVSQ Essais thermiques: https://www.ovsq.uvsq.fr/essais-thermiques, last access: 29 September 2022.

Pales, J. C. and Keeling, C. D.: The concentration of atmospheric carbon dioxide in Hawaii, J. Geophys. Res., 70, 6053–6076, https://doi.org/10.1029/JZ070i024p06053, 1965.

Palmer, P. I., O'Doherty, S., Allen, G., Bower, K., Bösch, H., Chipperfield, M. P., Connors, S., Dhomse, S., Feng, L., Finch, D. P., Gallagher, M. W., Gloor, E., Gonzi, S., Harris, N. R. P., Helfter, C., Humpage, N., Kerridge, B., Knappett, D., Jones, R. L., Breton, M. L., Lunt, M. F., Manning, A. J., Matthiesen, S., Muller, J. B. A., Mullinger, N., Nemitz, E., O'Shea, S., Parker, R. J., Percival, C. J., Pitt, J., Riddick, S. N., Rigby, M., Sembhi, H., Siddans, R., Skelton, R. L., Smith, P., Sonderfeld, H., Stanley, K., Stavert, A. R., Wenger, A., White, E., Wilson, C., and Young, D.: A measurement-based verification framework for UK greenhouse gas emissions: an overview of the Greenhouse gAs Uk and Global Emissions (GAUGE) project, Atmos. Chem. Phys., 25, 2018.

Paris, J.-D., Ciais, P., Nédélec, P., Ramonet, M., Belan, B. D., Arshinov, M. Yu., Golitsyn, G. S., Granberg, I., Stohl, A., Cayez, G., Athier, G., Boumard, F., and Cousin, J.-M.: The YAK-AEROSIB transcontinental aircraft campaigns: new insights on the transport of CO_2 , CO and O_3 across Siberia,

Tellus B: Chemical and Physical Meteorology, 60, 551–568, https://doi.org/10.1111/j.1600-0889.2008.00369.x, 2008.

Paris, J.-D., Riandet, A., Bourtsoukidis, E., Delmotte, M., Berchet, A., Williams, J., Ernle, L., Tadic, I., Harder, H., and Lelieveld, J.: Shipborne measurements of methane and carbon dioxide in the Middle East and Mediterranean areas and the contribution from oil and gas emissions, Atmos. Chem. Phys., 21, 12443–12462, https://doi.org/10.5194/acp-21-12443-2021, 2021.

Paris, J.-D., Stohl, A., Nédélec, P., Arshinov, M. Yu., Panchenko, M. V., Shmargunov, V. P., Law, K. S., Belan, B. D., and Ciais, P.: Wildfire smoke in the Siberian Arctic in summer: source characterization and plume evolution from airborne measurements, Atmos. Chem. Phys., 9, 9315–9327, https://doi.org/10.5194/acp-9-9315-2009, 2009.

Peng, S., Piao, S., Bousquet, P., Ciais, P., Li, B., Lin, X., Tao, S., Wang, Z., Zhang, Y., and Zhou, F.: Inventory of anthropogenic methane emissions in mainland China from 1980 to 2010, Atmos. Chem. Phys., 16, 14545–14562, https://doi.org/10.5194/acp-16-14545-2016, 2016.

Petäjä, T., Duplissy, E.-M., Tabakova, K., Schmale, J., Altstädter, B., Ancellet, G., Arshinov, M., Balin, Y., Baltensperger, U., Bange, J., Beamish, A., Belan, B., Berchet, A., Bossi, R., Cairns, W. R. L., Ebinghaus, R., El Haddad, I., Ferreira-Araujo, B., Franck, A., Huang, L., Hyvärinen, A., Humbert, A., Kalogridis, A.-C., Konstantinov, P., Lampert, A., MacLeod, M., Magand, O., Mahura, A., Marelle, L., Masloboev, V., Moisseev, D., Moschos, V., Neckel, N., Onishi, T., Osterwalder, S., Ovaska, A., Paasonen, P., Panchenko, M., Pankratov, F., Pernov, J. B., Platis, A., Popovicheva, O., Raut, J.-C., Riandet, A., Sachs, T., Salvatori, R., Salzano, R., Schröder, L., Schön, M., Shevchenko, V., Skov, H., Sonke, J. E., Spolaor, A., Stathopoulos, V. K., Strahlendorff, M., Thomas, J. L., Vitale, V., Vratolis, S., Barbante, C., Chabrillat, S., Dommergue, A., Eleftheriadis, K., Heilimo, J., Law, K. S., Massling, A., Noe, S. M., Paris, J.-D., Prévôt, A. S. H., Riipinen, I., Wehner, B., Xie, Z., and Lappalainen, H. K.: Overview: Integrative and Comprehensive Understanding on Polar Environments (iCUPE) – concept and initial results, Atmos. Chem. Phys., 20, 8551–8592, https://doi.org/10.5194/acp-20-8551-2020, 2020.

Peters, W., Jacobson, A. R., Sweeney, C., Andrews, A. E., Conway, T. J., Masarie, K., Miller, J. B., Bruhwiler, L. M. P., Petron, G., Hirsch, A. I.,

Worthy, D. E. J., van der Werf, G. R., Randerson, J. T., Wennberg, P. O., Krol, M. C., and Tans, P. P.: An atmospheric perspective on North American carbon dioxide exchange: CarbonTracker, P. Natl. Acad. Sci. USA, 104, 1892518930, doi:10.1073/pnas.0708986104, 2007.

Pinty, B., Janssens-Maenhout, G., M., D., Zunker, H., Brunhes, T., Ciais, P., Denier van der Gon, D. Dee, H., Dolman, H., M., D., Engelen, R., Heimann, M., Holmlund, K., Husband, R., Kentarchos, A., Meijer, Y., Palmer, P., and Scholze, M.: An Operational Anthropogenic CO_2 Emissions Monitoring and Verification Support capacity: Baseline Requirements, Model Components and Functional Architecture, European Commission Joint Research Centre, EUR 28736 EN, https://doi.org/10.2760/08644, 2017.

Ravikumar, A. P., Sreedhara, S., Wang, J., Englander, J., Roda-Stuart, D., Bell, C., Zimmerle, D., Lyon, D., Mogstad, I., Ratner, B., and Brandt, A. R.: Single-blind inter-comparison of methane detection technologies – results from the Stanford/EDF Mobile Monitoring Challenge, Elementa: Science of the Anthropocene, 7, 37, https://doi.org/10.1525/elementa.373, 2019.

Ren, X., Salmon, O. E., Hansford, J. R., Ahn, D., Hall, D., Benish, S. E., Stratton, P. R., He, H., Sahu, S., Grimes, C., Heimburger, A. M. F., Martin, C. R., Cohen, M. D., Stunder, B., Salawitch, R. J., Ehrman, S. H., Shepson, P. B., and Dickerson, R. R.: Methane Emissions From the Baltimore-Washington Area Based on Airborne Observations: Comparison to Emissions Inventories, J. Geophys. Res. Atmos., 123, 8869–8882, https://doi.org/10.1029/2018JD028851, 2018.

Reuter, M., Bovensmann, H., Buchwitz, M., Borchardt, J., Krautwurst, S., Gerilowski, K., Lindauer, M., Kubistin, D., and Burrows, J. P.: Development of a small unmanned aircraft system to derive CO_2 emissions of anthropogenic point sources, Atmospheric Measurement Techniques, 14, 153–172, https://doi.org/10.5194/amt-14-153-2021, 2021.

Rogelj, J., Forster, P. M., Kriegler, E., Smith, C. J., and Séférian, R.: Estimating and tracking the remaining carbon budget for stringent climate targets, Nature, 571, 335–342, https://doi.org/10.1038/s41586-019-1368-z, 2019.

Roscioli, J. R., Yacovitch, T. I., Floerchinger, C., Mitchell, A. L., Tkacik, D. S., Subramanian, R., Martinez, D. M., Vaughn, T. L., Williams, L., Zim-

merle, D., Robinson, A. L., Herndon, S. C., and Marchese, A. J.: Measurements of methane emissions from natural gas gathering facilities and processing plants: measurement methods, Atmos. Meas. Tech., 8, 2017–2035, https://doi.org/10.5194/amt-8-2017-2015, 2015.

Rutherford, J. S., Sherwin, E. D., Ravikumar, A. P., Heath, G. A., Englander, J., Cooley, D., Lyon, D., Omara, M., Langfitt, Q., and Brandt, A. R.: Closing the methane gap in US oil and natural gas production emissions inventories, Nat Commun, 12, 4715, https://doi.org/10.1038/s41467-021-25017-4, 2021.

Ryoo, J.-M., Iraci, L. T., Tanaka, T., Marrero, J. E., Yates, E. L., Fung, I., Michalak, A. M., Tadic, J., Gore, W., Bui, T. P., Dean-Day, J. M., and Chang, C. S.: Quantification of CO_2 and CH_4 emissions over Sacramento, California, based on divergence theorem using aircraft measurements, Atmos. Meas. Tech., 18, 2019.

Sanna, L., Ferrara, R., Zara, P., and Duce, P.: GHG Emissions Inventory at Urban Scale: The Sassari Case Study, Energy Procedia, 59, 344–350, https://doi.org/10.1016/j.egypro.2014.10.387, 2014.

Saunois, M., Bousquet, P., Poulter, B., Peregon, A., Ciais, P., Canadell, J. G., Dlugokencky, E. J., Etiope, G., Bastviken, D., Houweling, S., Janssens-Maenhout, G., Tubiello, F. N., Castaldi, S., Jackson, R. B., Alexe, M., Arora, V. K., Beerling, D. J., Bergamaschi, P., Blake, D. R., Brailsford, G., Brovkin, V., Bruhwiler, L., Crevoisier, C., Crill, P., Covey, K., Curry, C., Frankenberg, C., Gedney, N., Höglund-Isaksson, L., Ishizawa, M., Ito, A., Joos, F., Kim, H.-S., Kleinen, T., Krummel, P., Lamarque, J.-F., Langenfelds, R., Locatelli, R., Machida, T., Maksyutov, S., McDonald, K. C., Marshall, J., Melton, J. R., Morino, I., Naik, V., O'Doherty, S., Parmentier, F.-J. W., Patra, P. K., Peng, C., Peng, S., Peters, G. P., Pison, I., Prigent, C., Prinn, R., Ramonet, M., Riley, W. J., Saito, M., Santini, M., Schroeder, R., Simpson, I. J., Spahni, R., Steele, P., Takizawa, A., Thornton, B. F., Tian, H., Tohjima, Y., Viovy, N., Voulgarakis, A., van Weele, M., van der Werf, G. R., Weiss, R., Wiedinmyer, C., Wilton, D. J., Wiltshire, A., Worthy, D., Wunch, D., Xu, X., Yoshida, Y., Zhang, B., Zhang, Z., and Zhu, Q.: The global methane budget 2000–2012, Earth Syst. Sci. Data, 8, 697–751, https://doi.org/10.5194/essd-8-697-2016, 2016.

Saunois, M., Stavert, A. R., Poulter, B., Bousquet, P., Canadell, J. G., Jackson, R. B., Raymond, P. A., Dlugokencky, E. J., Houweling, S., Patra, P. K., Ciais, P., Arora, V. K., Bastviken, D., Bergamaschi, P., Blake, D. R., Brailsford, G., Bruhwiler, L., Carlson, K. M., Carrol, M., Castaldi, S., Chandra, N., Crevoisier, C., Crill, P. M., Covey, K., Curry, C. L., Etiope, G., Frankenberg, C., Gedney, N., Hegglin, M. I., Höglund-Isaksson, L., Hugelius, G., Ishizawa, M., Ito, A., Janssens-Maenhout, G., Jensen, K. M., Joos, F., Kleinen, T., Krummel, P. B., Langenfelds, R. L., Laruelle, G. G., Liu, L., Machida, T., Maksyutov, S., McDonald, K. C., McNorton, J., Miller, P. A., Melton, J. R., Morino, I., Müller, J., Murguia-Flores, F., Naik, V., Niwa, Y., Noce, S., O'Doherty, S., Parker, R. J., Peng, C., Peng, S., Peters, G. P., Prigent, C., Prinn, R., Ramonet, M., Regnier, P., Riley, W. J., Rosentreter, J. A., Segers, A., Simpson, I. J., Shi, H., Smith, S. J., Steele, L. P., Thornton, B. F., Tian, H., Tohjima, Y., Tubiello, F. N., Tsuruta, A., Viovy, N., Voulgarakis, A., Weber, T. S., van Weele, M., van der Werf, G. R., Weiss, R. F., Worthy, D., Wunch, D., Yin, Y., Yoshida, Y., Zhang, W., Zhang, Z., Zhao, Y., Zheng, B., Zhu, Q., Zhu, Q., and Zhuang, Q.: The Global Methane Budget 2000–2017, Earth Syst. Sci. Data, 12, 1561–1623, https://doi.org/10.5194/essd-12-1561-2020, 2020.

Scarpelli, T. R., Jacob, D. J., Maasakkers, J. D., Sulprizio, M. P., Sheng, J.-X., Rose, K., Romeo, L., Worden, J. R., and Janssens-Maenhout, G.: A global gridded (0.1° × 0.1°) inventory of methane emissions from oil, gas, and coal exploitation based on national reports to the United Nations Framework Convention on Climate Change, 13, 2020.

Scheutz, C., Kjeld, A., and Fredenslund, A. M.: Methane emissions from Icelandic landfills – A comparison between measured and modelled emissions, Waste Management, 139, 136–145, https://doi.org/10.1016/j.wasman.2021.12.028, 2022.

Schuster, U., Watson, A. J., Bates, N. R., Corbiere, A., Gonzalez-Davila, M., Metzl, N., Pierrot, D., and Santana-Casiano, M.: Trends in North Atlantic sea-surface f_{CO2} from 1990 to 2006, Deep Sea Research Part II: Topical Studies in Oceanography, 56, 620–629, https://doi.org/10.1016/j.dsr2.2008.12.011, 2009.

Schwietzke, S., Griffin, W. M., Matthews, H. S., and Bruhwiler, L. M. P.: Natural Gas Fugitive Emissions Rates Constrained by Global Atmospheric

Methane and Ethane, Environ. Sci. Technol., 48, 7714–7722, https://doi.org/10.1021/es501204c, 2014.

Schwietzke, S., Pétron, G., Conley, S., Pickering, C., Mielke-Maday, I., Dlugokencky, E. J., Tans, P. P., Vaughn, T., Bell, C., Zimmerle, D., Wolter, S., King, C. W., White, A. B., Coleman, T., Bianco, L., and Schnell, R. C.: Improved Mechanistic Understanding of Natural Gas Methane Emissions from Spatially Resolved Aircraft Measurements, Environ. Sci. Technol., 51, 7286–7294, https://doi.org/10.1021/acs.est.7b01810, 2017.

Shah, A., Pitt, J. R., Ricketts, H., Leen, J. B., Williams, P. I., Kabbabe, K., Gallagher, M. W., and Allen, G.: Testing the near-field Gaussian plume inversion flux quantification technique using unmanned aerial vehicle sampling, Atmos. Meas. Tech., 13, 1467–1484, https://doi.org/10.5194/amt-13-1467-2020, 2020.

Sherwin, E. D., Chen, Y., Ravikumar, A. P., and Brandt, A. R.: Single-blind test of airplane-based hyperspectral methane detection via controlled releases, Elementa: Science of the Anthropocene, 9, 00063, https://doi.org/10.1525/elementa.2021.00063, 2021.

Solazzo, E., Crippa, M., Guizzardi, D., Muntean, M., Choulga, M., and Janssens-Maenhout, G.: Uncertainties in the Emissions Database for Global Atmospheric Research (EDGAR) emission inventory of greenhouse gases, Atmos. Chem. Phys., 21, 5655–5683, https://doi.org/10.5194/acp-21-5655-2021, 2021.

Stanley, K. M., Grant, A., O'Doherty, S., Young, D., Manning, A. J., Stavert, A. R., Spain, T. G., Salameh, P. K., Harth, C. M., Simmonds, P. G., Sturges, W. T., Oram, D. E., and Derwent, R. G.: Greenhouse gas measurements from a UK network of tall towers: technical description and first results, Atmos. Meas. Tech., 11, 1437–1458, https://doi.org/10.5194/amt-11-1437-2018, 2018.

Stavert, A. R., Saunois, M., Canadell, J. G., Poulter, B., Jackson, R. B., Regnier, P., Lauerwald, R., Raymond, P. A., Allen, G. H., Patra, P. K., Bergamaschi, P., Bousquet, P., Chandra, N., Ciais, P., Gustafson, A., Ishizawa, M., Ito, A., Kleinen, T., Maksyutov, S., McNorton, J., Melton, J. R., Müller, J., Niwa, Y., Peng, S., Riley, W. J., Segers, A., Tian, H., Tsuruta, A., Yin, Y., Zhang, Z., Zheng, B., and Zhuang, Q.: Regional trends and drivers of the

global methane budget, Global Change Biology, 28, 182–200, https://doi.org/10.1111/gcb.15901, 2022.

Steele, L. P., Fraser, P. J., Rasmussen, R. A., Khalil, M. A. K., Conway, T. J., Crawford, A. J., Gammon, R. H., Masarie, K. A., and Thoning, K. W.: The global distribution of methane in the troposphere, J. Atmos. Chem., 5, 125–171, 1987.

Storm, I. M. L. D., Hellwing, A. L. F., Nielsen, N. I., and Madsen, J.: Methods for Measuring and Estimating Methane Emission from Ruminants, Animals, 2, 160–183, https://doi.org/10.3390/ani2020160, 2012.

Suto, H., Kataoka, F., Kikuchi, N., Knuteson, R. O., Butz, A., Haun, M., Buijs, H., Shiomi, K., Imai, H., and Kuze, A.: Thermal and near-infrared sensor for carbon observation Fourier transform spectrometer-2 (TANSO-FTS-2) on the Greenhouse gases Observing SATellite-2 (GOSAT-2) during its first year in orbit, Atmos. Meas. Tech., 14, 2013–2039, https://doi.org/10.5194/amt-14-2013-2021, 2021.

Sweeney, C., Karion, A., Wolter, S., Newberger, T., Guenther, D., Higgs, J. A., Andrews, A. E., Lang, P. M., Neff, D., Dlugokencky, E., Miller, J. B., Montzka, S. A., Miller, B. R., Masarie, K. A., Biraud, S. C., Novelli, P. C., Crotwell, M., Crotwell, A. M., Thoning, K., and Tans, P. P.: Seasonal climatology of CO_2 across North America from aircraft measurements in the NOAA/ESRL Global Greenhouse Gas Reference Network, Journal of Geophysical Research: Atmospheres, 120, 5155–5190, https://doi.org/10.1002/2014JD022591, 2015.

Tadić, J. M., Michalak, A. M., Iraci, L., Ilić, V., Biraud, S. C., Feldman, D. R., Bui, T., Johnson, M. S., Loewenstein, M., Jeong, S., Fischer, M. L., Yates, E. L., and Ryoo, J.-M.: Elliptic Cylinder Airborne Sampling and Geostatistical Mass Balance Approach for Quantifying Local Greenhouse Gas Emissions, Environ. Sci. Technol., 51, 10012–10021, https://doi.org/10.1021/acs.est.7b03100, 2017.

Thorpe, A. K., Frankenberg, C., Aubrey, A. D., Roberts, D. A., Nottrott, A. A., Rahn, T. A., Sauer, J. A., Dubey, M. K., Costigan, K. R., Arata, C., Steffke, A. M., Hills, S., Haselwimmer, C., Charlesworth, D., Funk, C. C., Green, R. O., Lundeen, S. R., Boardman, J. W., Eastwood, M. L., Sarture, C. M., Nolte, S. H., Mccubbin, I. B., Thompson, D. R., and McFadden, J. P.:

Mapping methane concentrations from a controlled release experiment using the next generation airborne visible/infrared imaging spectrometer (AVIRIS-NG), Remote Sensing of Environment, 179, 104–115, https://doi.org/10.1016/j.rse.2016.03.032, 2016.

Turner, A. J., Jacob, D. J., Wecht, K. J., Maasakkers, J. D., Lundgren, E., Andrews, A. E., Biraud, S. C., Boesch, H., Bowman, K. W., Deutscher, N. M., Dubey, M. K., Griffith, D. W. T., Hase, F., Kuze, A., Notholt, J., Ohyama, H., Parker, R., Payne, V. H., Sussmann, R., Sweeney, C., Velazco, V. A., Warneke, T., Wennberg, P. O., and Wunch, D.: Estimating global and North American methane emissions with high spatial resolution using GOSAT satellite data, Atmos. Chem. Phys., 15, 7049–7069, https://doi.org/10.5194/acp-15-7049-2015, 2015.

Turner, A. J., Jacob, D. J., Benmergui, J., Wofsy, S. C., Maasakkers, J. D., Butz, A., Hasekamp, O., and Biraud, S. C.: A large increase in U.S. methane emissions over the past decade inferred from satellite data and surface observations, Geophysical Research Letters, 43, 2218–2224, https://doi.org/10.1002/2016GL067987, 2016.

Tuzson, B., Graf, M., Ravelid, J., Scheidegger, P., Kupferschmid, A., Looser, H., Morales, R. P., and Emmenegger, L.: A compact QCL spectrometer for mobile, high-precision methane sensing aboard drones, Atmos. Meas. Tech., 13, 4715–4726, https://doi.org/10.5194/amt-13-4715-2020, 2020.

UNFCCC: National inventory submissions 2021, https://unfccc.int/ghg-inventories-annex-i-parties/2021, last access: 29 September 2022.

Unmanned systems research laboratory, the Cyprus Institute: https://usrl.cyi.ac.cy/, last access: 29 September 2022.

Vaughn, T. L., Bell, C. S., Pickering, C. K., Schwietzke, S., Heath, G. A., Pétron, G., Zimmerle, D. J., Schnell, R. C., and Nummedal, D.: Temporal variability largely explains top-down/bottom-up difference in methane emission estimates from a natural gas production region, Proc. Natl. Acad. Sci. U.S.A., 115, 11712–11717, https://doi.org/10.1073/pnas.1805687115, 2018.

Vechi, N. T., Mellqvist, J., and Scheutz, C.: Quantification of methane emissions from cattle farms, using the tracer gas dispersion method, Agri-

culture, Ecosystems & Environment, 330, 107885, https://doi.org/10.1016/j.agee.2022.107885, 2022.

Vernooij, R., Winiger, P., Wooster, M., Strydom, T., Poulain, L., Dusek, U., Grosvenor, M., Roberts, G. J., Schutgens, N., and van der Werf, G. R.: A quadcopter unmanned aerial system (UAS)-based methodology for measuring biomass burning emission factors, Atmos. Meas. Tech., 15, 4271–4294, https://doi.org/10.5194/amt-15-4271-2022, 2022.

Vinković, K., Andersen, T., de Vries, M., Kers, B., van Heuven, S., Peters, W., Hensen, A., van den Bulk, P., and Chen, H.: Evaluating the use of an Unmanned Aerial Vehicle (UAV)-based active AirCore system to quantify methane emissions from dairy cows, Science of The Total Environment, 831, 154898, https://doi.org/10.1016/j.scitotenv.2022.154898, 2022.

Vrekoussis, M., Pikridas, M., Rousogenous, C., Christodoulou, A., Desservettaz, M., Sciare, J., Richter, A., Bougoudis, I., Savvides, C., and Papadopoulos, C.: Local and regional air pollution characteristics in Cyprus: A long-term trace gases observations analysis, Science of The Total Environment, 845, 157315, https://doi.org/10.1016/j.scitotenv.2022.157315, 2022.

Wania, R., Melton, J. R., Hodson, E. L., Poulter, B., Ringeval, B., Spahni, R., Bohn, T., Avis, C. A., Chen, G., Eliseev, A. V., Hopcroft, P. O., Riley, W. J., Subin, Z. M., Tian, H., van Bodegom, P. M., Kleinen, T., Yu, Z. C., Singarayer, J. S., Zürcher, S., Lettenmaier, D. P., Beerling, D. J., Denisov, S. N., Prigent, C., Papa, F., and Kaplan, J. O.: Present state of global wetland extent and wetland methane modelling: methodology of a model intercomparison project (WETCHIMP), Geosci. Model Dev., 6, 617–641, https://doi.org/10.5194/gmd-6-617-2013, 2013.

Watai, T., Machida, T., Ishizaki, N., and Inoue, G.: A Lightweight Observation System for Atmospheric Carbon Dioxide Concentration Using a Small Unmanned Aerial Vehicle, JOURNAL OF ATMOSPHERIC AND OCEANIC TECHNOLOGY, 23, 11, 2006.

Waxman, A. R., Khomaini, A., Leibowicz, B. D., and Olmstead, S. M.: Emissions in the stream: estimating the greenhouse gas impacts of an oil and gas boom, Environ. Res. Lett., 15, 014004, https://doi.org/10.1088/1748-9326/ab5e6f, 2020.

Weller, Z. D., Roscioli, J. R., Daube, W. C., Lamb, B. K., Ferrara, T. W., Brewer, P. E., and von Fischer, J. C.: Vehicle-Based Methane Surveys for Finding Natural Gas Leaks and Estimating Their Size: Validation and Uncertainty, Environ. Sci. Technol., acs.est.8b03135, https://doi.org/10.1021/acs.est.8b03135, 2018.

WMO GAW Central Calibration Laboratories: https://gml.noaa.gov/ccl/, last access: 29 September 2022.
WMO Greenhouse Gas Bulletin (GHG Bulletin)-No.15: The State of Greenhouse Gases in the Atmosphere Based on Global Observations through 2017, WMO, https://library.wmo.int/doc_num.php?explnum_id=5455, last access 29 September 2022, 2018.

WMO Greenhouse Gas Bulletin (GHG Bulletin)-No.15: The State of Greenhouse Gases in the Atmosphere Based on Global Observations through 2018, WMO, https://library.wmo.int/index.php?lvl=notice_display&id=21620#.YzVW4kxBxaQ, last access 29 September 2022, 2019.

WMO Greenhouse Gas Bulletin (GHG Bulletin)-No.17: The State of Greenhouse Gases in the Atmosphere Based on Global Observations through 2020, WMO, https://library.wmo.int/doc_num.php?explnum_id=10904, last access 29 September 2022, 2021.

Wolf, J., Asrar, G. R., and West, T. O.: Revised methane emissions factors and spatially distributed annual carbon fluxes for global livestock, Carbon Balance Manage, 12, 16, https://doi.org/10.1186/s13021-017-0084-y, 2017.

Wright, L. A., Kemp, S., and Williams, I.: 'Carbon footprinting': towards a universally accepted definition, Carbon Management, 2, 61–72, https://doi.org/10.4155/cmt.10.39, 2011.

Wunch, D., Toon, G. C., Hedelius, J. K., Vizenor, N., Roehl, C. M., Saad, K. M., Blavier, J.-F. L., Blake, D. R., and Wennberg, P. O.: Quantifying the loss of processed natural gas within California's South Coast Air Basin using long-term measurements of ethane and methane, Atmos. Chem. Phys., 16, 14091–14105, https://doi.org/10.5194/acp-16-14091-2016, 2016.

Wunch, D., Wennberg, P. O., Osterman, G., Fisher, B., Naylor, B., Roehl, C. M., O'Dell, C., Mandrake, L., Viatte, C., Kiel, M., Griffith, D. W. T., Deutscher, N. M., Velazco, V. A., Notholt, J., Warneke, T., Petri, C., De Maziere, M., Sha, M. K., Sussmann, R., Rettinger, M., Pollard, D., Robinson, J., Morino, I., Uchino, O., Hase, F., Blumenstock, T., Feist, D. G., Arnold, S. G., Strong, K., Mendonca, J., Kivi, R., Heikkinen, P., Iraci, L., Podolske, J., Hillyard, P. W., Kawakami, S., Dubey, M. K., Parker, H. A., Sepulveda, E., García, O. E., Te, Y., Jeseck, P., Gunson, M. R., Crisp, D., and Eldering, A.: Comparisons of the Orbiting Carbon Observatory-2 (OCO-2) X_{CO2} measurements with TCCON, Atmos. Meas. Tech., 10, 2209–2238, https://doi.org/10.5194/amt-10-2209-2017, 2017.

Yver Kwok, C., Laurent, O., Guemri, A., Philippon, C., Wastine, B., Rella, C. W., Vuillemin, C., Truong, F., Delmotte, M., Kazan, V., Darding, M., Lebègue, B., Kaiser, C., Xueref-Rémy, I., and Ramonet, M.: Comprehensive laboratory and field testing of cavity ring-down spectroscopy analyzers measuring H_2O, CO_2, CH_4 and CO, Atmos. Meas. Tech., 8, 3867–3892, https://doi.org/10.5194/amt-8-3867-2015, 2015.

Yver-Kwok, C., Philippon, C., Bergamaschi, P., Biermann, T., Calzolari, F., Chen, H., Conil, S., Cristofanelli, P., Delmotte, M., Hatakka, J., Heliasz, M., Hermansen, O., Komínková, K., Kubistin, D., Kumps, N., Laurent, O., Laurila, T., Lehner, I., Levula, J., Lindauer, M., Lopez, M., Mammarella, I., Manca, G., Marklund, P., Metzger, J.-M., Mölder, M., Platt, S. M., Ramonet, M., Rivier, L., Scheeren, B., Sha, M. K., Smith, P., Steinbacher, M., Vítková, G., and Wyss, S.: Evaluation and optimization of ICOS atmosphere station data as part of the labeling process, Atmos. Meas. Tech., 14, 89–116, https://doi.org/10.5194/amt-14-89-2021, 2021.

Zavala-Araiza, D., Lyon, D. R., Alvarez, R. A., Davis, K. J., Harriss, R., Herndon, S. C., Karion, A., Kort, E. A., Lamb, B. K., Lan, X., Marchese, A. J., Pacala, S. W., Robinson, A. L., Shepson, P. B., Sweeney, C., Talbot, R., Townsend-Small, A., Yacovitch, T. I., Zimmerle, D. J., and Hamburg, S. P.: Reconciling divergent estimates of oil and gas methane emissions, Proc Natl Acad Sci USA, 112, 15597–15602, https://doi.org/10.1073/pnas.1522126112, 2015.

Zavala-Araiza, D., Omara, M., Gautam, R., Smith, M. L., Pandey, S., Aben, I., Almanza-Veloz, V., Conley, S., Houweling, S., Kort, E. A., Maasakkers,

J. D., Molina, L. T., Pusuluri, A., Scarpelli, T., Schwietzke, S., Shen, L., Zavala, M., and Hamburg, S. P.: A tale of two regions: methane emissions from oil and gas production in offshore/onshore Mexico, Environ. Res. Lett., 16, 024019, https://doi.org/10.1088/1748-9326/abceeb, 2021.

Zhang, X., Lee, X., Griffis, T. J., Baker, J. M., and Xiao, W.: Estimating regional greenhouse gas fluxes: an uncertainty analysis of planetary boundary layer techniques and bottom-up inventories, Atmos. Chem. Phys., 14, 10705–10719, https://doi.org/10.5194/acp-14-10705-2014, 2014.

Zhou, M., Langerock, B., Sha, M. K., Kumps, N., Hermans, C., Petri, C., Warneke, T., Chen, H., Metzger, J.-M., Kivi, R., Heikkinen, P., Ramonet, M., and De Mazière, M.: Retrieval of atmospheric CH₄ vertical information from TCCONFTIR spectra, Gases/Remote Sensing/Data Processing and Information Retrieval, https://doi.org/10.5194/amt-2019-94, 2019.

Zimmerle, D., Vaughn, T., Luck, B., Lauderdale, T., Keen, K., Harrison, M., Marchese, A., Williams, L., and Allen, D.: Methane Emissions from Gathering Compressor Stations in the U.S., Environ. Sci. Technol., 54, 7552–7561, https://doi.org/10.1021/acs.est.0c00516, 2020.

Zittis, G., Hadjinicolaou, P., Fnais, M., and Lelieveld, J.: Projected changes in heat wave characteristics in the eastern Mediterranean and the Middle East, Reg Environ Change, 16, 1863–1876, https://doi.org/10.1007/s10113-014-0753-2, 2016.

Zittis, G., Almazroui, M., Alpert, P., Ciais, P., Cramer, W., Dahdal, Y., Fnais, M., Francis, D., Hadjinicolaou, P., Howari, F., Jrrar, A., Kaskaoutis, D. G., Kulmala, M., Lazoglou, G., Mihalopoulos, N., Lin, X., Rudich, Y., Sciare, J., Stenchikov, G., Xoplaki, E., and Lelieveld, J.: Climate Change and Weather Extremes in the Eastern Mediterranean and Middle East, Reviews of Geophysics, 60, e2021RG000762, https://doi.org/10.1029/2021RG000762, 2022.

APPENDIX A: AIRBORNE MEASUREMENTS OF METHANE IN CYPRUS

We conducted three airborne GHG surveys on April 9, May 24 and June 8 2021. The LGR-ICOS™ GLA133 Series Greenhouse gas analyzer using patented off-Axis integrated Cavity output Spectroscopy (OA-ICOS) technology was employed to measure CH_4 at 1 Hz resolution. The analyzer was installed into a small aircraft (5B-CMD) with a GPS device (NEO-M8N-0-10 U-Blox), as shown in Fig.S1.1. The air inlet was added to the outside of the window (Figure S1.1). The instrument was tested and calibrated following the WMO X2004 scale (Yver Kwok et al., 2015) at Le Laboratoire des Sciences du Climat et de l'Environnement (LSCE) before shipped to Cyprus. The analyzer was calibrated before and after each flight. All the data reported were quality controlled by the Integrated Carbon Observation System-Atmosphere Thematic Center (ICOS-ATC). The precision of CH_4 is 0.65 ppb (1σ) at 1 Hz.

The duration of each flight was about 2.5 h. The aircraft took off at the Larnaca international airport heading to Limassol and Paphos, then returned to the Akamas national park back to Larnaca. The survey dates were selected when the wind came from the west or northwest with the wind speed above 2 m s^{-1}. Due to the limitation of the government regulation on the flight path, the aircraft could not fly over the sea. The bottom second percentile of methane mole fractions was measured in each survey as the daily background concentration. Methane mole fractions were further documented with the GPS device. Figure S1.2 presents the mapping and time series plot of methane measurements of the flight on April 9, 2021. Since there were no significant emission plumes captured during the second flight, estimates of methane emissions were calculated through the other two flights. These data have been processed and analyzed by the master student Ms. Assia Palagi, during her internship at LSCE, based on the Lagrangian particle transport and dispersion model FLEXPART (FLEXible PARTicle dispersion model) and the mass balance approach (Palagi, 2022). The preliminary analysis indicated that the measured methane emissions were mainly emanating from local emissions in Cyprus.

Figure S1.1 The setup of the airborne measurement system.

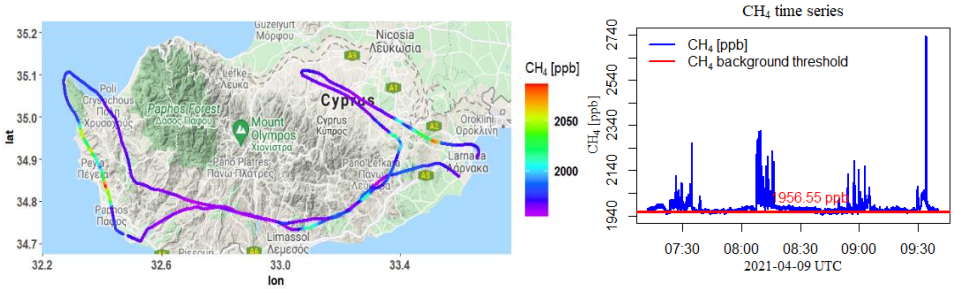

Figure S1.2 Methane mapping (on the left) and time series plot (on the right).

APPENDIX B : SUPPLEMENTARY MATERIAL TO SECTION 4.2

Supplement of

Improvements of a low-cost CO_2 commercial NDIR sensor for UAV atmospheric mapping applications

Liu et al.

Correspondence to: Yunsong Liu (yunsong.liu@lsce.ipsl.fr)

Figures and pictures

(a)  (b) 

Figure S1 the setup of the system onboard a small aircraft (a) and the manned aircraft platform Beechcraft Baron 58 (b).

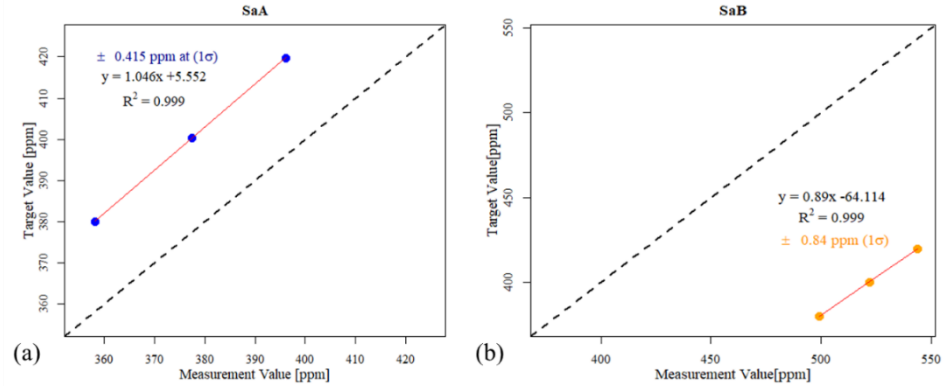

Figure S2 Calibration linear fits calculated for SaA (a) and SaB (b).

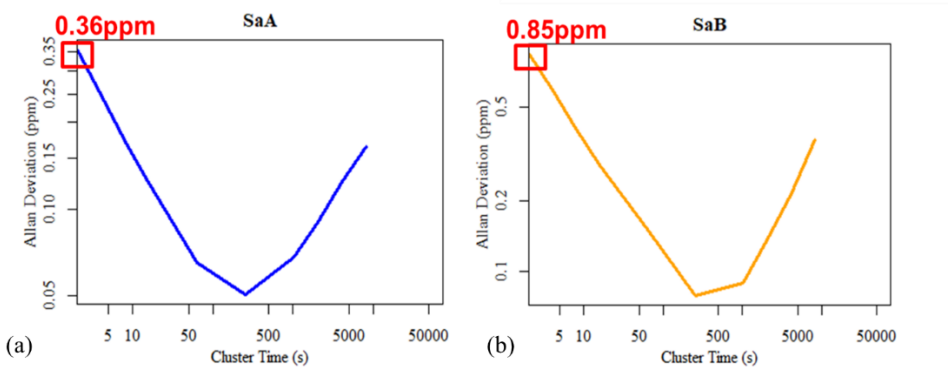

Figure S3 Allan deviation test results for SaA (a) and SaB (b).

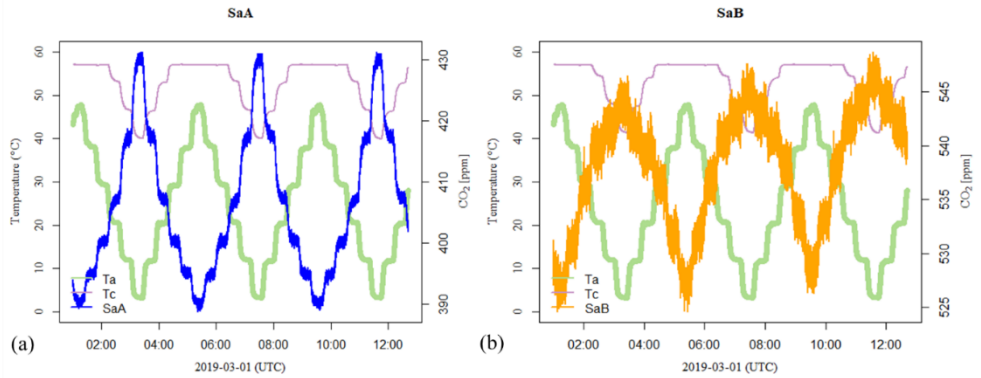

Figure S4 Temperature sensitivity test diagrams, (a) shows the time series of chamber temperature, the sensor cell temperature of SaA and CO_2 readings from SaA; (b) shows the time series of chamber temperature, the sensor cell temperature of SaB and CO_2 readings from SaB.

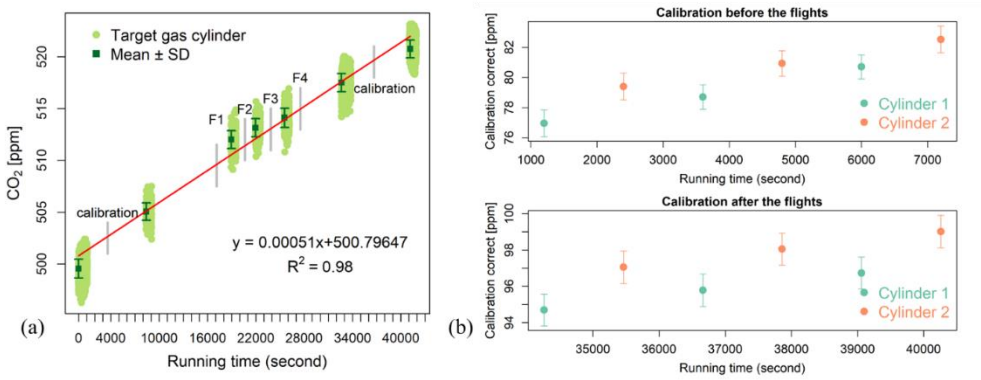

Figure S5 (a) the evolution of target cylinder measurements for SaB and the red line is the linear regression of CO_2 (ppm) against time; (b) presents the calibrations before and after the flights.

APPENDIX C : RESUME SUBSTANTIEL EN FRANÇAIS

Le méthane (CH_4) et le dioxyde de carbone (CO_2), les deux gaz à effet de serre (GES) les plus abondants et les plus importants dans l'atmosphère, sont les principaux moteurs du changement climatique. Par conséquent, caractériser et quantifier avec précision leurs émissions par secteur est une condition préalable essentielle pour mettre en place des actions et des politiques d'atténuation efficaces. Cette thèse vise à déterminer les émissions de CH_4 et de CO_2 grâce au développement et déploiement de différentes plateformes mobiles (véhicules, drones, et avions) de l'échelle locale à nationale.

Le chapitre 2, basé sur des mesures mobiles en voiture (24 jours d'enquête), propose une tentative de quantification indépendante des émetteurs de méthane importants pour l'ile-pays de Chypre et d'en déduire de nouvelles contraintes fortes pour l'inventaire national. Les zones étudiées de mesures mobiles comprennent les décharges et les zones d'élevage bovin. Les taux d'émission ont été estimés à l'aide d'un modèle de panache gaussien. Les émissions de méthane calculées provenant des décharges (Koshi et Kotsiatis) et de la fermentation entérique du bétail étaient environ 160% et 40% plus élevées respectivement que les estimations sectorielles ascendantes utilisées dans l'inventaire national de la UNFCCC. La paramétrisation du modèle de panache gaussien domine l'incertitude de la méthode, avec une incertitude typique de 21%. Ces enquêtes mobiles montrent que l'utilisation d'un ensemble de mesures in situ ciblant des points chauds d'émission de méthane représentatifs avec une couverture temporelle et spatiale cohérente peut largement améliorer les inventaires nationaux d'émissions.

Dans le but de mieux évaluer les performances des systèmes mobiles de mesure des gaz à effet de serre, le chapitre 3 se concentre sur l'évaluation de dix systèmes de quantification de méthane commerciaux, en s'appuyant sur une série d'expériences de libération de gaz contrôlée dans une station de compression inerte. Les plates-formes de mesure comprennent des mesures atmosphériques aéroportées, mobiles et fixes au sol, ainsi que des systèmes portables. De plus, les rejets contrôlés couvrent un large éventail de situations, telles que différents débits allant de 0,01 kg h^{-1} à 50 kg h^{-1}, des hauteurs de rejet allant de 1 m à 28 m et différents types de sorties de gaz.

Le niveau d'erreurs des différents systèmes n'a pas varié en fonction des taux de rejet pour les rejets supérieurs à 0,1 kg h^{-1}. Les systèmes au niveau de la source sous-estiment généralement les émissions tandis que les systèmes au niveau du site, reposant sur la dispersion atmosphérique, ont surestiment légèrement les taux d'émission. L'analyse des estimations d'émissions disponibles pour les sources individuelles lors de rejets multi-sources encourage la définition de nouveaux protocoles exploitant la combinaison de systèmes de quantification au niveau de la source et au niveau du site afin d'obtenir une connaissance complète des bilan d'émission et de leur distribution spatiale.

Les drones (UAV) offrent une possibilité potentiellement intéressante de combler l'écart entre les observations au sol et les observations aéroportées. Le chapitre 4 décrit l'intégration et la validation d'un nouveau système de capteur UAV-CO_2 portable basé sur un capteur NDIR commercial de CO_2 à faible coût. La charge utile est de 1058 g avec des dimensions de 15 cm × 9,5 cm × 11 cm, y compris la batterie. Avant l'intégration, la précision et la linéarité du capteur de CO_2 ont été assurées par une série de tests en laboratoire, qui ont montré que la précision reste à ± 1 ppm (1σ) à 1 Hz. Des corrections dues aux changements de température et de pression ont été appliquées à la suite d'expériences en chambre climatique. Les performances de ce système ont également été validées dans des conditions ambiantes par rapport à un instrument de référence à bord d'un aéronef piloté et ont été trouvées à ± 2 ppm (1σ) à 1 Hz et ± 1 ppm (1σ) à 1 min. Comme preuve de concept, des vols intensifs du système développé ont été présentés dans la zone urbaine (Nicosie, Chypre). Il est démontré que le système est facile à reproduire, permettant une large gamme d'applications sur le terrain, telles que la surveillance des émissions urbaines et ponctuelles.

Les résultats de cette thèse ont permis de vérifier les émissions nationales de méthane à Chypre sur la base de mesures mobiles in situ et ont proposé une tentative de quantification indépendante des émetteurs importants à l'échelle nationale pour en déduire de nouvelles contraintes fortes pour l'inventaire national. L'évaluation et les comparaisons de dix approches prometteuses de quantification du méthane basées sur des expériences de libération contrôlée fournissent une mise à jour sur les capacités actuelles et améliorent la connaissance des émissions fugitives de méthane des systèmes de gaz naturel pour élaborer des politiques et des actions d'atténuation efficaces. De plus, un système de capteur UAV-CO_2 portable et peu coûteux est développé pour prendre en charge les futures applications de plate-forme

UAV pour les mesures de gaz traces atmosphériques, et a le potentiel d'accueillir d'autres capteurs pour effectuer des mesures de taux d'émission de cheminée, ouvrant ainsi de futures opportunités interessantes.